Cellular locomotion and adhesion in the context of different substrate properties

Dissertation

for the award of the degree

“Doctor rerum naturalium”

of the Georg-August-University Göttingen

within the doctoral program “*Molecular Biology of Cells*”

of the Georg-August-University School of Science (GAUSS)

submitted by

Thilo Baronsky

from Bonn

Göttingen 2016

Thesis Committee

Prof. Dr. Andreas Janshoff

Institute of Physical Chemistry

Georg-August-University Göttingen

Prof. Dr. Tomas Pieler

Department of Developmental Biochemistry

Center for Biochemistry and Molecular Biology

Georg-August-University Göttingen

Prof. Dr. Andreas Wodarz

Microscopic Anatomy and Molecular Cell Biology

University of Cologne

Member of the Examination Board

1st Referee:

Prof. Dr. Andreas Janshoff, Institute of Physical Chemistry, Georg-August-University Göttingen

2nd Referee:

Prof. Dr. Tomas Pieler, Department of Developmental Biochemistry, Georg-August-University Göttingen

Further members of the Examination Board

Prof. Dr. Andreas Wodarz, Microscopic Anatomy and Molecular Cell Biology, University of Cologne

Prof. Dr. Sarah Köster, Institute for X-Ray Physics, Georg-August-University Göttingen

Prof. Dr. Michael Meinecke, Molecular Membrane Biology, European Neuroscience Institute Göttingen

Prof. Dr. Jörg Großhans, Department of Developmental Biochemistry, Georg-August-University Göttingen

Date of oral examination: 10.06.2016

I, Thilo Baronsky, hereby certify that my doctoral thesis entitled “Cellular locomotion and adhesion in the context of different substrate properties” has been written independently and with no other sources and aids than quoted.

Thilo Baronsky
28.04.2016
Göttingen, Germany

Meiner Familie

“Das Lernen macht stets dann Verdruß wenn man’s nicht will, es aber muß.“

Heinz Erhardt

Abstract

This work comprises three different projects dealing with the interplay of cellular locomotion and adhesion to establish a better understanding of the response of cells to their environment.

In the first part of this thesis the dependence of migration and adhesion of *Xenopus laevis* primordial germ cell (PGCs) on E-cadherin expression was investigated. With single cell force spectroscopy (SCFS) different stages during embryogenesis were analyzed. Here we found that the adhesion force between migratory PGCs and the cadherin-coated surface was significantly reduced compared to non-migratory PGCs and reached almost the level of E-cadherin knock down PGCs. Secondly, the influence of the biological process epithelial-mesenchymal transition (EMT) on cellular locomotion and adhesion was investigated. In this project the cell-substrate distance alteration during EMT on mouse breast epithelial cells (NMuMG) was analyzed by metal induced energy transfer (MIET) and electric cell-substrate impedance sensing (ECIS). The results demonstrated that in the very first hours of the transition the cell-substrate distance increased and in the course of the transition the distance is reduced again to the level of untreated cells and stayed constant for the mesenchymal state. The last project shed light on the alteration of biochemical properties of the extracellular matrix (ECM) in response to the knock-out of the surface receptor discoidin domain receptor 2 (DDR2) in mice. Therefore the stiffness of dermal skin was analyzed by atomic force microscopy (AFM) and rheometry. Both methods confirmed that in response of the DDR2 knock out the dermis of mice became significantly stiffer than the wild type. This could make the DDR2 knock out mice a suitable model to investigate the mechanobiological effect of the environment during tumor progression.

Table of contents

1 Introduction

In cellular locomotion and adhesion cells highly interact with the surrounding microenvironment. Both phenomena are tightly coupled and play a fundamental role in different aspects of life (Ladoux and Nicolas, 2012). In development and embryogenesis for example, they mediate the establishment of the embryonic architecture (Locascio and Nieto, 2001). Cells can move either in a collective manner, in small groups or individually. One example for collective migration is the process of gastrulation (Keller, 2005) where cells are influenced by interaction with their neighbors (Theveneau and Mayor, 2013, Locascio and Nieto, 2001). The active migration of primordial germ cells (PGCs) across the embryo (Terayama et al., 2013) is an example of individual cell migration and requires the loss of cell-cell contacts. Also in the adult organism migration and adhesion play a central role and are essential for inflammatory response or wound healing (Lauffenburger and Horwitz, 1996, Martin, 1997, Muller, 2003). Additionally, they are also important in the context of cancer. A dysregulation of cell attachment could lead to cancer invasion and metastasis (Ladoux and Nicolas, 2012), where the cancer cells actively migrate from the primary tumor into adjacent tissues (Yamaguchi et al., 2005).

One process which causes cellular locomotion and an alteration of adhesion is the so called epithelial-mesenchymal transition (EMT). EMT appears apart from cancer progression in embryogenesis, tissue regeneration and wound healing (Kalluri and Weinberg, 2009, Son and Moon, 2010, Lamouille et al., 2014). In EMT the polarized epithelial cells undergo multiple biochemical changes to transform into a mesenchymal phenotype which leads to an enhanced migratory capacity and invasiveness (Kalluri and Weinberg, 2009, Lamouille et al., 2014).

Cellular locomotion and adhesion are largely influenced by the microenvironment around the cells. One main component of this environment is the extracellular matrix (ECM). The ECM has the ability to regulate the mechanism of cell adhesion and migration by its physical properties including stiffness and ligand density (Pathak and Kumar, 2011). The study of the role of the ECM in diseases, such as cancer, is also a task in the modern research since it could be shown

that the ECM regulates almost all cellular behavior and has an influence on main developmental processes (Wiseman et al., 2003, Stickens et al., 2004, Lu et al., 2011).

To get a deeper understanding of these cellular processes it is necessary to know what role single cellular properties play for the interplay with the direct environment. Therefore, this work deals with the investigation of cellular locomotion and adhesion in the context of different substrate properties. Three different fields concerning cellular locomotion and adhesion were investigated. Firstly, we studied the function of E-cadherin in the context of active migration and adhesion in early embryonic stage of primordial germ cell (PGCs) of the model system *Xenopus laevis*. Here the interaction between E-cadherin coated surfaces and modified PGCs of different embryonic stages was analyzed with single cell force spectroscopy (SCFS). SCFS is based on atomic force spectroscopy and gives information of the adhesion strength and interaction between cell and surface. It enables to measure overall cellular adhesion but also single interactions between cell and E-cadherin (Helenius et al., 2008) which gives an good overview to characterize the dependency of E-cadherin mediated adhesion in the active migration of *Xenopus* PGCs.

Secondly, the progress of the biological important epithelial-mesenchymal transition (EMT) on cellular locomotion and adhesion of mouse breast epithelial cells (NMuMG) was monitored. Global and individual height alterations during EMT were analyzed with metal induced energy transfer (MIET) and electric cell-substrate impedance sensing (ECIS). MIET visualizes and quantifies the distance between the cell and the substrate with spatial nanometer resolution and gives an insight into the local cell-substrate changes. The distance between the fluorophore labelled cell membrane and the used metal surface can be calculated from the locally recorded fluorescence lifetime (Chizhik et al., 2014). ECIS is a real time, non-invasive method to monitor globally the morphological changes of cells like cell-cell as well as cell-substrate interaction and cellular locomotion by measure the impedance signal (Wegener et al., 2000, Lovelady et al., 2007, Tarantola et al., 2009, Lo et al., 1995, Giaever and Keese, 1991). The combination of both methods enabled us to monitor changes in the cell-substrate distance during EMT on different spatial length scales ranging from single adhesion spots to entire cell cluster attachment. In these studies the EMT is

induced by the cytokine transforming growth factor-ß1 (TGF-ß1) which is known to promote EMT in NMuMG cells (Xu et al., 2009, Gal et al., 2008).

Lastly, we shed light on the interplay between extracellular matrix (ECM) and cellular adhesion and migration. Here, we studied if the knock-out of the surface receptor discoidin domain receptor 2 (DDR2) in mice alters the stiffness of the ECM. This setup could serve as a suitable model system for investigating the mechanobiological effect on the tumor environment on tumor progression. The stiffness of dermal skin samples was measured with AFM and rheology to probe spots of micrometer scale on the one hand and macroscopic skin samples of several centimeter on the other hand.

This work comprises three different projects in the context of cellular processes of locomotion and adhesion. Each part handles the interplay of these processes with different substrates to accomplish a better understanding of the response of a cell on its direct environment.

2 Cellular locomotion and adhesion

As already mentioned cellular locomotion and adhesion are tightly coupled phenomena which are used from the cell to interact with the surrounding microenvironment. This work deals with the locomotion of single cells in three different processes. The active migration at early embryonic stages from single primordial germ cells (PGCs) to the gonad formation. Epithelial-mesenchymal transition where epithelial cells change to a mesenchymal phenotype to start migration individually. And the individual cellular locomotion in response to altering extracellular matrix.

This chapter gives insights into these processes and the biological relevant components like the epithelial marker E-cadherin, the actin cytoskeleton (F-actin), the cytokine transforming growth factor-ß1 (TGF-ß1) and the surface receptor Discoidin Domain Receptor 2 (DDR 2).

2.1 Active migration at early embryonic stages

Cellular locomotion is essential in embryogenesis for embryonic architecture. During embryonic development two types of cell movements can occur. One type of movement is a collective migration whereby tissue moves in a coordinated manner and the cells are influenced by interaction with their neighbors (Theveneau and Mayor, 2013, Locascio and Nieto, 2001). One example is the gastrulation in the morphogenetic process where coordinated cell migration is responsible for the formation of the three germ layers (ectoderm, mesoderm and endoderm) (Keller, 2005). The other type of movement is the migration of individual or small groups of cells, which requires the loss of cell-cell contacts first. Then individual cells exhibit a directional polarity with a leading edge at the front and a lagging edge at the back. One example, which will be discussed next, is the active migration from primordial germ cells (PGCs) across the embryo.

PGCs are precursors to sperms and eggs and arise at a distance from the future gonadal region at early embryonic stages and have to migrate toward the gonad

formation. This phenomena can be found in many animals and has been investigated in several model systems over the last years. The model genetic organisms are *Drosophila melanogaster*, zebrafish, *Xenopus laevis* and mice (Terayama et al., 2013, Richardson and Lehmann, 2010). The biological process itself provides a useful model system to study the cellular locomotion in the context of development. The migration path for PGCs goes through various developing tissues, therefore, it requires precise regulation. With the understanding of PGC migration a conceptual framework for the investigation of other migrating cell types can build up (Richardson and Lehmann, 2010).

As the migration of PGCs goes through different types of tissue and over long distances they are assumed to exhibit not only a high motility but also a highly dynamic migratory mechanism. In response to this requirements they reveal different migration stages as the initiation of migration, directional movement and completion at destination (Terayama et al., 2013).

In the following chapter focus lies on the migration of PGC from the organism *Xenopus laevis*.

In the initiation phase, the PGC must become motile and start to migrate. In *Xenopus* the separation process from the PGC cluster and cell elongation start at stage 28 in the endoderm. At stage 33/34 the scattered cells already migrate towards the dorsal side. Here, they reveal the stage of directional movement. The PGCs reaches the completion at destination at stage 41, where more than half of the PGCs form clusters in the most dorsal region of the endoderm. The *Xenopus* PGC locomotion is guided by the ROCK/RhoA signaling pathway (Terayama et al., 2013). To fulfill the different migration stages during their active migration the PGCs change their morphology from round cells with small blebs, over an elongated cell shape to rugged PGCs and then back to round cells. The elongated shape accompanies the locomotive phase to move in the longitudinal direction with the help of large membrane blebs at the leading front. The bleb formation for the locomotive phase is associated with actin polymerization and myosin-based contractions. The rugged PGCs exhibit several bleb-like protrusions but show no clear locomotion and occur in the so called pause phase. It could be observed that the PGCs uses these two morphologies of elongated and rugged cells to alternate between the locomotive phase and the pause

phase. Before and after the entire migration process the cells exhibit an indistinguishable spherical round morphology. This morphology is similar to somatic endodermal cells. Somatic cells surrounding the PGCs, don't undergo the active migration during the embryogenesis and can serve as a reference against PGCs (Terayama et al., 2013, Dzementsei and Pieler, 2014).

In zebrafish it was revealed that apart from increased formation of cellular protrusions also differences in the expression and stability of adhesion molecules caused the migratory behavior. A special role was found for the epithelial E-cadherin (Richardson and Lehmann, 2010, Kardash et al., 2010). During the locomotion process of the PGCs the level of E-cadherin expression is down-regulated in order to induce a fast turnover of adhesion contacts. Despite that, E-cadherin also mediates the formation of contacts on neighboring somatic cells to generate traction force for the cellular movement (Kardash et al., 2010, Goudarzi et al., 2012).

If E-cadherin also plays a significant role in the process of the active migration of PGCs from *Xenopus laevis* has to be clarified. In this work the role of E-cadherin in the context of active migration and adhesion in early embryonic stage of primordial germ cell (PGCs) of *Xenopus laevis* is analyzed. The study of Dzementsei et al., already indicated that E-cadherin is also down regulated in response to the migration by qPCR analysis from isolated PGCs (Dzementsei et al., 2013). This work proofs if the PGCs really exhibit a reduced E-cadherin expression through migration.

2.2 Epithelial-mesenchymal transition

Epithelial-mesenchymal transition (EMT) is a biological process where polarized epithelial cells undergo multiple biochemical changes to transform into a mesenchymal phenotype, either fully or partially (Lamouille et al., 2014, Kalluri and Weinberg, 2009). This transition results an increase in migratory capacity, invasiveness and resistance to apoptosis (Kalluri and Weinberg, 2009). EMT occurs in embryogenesis, tissue regeneration and wound healing but also in fibrosis or cancer progression (Kalluri and Weinberg, 2009, Son and Moon, 2010, Lamouille et al., 2014).

This process can also happen the other way around where mesenchymal cells convert to epithelial derivatives. This is called mesenchymal-epithelial transition (MET) (Kalluri and Weinberg, 2009). The difference of an epithelial versus a mesenchymal state is not very distinct and a partial EMT/MET can also occur. The enormous flexibility of the assumedly differentiated cells during morphogenesis is shown by their transition dynamics (Tsai and Yang, 2013).

For initiation of the EMT a distinct number of molecular processes are involved and are essential for the transformation. These processes are expression of specific cell-surface proteins, reorganization and expression of cytoskeletal proteins, activation of transcription factors, changes in expression of specific microRNAs and production of ECM-degrading enzymes (Kalluri and Weinberg, 2009). Figure 2-1 shows the functional transition of polarized epithelial cells into mesenchymal cells. The cells change from epithelial phenotype over intermediate phenotypes to mesenchymal cells. They lose their cell contacts, polarized cell shape and epithelial markers like E-cadherin, ZO-1 or Laminin-1 and became elongated single cells with mesenchymal markers like N-cadherin, Vimentin.

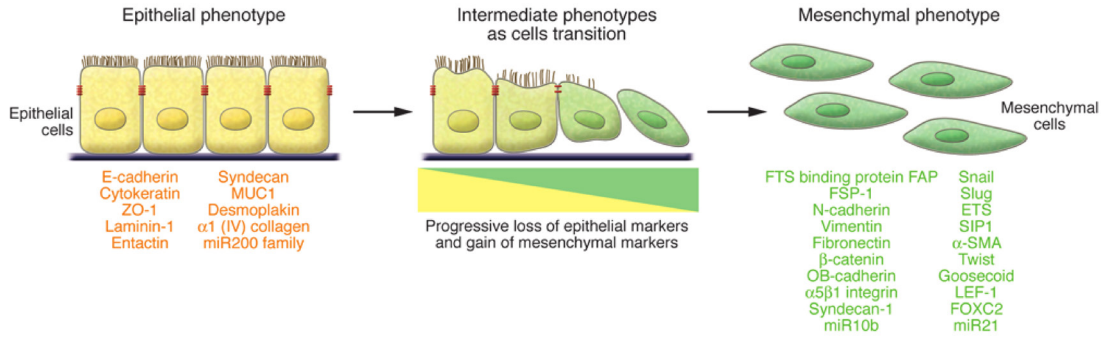

Figure 2-1 **Overview of EMT**. Functional transition from polarized epithelial cells to mesenchymal cells with the commonly used epithelial and mesenchymal cell markers (Kalluri and Weinberg, 2009).

The key characteristics in EMT for epithelial cells is the loss of cell junctions and apical-basal polarity, reorganization of their cytoskeletal architecture, change of cell shape and gene expression (Lamouille et al., 2014, Kalluri and Weinberg, 2009, Kalluri, 2009, Thiery et al., 2009, Thiery and Sleeman, 2006) which can also be seen in Figure 2-2.

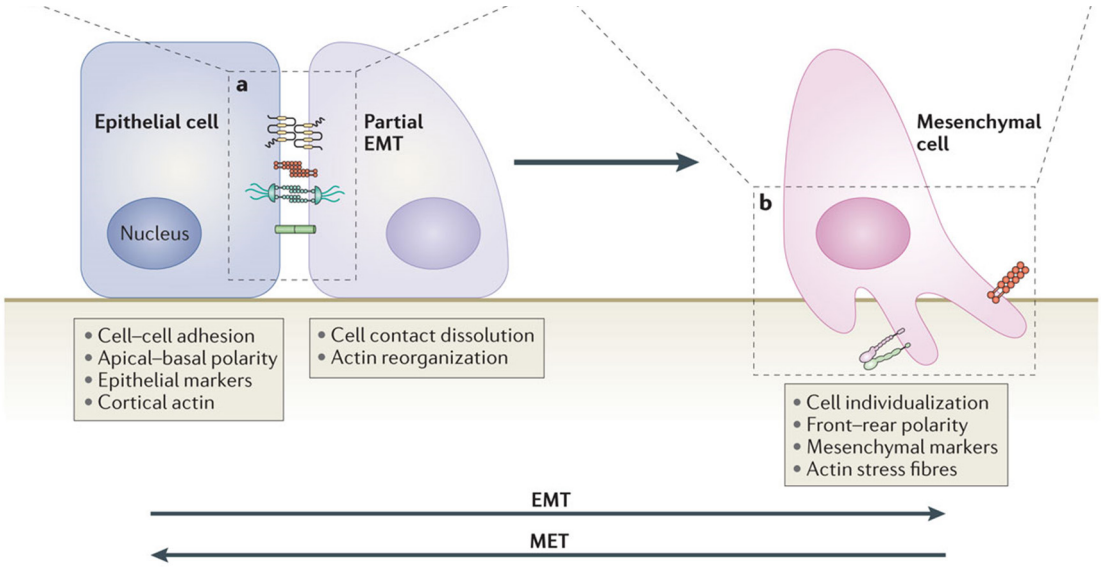

Figure 2-2 **Cellular processes during EMT.** a) The disassembly of epithelial cell-cell contacts in tight junctions, adherens junctions, desmosomes and gap junctions and the loss of cell polarity are the first steps of EMT. Additionally, the expression of epithelial genes is down regulated and simultaneously the expression of mesenchymal genes is activated. b) In the mesenchymal state the actin architecture is reorganized and the cells exhibit motility and invasive capacities (Lamouille et al., 2014).

EMT can be observed in three distinct biological settings which entail different functional consequences. First type of EMT is associated with embryogenesis, implantation and organ development. Here EMT generates diverse cell types that share a general mesenchymal phenotype and does not cause fibrosis or induce an invasive phenotype. The generated mesenchymal cells have a higher potential to subsequently undergo a MET to create secondary epithelia (Kalluri and Weinberg, 2009, Zeisberg and Neilson, 2009).

Tissue regeneration, wound healing and organ fibrosis are in conjunction with the second type of EMT. The repair-associated process normally recruit fibroblasts and other related cells which are responsible to reconstruct tissues following trauma and inflammatory injury. In the context of organ fibrosis the EMT can continue to respond to ongoing inflammation which can then cause organ destruction (Kalluri, 2009, Kalluri and Weinberg, 2009, Rastaldi et al., 2002).

Last type of EMT appears in carcinoma progression and metastasis. Carcinoma cells undergo EMT type 3 for the final stage of cancer progression to invade and metastasize. In response to this EMT the tumor cells facilitate reaching the malignant phase of tumor growth and the cancer cells are able to enter the circulation and exit the blood stream to form metastases (Tsai and Yang, 2013, Kalluri and Weinberg, 2009, Yilmaz and Christofori, 2009).

EMT can be induced in different ways. The well-known cytokine transforming growth factor-ß1 (TGF-ß1) is a major inducer of EMT. (Xie et al., 2003, Xu et al., 2009, Zhang et al., 2014). Besides TGF-ß1, the other two key signaling pathways which induce EMT are Wnt and Notch (Son and Moon, 2010).

This work goes into the matter of how the adhesion between cell and surface alter during the transition from epithelial to mesenchymal phenotype. Two hallmarks of the EMT are the down regulation of the epithelial marker E-cadherin and the reorganization of the F-actin. Both are key steps in EMT (Lamouille et al., 2014) and play an important role in the context of this work. Therefore, the next two chapters deal with the function and composition of these two candidates.

2.2.1 E-cadherin

Cadherins are one of the key cellular adhesion molecules that regulate and communicate many cellular processes like cell motility, cell signaling and also intercellular adhesion (Lekka et al., 2011, Gooding et al., 2004). They are a superfamily of calcium (Ca^{2+})-dependent homophilic cell-cell adhesion proteins, apart from some exceptions, which have an influence on morphogenesis, tissue repair and carcinogenesis (Oroz et al., 2011, Conacci-Sorrell et al., 2002).

Cadherin are calcium sensitive (Oroz et al., 2011) since mature cadherin interaction are disturbed upon depletion of Ca^{2+}. In the absence of calcium the cadherin ectodomain loses its rigidity and becomes a very flexible structure, which is hindered to form an explicit interaction (Haussinger et al., 2002, Oroz et al., 2011).

E-cadherin is one part of the cadherin family and is functionally linked to the epithelial tissue (Tian et al., 2011, Jeanes et al., 2008). It can be found at the intercellular adherens junctions. It is part of the classical cadherins, which are single pass transmembrane glycoproteins of 720-750 amino acids and exhibit both extracellular and cytoplasmic domains. The extracellular region (ectodomain or EC) is a rod-like structure existing of five autonomously folded domains with binding sites for calcium (EC_1-EC_5), which establish homophilic interactions in *cis* and *trans* position (Figure 2-3). Each interdomain region between the EC can bind three Ca^{2+} ions which leads to an entire capacity of 12 Ca^{2+} ions. The calcium binding has a marked effect on the conformation of the protein which was mentioned before (Lekka et al., 2011, Oroz et al., 2011).

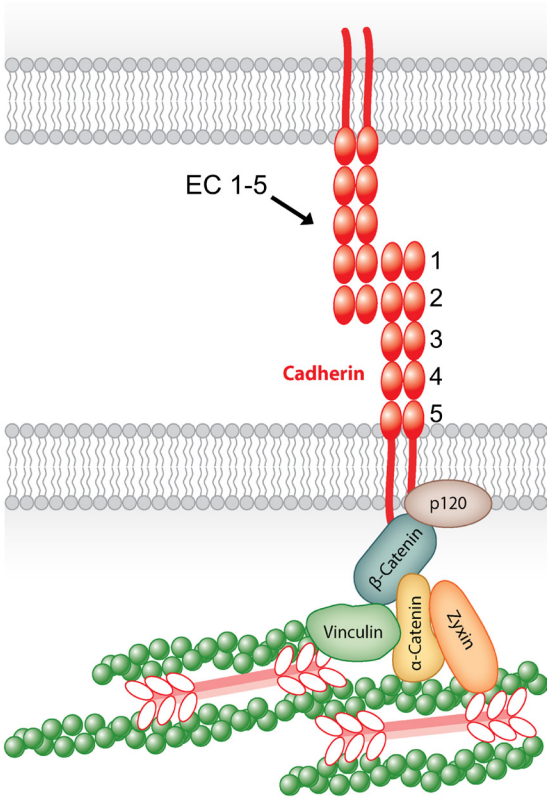

Figure 2-3 **Schematic depiction of classical cadherin junctions**. Classical cadherins, like E-cadherin, form adhesive contacts through the extracellular region. The main proteins which binds to the cytoplasmic region are *β*- and p120-catenin. *α*-catenin serves as a linker to bind directly to F-actin or indirectly to other actin-binding proteins like vinculin. Modified from (Leckband and de Rooij, 2014).

The intracellular region connects to the cytoskeleton network through several adaptor proteins. The most important proteins which are involved in the formation of cadherin complexes are *α*-, *β*-, *γ*- (plakoglobin) and p120-catenin (Tian et al., 2011, Ozawa and Kemler, 1998). P120 catenin binds to the juxtamembrane portion of the cytoplasmic region of cadherin and tunes cell cohesion by regulating cadherin abundance at the membrane (Niessen et al., 2011). *β*- or *γ*-catenin also directly associate to the cytoplasmic domain of E-cadherin. *α*-catenin serves as a dynamic linker between *β*-catenin and F-actin (Tian et al., 2011, Lekka et al., 2011, Bajpai et al., 2009) (Figure 2-3).

Apart from the cadherin structure the binding mechanism of cadherins are also a matter of debate. The original model states that lateral *cis*-dimerization of cadherin proteins has to occur first and that this functional unit form a *trans*-interaction with a corresponding dimer of an opposing cell (van Roy and Berx, 2008, Niessen et al., 2011, Shapiro et al., 1995). But over the last years another

model has become more favorable. Instead of forming *cis*-dimers, EC1-EC2 interdomains of two cadherins form a fast-binding X-dimer, which is an intermediate trans-contact and then promotes formation of more stable swapped *trans*-dimer. With this model lateral dimerization and clustering have a promoting effect by raising the probability of trans-dimer formation (Fichtner et al., 2014, Sivasankar, 2013, Hong et al., 2011, Leckband and de Rooij, 2014). The new favored model can be seen in Figure 2-4:

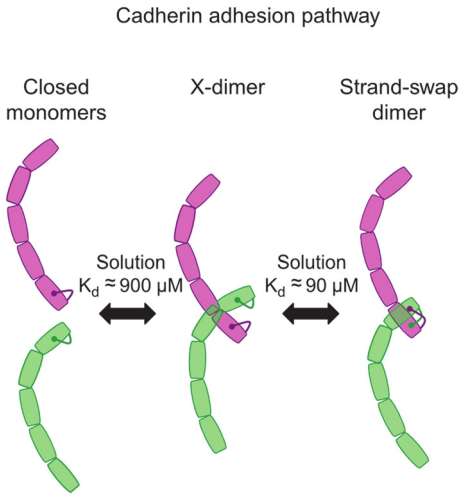

Figure 2-4 **Pathway for cadherin binding**. E-cadherin monomers from two opposing cells come into contact and form first a so called “X-dimer” and then proceed to swap residues and finally form a strand-swap dimer (Sivasankar, 2013).

2.2.2 Actin cytoskeleton

Actin filaments (F-actin) are part of the cytoskeleton which consist apart from F-actin also of intermediate filaments and microtubules. The main task for these three biopolymers is to provide the mechanical stability of the cell and maintain its shape. Actin filaments provide, together with microtubules, binding sites for ATP-powered motor proteins that cause most cellular movements, including muscle contraction, cellular locomotion, mitosis or transport of organelles through the cytoplasm. A network of cross-linked actin filaments, which is anchored to the plasma membrane, supports the surface of the cell. In contrast filopodia or microvilli are supported by tightly packed bundles of actin. These finger-like protrusions of the plasma membrane increase the surface area for transporting nutrients and other processes like cellular migration (Pollard et al., 2008).

Actin filaments are involved in the assembly of F-actin which results in some movements, like the extension of pseudopods. The force which is produced by the motor protein myosin by moving along actin filaments causes an alternative movement. F-actin with microtubules and intermediate filaments provide mechanical support for the cytoplasm that is increased by interactions between these biopolymers (Pollard et al., 2008).

Actin filaments are polarized, one end is called barbed end and the other is called pointed end. The subunits in actin filaments are in a helical arrangement and the polymerization is driven by a series of bimolecular reactions. The subunits are stabilized by hydrogen bonds, electrostatic bonds and hydrophobic interactions (Pollard et al., 2008). The starting point for filament growth are actin trimers because they have the advantage, compared to a dimer that they are more stable and can add further monomers rapidly. Also they form the smallest oligomer with a complete set of intermolecular bonds. During polymerization the polar filament exhibits different rates of association and dissociation at the two ends (Figure 2-5). In total, the filament moves forward and keeps the same length which is also called “treadmilling”. Therefore, the protrusive force of F-actin, which is thought to push the membrane to form a lamellipodium, is determined by the control of actin polymerization at the barbed end and depolymerization at the pointed end. During polymerization there is a critical concentration of actin monomers (Figure 2-5). Below this critical actin concentration the polymer shrinks (Pollard et al., 2008, Le Clainche and Carlier, 2008).

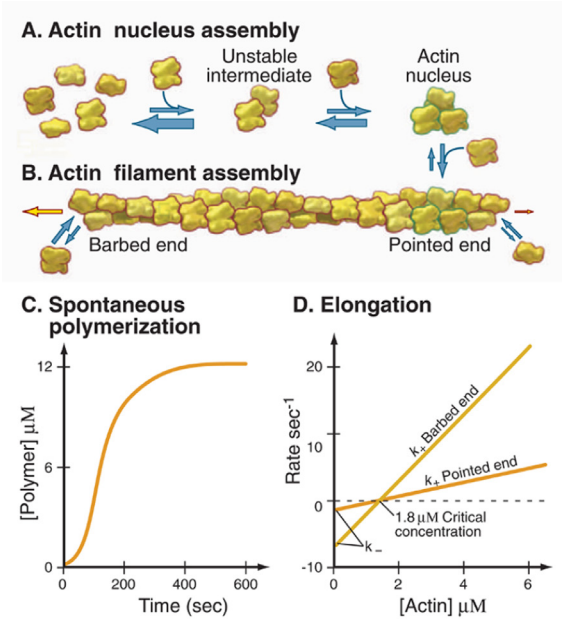

Figure 2-5 **Overview of actin filament polymerization.** A) Monomers build up a trimeric nucleus. B) Elongation of the nucleus at the two ends by association and dissociation of monomers. C) Time dependency of spontaneous polymerization of purified ADP-actin under physiological conditions. D) Different elongation rates of the two ends of a filament on the concentration of ADP-actin monomers (Pollard et al., 2008).

Polymerization itself is also dependent on the presence of ATP or ADP and divalent cations. Actin can polymerize in an ATP- as well as an ADP-bound state. But as actin hydrolyzes ATP upon polymerization, the critical concentration for ATP-actin is about 20 times lower than for ADP-actin. (Le Clainche and Carlier, 2008, Pollard et al., 2008).

Additionally, one form of appearance of F-actin has to be highlighted in this context. The so-called stress fibers play an important role in many cellular functions, like adhesion, motility or morphological stability. Stress fibers are bundles of actin filaments sheared by actin-myosin interactions and stably cross-linked by myosin light chain, *α*-actinin, tropomyosin and other proteins. Proteins like vinculin, paxilin, talin or zyxin connect each end of a ventral stress fiber to a focal adhesion. This allows to transmit the forces at the basal surface out of and into the cytoskeleton of the cell to interact with the surrounding extracellular matrix (ECM). This central role of stress fibers influences many cellular functions, such as adhesion, wound healing, shape stability or apoptosis and others (Lu et al., 2008, Deguchi et al., 2006).

2.2.3 Transforming growth factor-ß cytokine

Transforming growth factor beta (TGF-ß) is a well-known cytokine. Beside the activation of EMT, TGF-ß plays also an important role in a wide range of cellular processes like differentiation, cell growth, embryonic development, apoptosis and also cancer progression (Xie et al., 2003, Xu et al., 2009, Zhang et al., 2014).

TGF-ß is the prototype of a large family of more than 40 members of signaling molecules. It triggers type I receptor (TßRI) and type II receptor (TßRII) serine/threonine kinase receptors, Smad transcriptional regulators and also many other signaling pathways (Xie et al., 2003, Yue and Mulder, 2001, Son and Moon, 2010). Different types of TGF-ß can be found. In the context of EMT TGF-ß1 plays apart from TGF-ß2 and TGF-ß3 a major role. The signaling of TGF-ß1 induces EMT in cancer, wound healing and fibrosis (Lamouille et al., 2014).

In tumorigenesis TGF-ß plays an important but also complex role. The most studied TGF-ß response is growth inhibition but in many epithelial originate tumors the cells become resistant against this inhibition and exhibit the EMT to increase tumor invasion and metastasis (Xie et al., 2003, Lamouille et al., 2014).

The main regulatory network for inducing EMT is composed of two transcription factors (*SNAIL1*; *ZEB1*), TGF-ß and two families of microRNAs (*miR-34*; *miR-200*) (Zhang et al., 2014). Several feedback loops exist in this core network to modulate EMT. A schematic illustration of this regulatory network can be found in Figure 2-6.

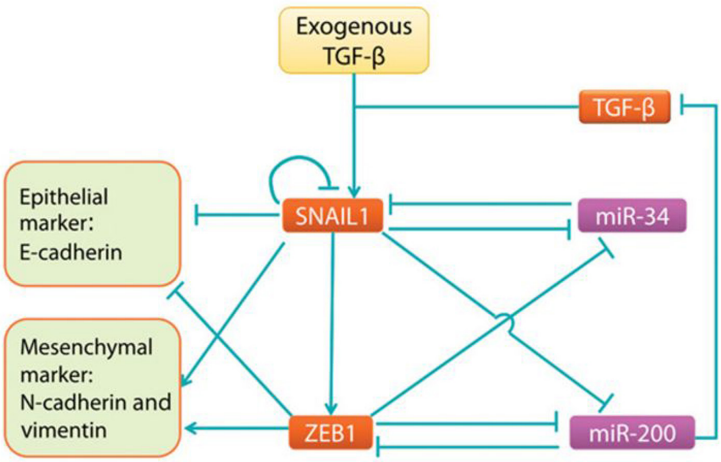

Figure 2-6 **Schematic illustration of the core regulatory network of TGF-ß induced EMT** (Zhang et al., 2014)**.**

The schematic of the network in Figure 2-6 (Zhang et al., 2014) reveals how the TGF-ß induced EMT is regulated. The exogenous TGF-ß induces *SNAIL1* expression. *SNAIL1* stimulates the expression of *ZEB1* and promotes the mesenchymal markers N-cadherin and vimentin. Additionally it participate in a double-negative feedback loop with *miR-34* and inhibits the expression of *miR-200* over *ZEB1* and also inhibits its own expression. The autocrine production of TGF-ß is hindered by *miR-200*. *MiR-200* also exhibit another similar double-negative feedback loop with *ZEB1*. Apart from this *SNAIL1* and *ZEB1* also inhibit the expression of the epithelial cell marker E-cadherin and induce the expression of mesenchymal markers like N-cadherin. The entire EMT is driven by this core regulation network (Zhang et al., 2014, Gregory et al., 2011, Siemens et al., 2011, Wellner et al., 2009, Nieto, 2002).

2.3 Role of extracellular matrix in cellular behavior

The Extracellular matrix (ECM) is a large collection of different components including proteins, polysaccharides, glycoproteins and proteoglycans with different biochemical and physical characteristics. For the ECM we distinguish between basement membrane and interstitial matrix. The basement membrane separates epithelium or endothelium from stroma and is produced by epithelial, endothelial and stromal cells. This specialized ECM appears less porous and more compact compared to the interstitial matrix. The basement membrane contains collagen type IV, fibronectin, laminin and linker proteins like nidogen and entactin which link collagens with other protein components. In contrast, the interstitial matrix is rich in proteoglycans, fibrillar collagens and various glycoproteins such as fibronectin. This fact makes the matrix highly charged, hydrated and accounts greatly for the tensile strength of tissues (Lu et al., 2012, Egeblad et al., 2010).

ECM regulates almost all cellular behavior and is essential for main developmental processes (Wiseman et al., 2003, Stickens et al., 2004, Lu et al., 2011). Apart from normal development it also has a strong influence in the context of different diseases.

In cancer development for example the surrounding microenvironment of a cancer cell plays an important role. One main component of this microenvironment is the extracellular matrix (ECM), which consist of a complex network of macromolecules with distinct biochemical, biomechanical and physical properties (Lu et al., 2012, Pupa et al., 2002, Bosman and Stamenkovic, 2003).

The ECM components exhibit unique biochemical, physical and biomechanical properties, which are essential for regulating cell behavior. The review of Pengfei Lu et al. illustrates nicely the important functions of the ECM for cells (Figure 2-7).

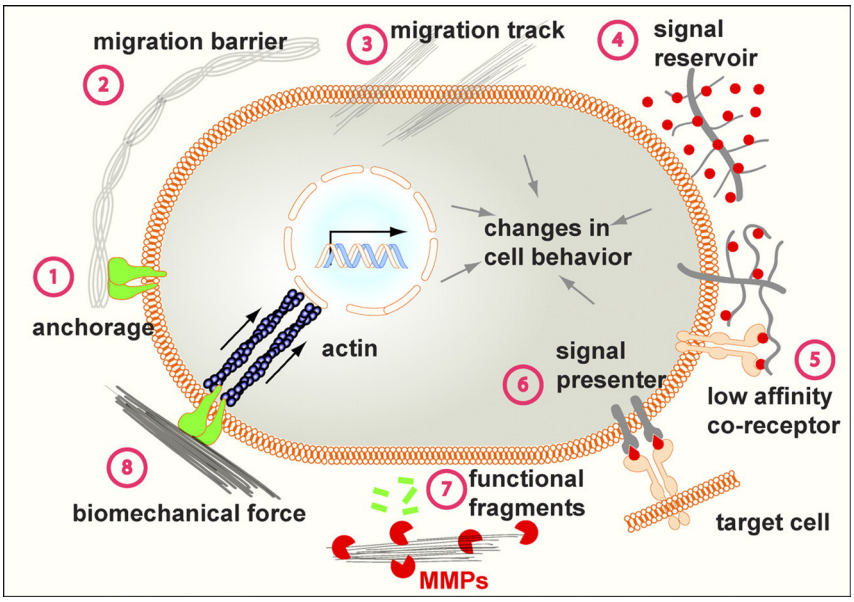

Figure 2-7 **Different functions of the ECM;** Anchorage to the basement membrane for e.g. maintenance of tissue polarity (1); Migration barrier to block cell migration (2); Migration track for support cell migration (3); Signal reservoir by binding growth factor signaling molecules for maintain concentration gradient (4). Signal coreceptor over the bonded growth factors (5) or as a presenter (6) Direct communication to the cell by functional fragments, which are processed by proteases like MMPs (7); Direct binding to sense the biomechanical properties of the ECM like stiffness (8) (Lu et al., 2012)**.**

ECM is responsible for various biological processes, like maintenance of tissue polarity or asymmetric cell division in stem cell biology where the anchorage to the basement membrane is essential (1). Physical properties and functions of the ECM influence the role in cell migration negatively as well as positively (2, 3). The ability of the ECM to bind growth factor signaling molecules leads the ECM to establish a concentration gradient (4). Apart from this, certain parts of the ECM can serve as a single coreceptor (5) or as a presenter (6). The ECM can also transmit signals directly to the cell by using for example matrix metalloprotease (MMP) (7). Last possible interaction with the ECM is that the cell directly sense the biomechanical properties of the ECM, like its stiffness and subsequently changes its behaviors (8).

Since the ECM and its function plays an important role in a wide range of cellular processes it is only logical that the abnormal deregulation of ECM dynamics reveals a hallmark of cancer (Lu et al., 2012). In diseases, such as cancer, the ECM gets deregulated and becomes disorganized compared to embryonic development and organ homeostasis, where the ECM is highly controlled. With its key role it can directly affect cancer progression through promoting cellular

transformation, invasiveness and metastasis (Lu et al., 2012, Marastoni et al., 2008). But in contrast it can also impair cell viability through individual ECM molecules and could be a putative tool for cancer therapy (Marastoni et al., 2008).

Abnormal changes in the composition and amount of the ECM can dramatically alter biochemical properties of the ECM and rise the oncogenic effects of various growth factor signaling pathways and negatively influence cell behaviors during malignant transformation. Also changes in the biochemical properties of ECM occur in the context of disease conditions. For example the typical tumor stroma is stiffer than normal one (Lu et al., 2012).

Looking on the biochemical properties of the ECM, the data (Lu et al., 2012, Lu et al., 2011, Marastoni et al., 2008) illustrated that abnormal regulation of ECM stiffness and also deregulation of collagen cross-linking play a grave role in cancer pathogenesis and are more than just a side effect.

In this context this work concentrates on the stiffness of the ECM. Do the mechanical forces, which are exerted from the ECM itself to the cell, have the ability to influence cell functions like induction of signal cascades to enhance the invasive potential, migration and also the tumor progression itself? Does different rigidity in ECM have a strong impact on migratory behavior of the cancer cell or on metastasis? For this approach the cell surface receptors like the family of receptor tyrosine kinases (RTKs) play a supporting role.

2.3.1 Discoidin domain receptor 2

The transmission of signals from ECM proteins through the plasma membrane into the cell is regulated by surface receptors which bind to ECM proteins. The family of receptor tyrosine kinases (RTKs) provides many types of these receptors. One subfamily of the RTKs are the Discoidin Domain Receptors (DDRs).

The two main candidates are DDR1 and DDR2. In solid tissues DDR1 is expressed in epithelial cells, DDR2 in mesenchymal cells. Both have the ability to bind fibrillary as well as non-fibrillary collagens. In this chapter only DDR2 is discussed.

DDR2 shows a functional relevance for reconstruction of the ECM since it is expressed for example in the stroma of fibroblast and activates MMP (Labrador et al., 2001, Vogel et al., 2006). DDR2 is activated by binding of fibrillary collagens like collagen type I and type III (Vogel et al., 2006, Shrivastava et al., 1997) and has only one isoform. In the cellular membrane DDR2 exists as dimers to build up a ligand independent manner by interactions mediated in response to their transmembrane domains. The receptor activation occurs by the interaction of collagen with the pre-formed DDR dimers which results in dimer oligomerization and conformational changes (Borza and Pozzi, 2014).

The initiating signaling pathways from DDRs are in a context and cell type-dependent manner. DDR2 for example could be shown to promote EMT. DDR2 expression is increased during the EMT in MDCK cells. The cytokine transforming growth factor-ß (TGF-ß), which is commonly used to induce EMT, also promotes DDR2 expression. Additionally, the EMT driver *SNAIL1* reveals a higher stability by collagen I-mediated DDR2 activation. This activation also benefits breast cancer cell invasion in vitro and also raises metastasis in vivo (Borza and Pozzi, 2014, Maeyama et al., 2008, Walsh et al., 2011, Zhang et al., 2013).

It could be shown that apart from mediating direct collagen-dependent signaling, DDRs are also capable to modulate signaling pathways by transmembrane receptors (e.g. insulin receptor), cytokines (e.g. TGF-ß) and other matrix receptors like integrins (Borza and Pozzi, 2014).

Knock out of DDR2 in mice reveals a reduced bone growth during development due to reduced chondrocyte proliferation. Additionally, the healing of epidermal wounds is significantly delayed. Fibroblasts in DDR2 knock out mice are unable to migrate through a reconstituted basement membrane and also reveal reduced MMP2 activity which is a key feature of defective wounding response and causes the delay of healing (Olaso et al., 2011b, Vogel et al., 2006, Borza and Pozzi, 2014).

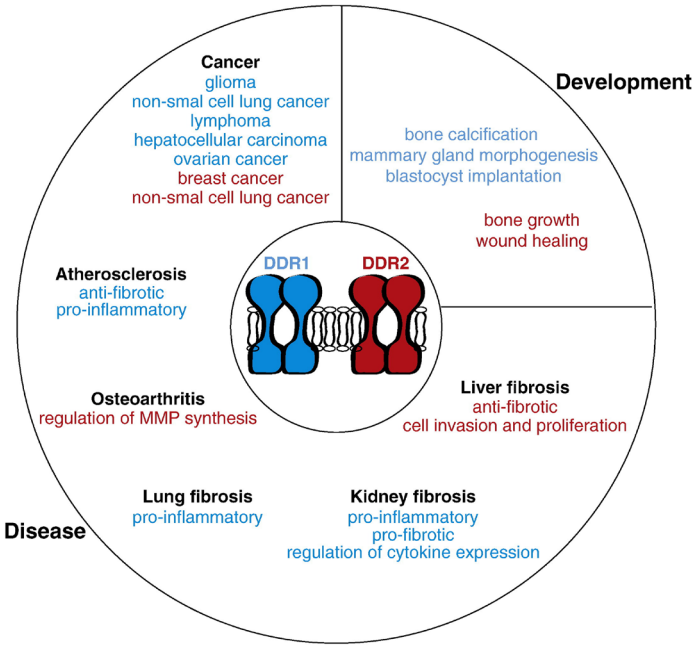

Figure 2-8 **Influence of DDR**; DDR expression and/or activation has an influence in physiological (e.g. development) and pathological (e.g. cancer, fibrosis) conditions by controlling key cellular processes (Borza and Pozzi, 2014).

Apart from embryonic development DDRs have been linked to a number of diverse diseases like cancer or lung and liver fibrosis. Figure 2-8 illustrates the impact of DDR expression or activation on different diseases or on development. As DDRs are associated with a wide range of key cellular processes like cytokine secretion, matrix production, cell migration or protease production, they have a potential importance in human health and disease and could serve as a target for therapeutic interventions (Vogel et al., 2006, Borza and Pozzi, 2014).

In this work the function of DDR2 on ECM in mice is investigated. Does the knockout of DDR2 apart from increased collagen deposition also change the stiffness of mice skin? If this is the case, the DDR2-deficient mice could be used as a model for the analysis of tumor progression in ECM of different stiffnesses.

3 Materials and methods

Detailed Information about the used chemicals and devices can be found in chapter **9** (*p.* 151).

3.1 Atomic force microscopy

The atomic force microscopy (AFM) is a member of scanning probe microscopes invented in the 1980s by Binnig, Quate and Gerber (Binnig et al., 1986). It is one follower of the scanning tunneling microscope (STM) which was also invented by Binning and Rohrer (Binnig and Rohrer, 1983).

AFM has become the most important scanning probe microscope and allows the imaging of samples in subnanometer resolution. Apart from imaging the AFM is also a sensitive force measuring device which can detect or exert forces down to the piconewton range (Janshoff et al., 2000, Butt et al., 2005). The advantage of AFM is the possibility to investigate samples with little or no modification under physiologically-relevant conditions which make it eligible for investigating biological samples, including living cells or tissues (Franz and Puech, 2008, Fotiadis et al., 2002).

3.1.1 Setup

The AFM uses a tip which is attached to a flexible cantilever to sensor the interaction with the sample. To detect these interactions the AFM uses an infrared laser to measure the deflection of the cantilever when the tip is moved toward and away from the surface. The laser is reflected at the back of the cantilever and guided to a four-quadrant photodiode which serves as a detector that measures the laser spot position in two directions (Figure 3-1).

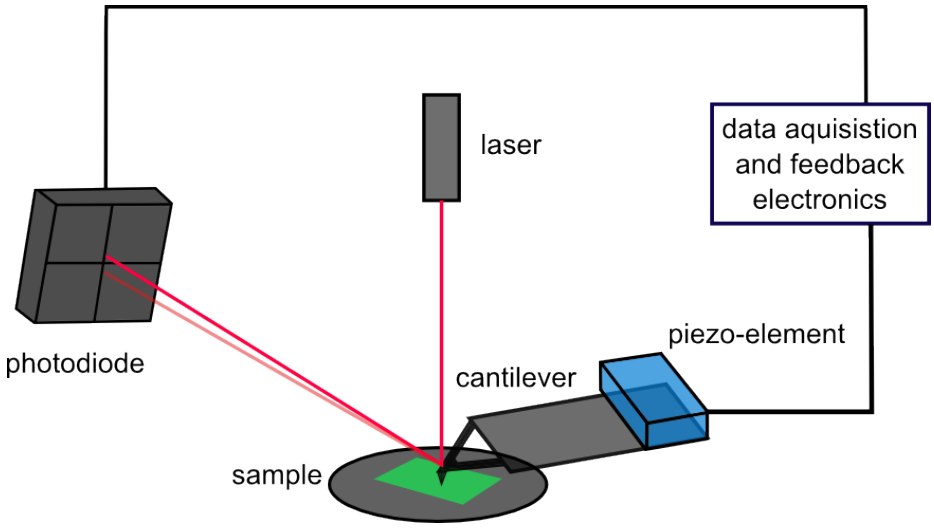

Figure 3-1 **Schematic of an atomic force microscope (AFM)**.

For the sample movement in x-, y- and the cantilever in z-direction the AFM uses a piezo element. Piezo elements have the effect that they generate an electric charge proportional to an applied mechanical stress. On the other way around they become strained proportional to an applied electric field. This is known as the direct and inverse piezoelectric effect, respectively (Holterman and Groen, 2013). With the piezo element the cantilever can be positioned in a precision of a few nanometers.

The heart of the AFM is the cantilever with his tip, which is brought in contact with the sample. It is a small micro-precision-machined triangular or rectangular piece of silicon nitride or silicon. The AFM device measures the deflection of the cantilever as it comes in contact with the sample and built up from this information a three-dimensional image of the sample. Typically the tip is a few microns long, and shaped like a cone or pyramid but also a sphere with different diameters are possible for a cantilever tip. Cantilevers have a characteristic spring constant. The spring constants of the commercially available cantilevers vary over four orders of magnitude (JPK_Instruments, 2015).

Hooke's Law described that the force applied to the sample is proportional to the deflection of the cantilever:

$$F = -k_c * x \qquad (3\text{-}1)$$

With the force F, the spring constant k_c of the cantilever and the deflection x. The spring constant depends on the dimensions of the cantilver and the material it is made of. For force measurements with an AFM the spring constant has to be determined. The calculation of the spring constant can be done by different methods. The most common method, which is also used here, is the thermal noise method (Butt et al., 2005, Hutter and Bechhoefer, 1993).

In brief, first the cantilever is brought into contact with a hard substrate to determine only the deflection of the cantilever. With this step the distance of the actually cantilever defelction is calibrated for a certain measured change in photodetector voltage. The generated force curve is used to determine the sensivity of the setup. The factor for converting Volts into nanometer is gained out of the linear slope of the contact part of the generated force curve. Afterwards the spring constant is calculated from the thermal noise spectrum of the cantilever defelction by integration over the first resonance peak. By knowing the spring constant the four-quadrant photodiode signal can easily be converted into a force as described in Hooke's law (3-1) (Butt et al., 2005, JPK_Instruments, 2015).

3.1.2 Force spectroscopy

AFM is a well-known tool to sense or exert forces between tip und sample. It can detect a wide range of forces, from several tens to hundreds of piconewtons (Puchner and Gaub, 2009). With AFM it is possible to determine and quantify inter- and intramolecular forces (Lee et al., 2007).

The vertical deflection of the cantilever vs the height position for the approach/trace (red) or retract/retrace (blue) of the cantilever is plotted in so called "force distance" curves (Figure 3-2). The gap between the baseline of trace and retrace curve is caused by hydrodynamic effects, which occur when the cantilever is moved through a liquid. Depending on the analyzed force distance curve this effects were corrected by setting the baseline of the trace or retrace curve respectively at the level zero. With this step the hydrodynamic effects were rectified.

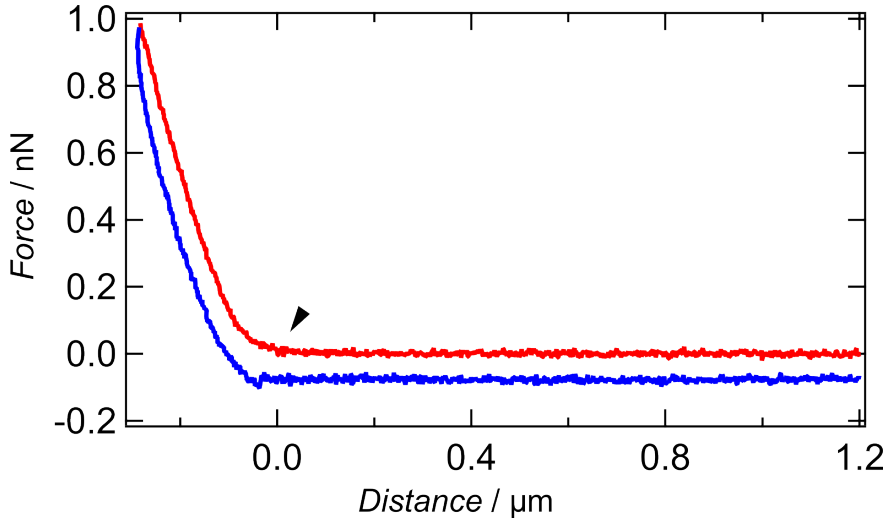

Figure 3-2 **Typical force distance curve** after correcting the height for cantilever bending (tip sample separation) with trace (red) and retrace (blue) curve. Contact point marked by black arrow. (Set point 1 nN; velocity 3 µm/s).

The force distance curve in Figure 3-2 shows that after the first contact point the force on the tip increases. After reaching the force setpoint the cantilever is retracting again from the surface. In this retraction many different adhesion events can be observed (see section 3.2; *p.* 33).

From the trace curve we can gain the information how deep the cantilever tip penetrates into the sample. The so-called indentation depth δ is defined as the subtraction of the measured cantilever deflection (*d*) from the z-piezo extension (*z*) (Jiao and Schaffer, 2004):

$$\delta = (z - z_0) - (d - d_0) \qquad (3\text{-}2)$$

z_0 is the position of the *z*-piezo where the tip first comes into contact with the sample surface.

With this indentation depth it is possible to calculate elastic properties of the sample from the measured force indentation curve. To fit the curves different contact mechanical models are used (Butt et al., 2005, Sneddon, 1965) which provide the elastic Young's modulus *E*.

The two most common used mechanical models are the Hertzian model (3-3) and the Sneddon model (3-4). The Hertzian model is valid for a cantilever with a spherical indenter on a flat surface and is described as (Hertz, 1881, Johnson, 1985):

$$F = \frac{4}{3}\frac{E}{(1-\nu^2)}\sqrt{R_{\text{tip}}}\,\delta^{\frac{3}{2}} \tag{3-3}$$

With the radius of the tip (R_{tip}) and ν for the Poisson's ratio of the sample. For a conical indenter the Sneddon model is used (Sneddon, 1965, Jiao and Schaffer, 2004) with the opening half-angle α of the cone:

$$F = \frac{2}{\pi}\frac{E}{(1-\nu^2)}\tan(\alpha)\delta^2 \tag{3-4}$$

3.1.3 Experimental procedure

Force spectroscopy measurements were carried out for chapter **4.3** (*p.* 105).

3.1.3.1 Preparation

Skin samples of DDR 2 deficient and wild type mice (C57BL/6) were prepared by the working group of Dr. Missbach-Güntner (Göttingen University Medical School, Dept. of Diagnostic and Interventional Radiology). After preparation, the 30 µm thick native skin cross sections which were glued on microscope glass slides (76x26x1mm^3) are stored at -80 °C. For force measurements the samples were thawed and moisten with PBS^{--} (without Ca^{2+} and Mg^{2+} denoted as PBS^{--}). All measurements were performed using a NanoWizard II™ AFM (JPK Instruments) mounted on top of an Olympus IX81 microscope or a MFP-3D™ (Asylum Research) setup also on top of on an inverted Olympus IX51 microscope. Force-indentation curves were recorded at room temperature using cantilevers with a sphere attached on the tip ((CP-PNPL-SiO-A, sQube)

(diameter: 2 µm) and CP-PNPL-Au-C-8 (diameter: 5.5 µm)) and a nominal spring constant of 0.08 N/m. The cantilever spring constant was determined before each measurement as described in section 3.1.1 (*p.* 25).

3.1.3.2 Settings and parameters

For calibrating the cantilever following parameters were used:

	Set point	**Velocity**	**Contact time**	**Sample rate**
NanoWizard II	0.5 V	1 µm/s	0 s	2.48 kHz
MFP-3D	1 V	3 µm/s	0 s	2 kHz

Table 3-1 Parameters for calibrating the cantilever at AFM force measurements

The indentation experiments were carried out by taking force maps on different spots of the skin samples. At least three different mouse skin probes were investigated per category. Following parameters were used:

	Set point	**Velocity**	**Sample rate**	**Force map**	
				Size	**Points**
NanoWizard II	1 nN	3 µm/s	2.48 kHz	50 x 50 µm^2	20 x 20
MFP-3D	1 nN	3 µm/s	2 kHz	50 x 50 µm^2	20 x 20

Table 3-2 Parameters for AFM force measurements

3.1.3.3 Analysis of data

For the analysis of the force maps a home-made Matlab script was used. The force curves which were obtained from the Nano Wizard II first to be processed first with the JPK Data Processing software. Here the force map was split into separate force files and each force distance curve was treated with the same working steps through a batch process.

Following steps were done:

1) Baseline of the curve was corrected by adding an offset and subtract a linear fit
2) Contact point was set
3) Tip-sample separation was generated by correcting the height for cantilever bending. Here the unsmoothed height was selected.

After executing these steps each force distance curve was saved as a text file (.txt) to be analyzed with the home-made Matlab script.

The matlab script (provided by Dr. Ingo Mey; Georg-August-University, Institute for Organic and Biomolecular Chemistry, Göttingen, Germany) calculates the Young's modulus *E* from the trace of the force distance curves by fitting the slope with the Hertz Model (3-3). The Poisson ratio of for the skin sample was assumed to be $\nu = 0.5$ for a soft, incompressible material (Boudou et al., 2006, Soofi et al., 2009, Radmacher, 1997) and a radius of $R_{tip} = 1$ µm or 2.75 µm (dependent on the used cantilever) was used. Only force distance curves, which were evaluable and where the Hertzian fit was applicable the Young's modulus *E* were taken.

The results were illustrated with the software IGOR. The criteria for the used box-whisker-plots: line denotes the median of the distribution, boxes comprise the 25^{th} and 75^{th} percentile, whisker tops and bottoms are drawn to the 10^{th} and 90^{th} percentiles, respectively.

3.2 Single cell force spectroscopy

Single cell force spectroscopy (SCFS) is a modified version of atomic force spectroscopy and is used to quantify cellular adhesion. SCFS uses the combination of AFM and optical microscopy to investigate cellular interactions between a cell, which is attached to a cantilever, and a functionalized surface, tissue or an another cell (Helenius et al., 2008, Benoit et al., 2000). This method is one of three types of single-cell force spectroscopy assays. It allows to reach the widest practical force range from 10 pN to 10^6 pN (Helenius et al., 2008). Alternative to the AFM based SCFS is the micropipette assay to grasp and hold cells, which is also the oldest method (Evans et al., 1995). The third alternative is to use a laser trap to determine the strength of interactions between the cell, which is hold by a pipette, and a functionalized bead (Litvinov et al., 2002).

By using the SCFS with an AFM the occurring forces are measured by the deflection of the cantilever. Here, we also have the advantage to measure living single cells under nearly physiological conditions and also to characterize the interaction between single molecules. Therefore, it is possible not only to investigate overall cellular adhesion but also forces from single recpetor and ligand interactions (Helenius et al., 2008).

3.2.1 Setup and procedure

For the SCFS an atomic force microscope is used to fix a cell on a functionalized cantilever and investigate the interaction with the underlying surface or other cells with a certain set force, velocity and contact time. Therefore, suspended cells were seeded on petri dishes and allowed to settle. Afterwards the functionalized tipless cantilever is pressed onto a cell for a defined time, set point and after retraction of the cantilever it sticks to the cantilever Figure 3-3.

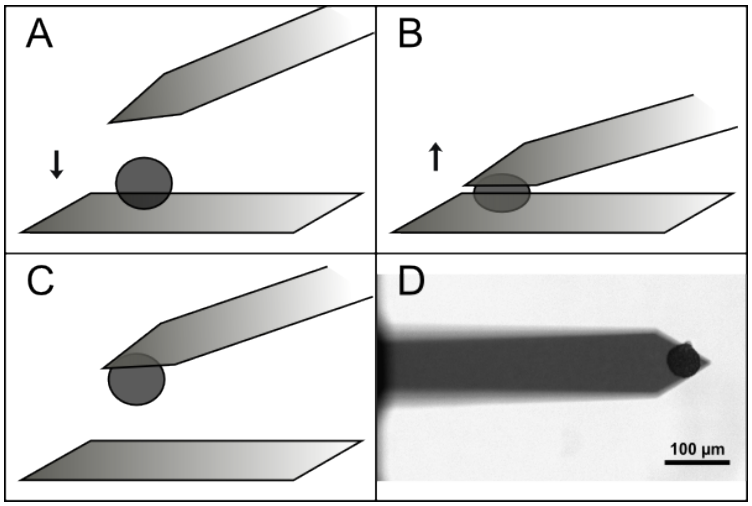

Figure 3-3 **SCFS cycle**: Functionalized cantilever is moved to the settled cell (A), pressed onto the cell with a certain force (B) and retracted again with the picked cell (C). Example for bright-field image of a picked somatic endodermal cell (*Xenopus laevis*) (D).

After picking the cell the interaction to the surface or other cells can be investigated. The occurring interactions are recorded by the deflection of the cantilever in the so called force distance curve (Figure 3-4). This curve gives an insight of the cell adhesion, where both specific and nonspecific adhesion processes are included. For analysis of the interaction forces the retrace curve is used. The approach curve displays the elastic response of the cell and can also be used for analysis, e.g. to determine the cortical tension of cells by fitting the slope of the curve since the deformation of the cell and substrate is recorded during contact (Friedrichs et al., 2013).

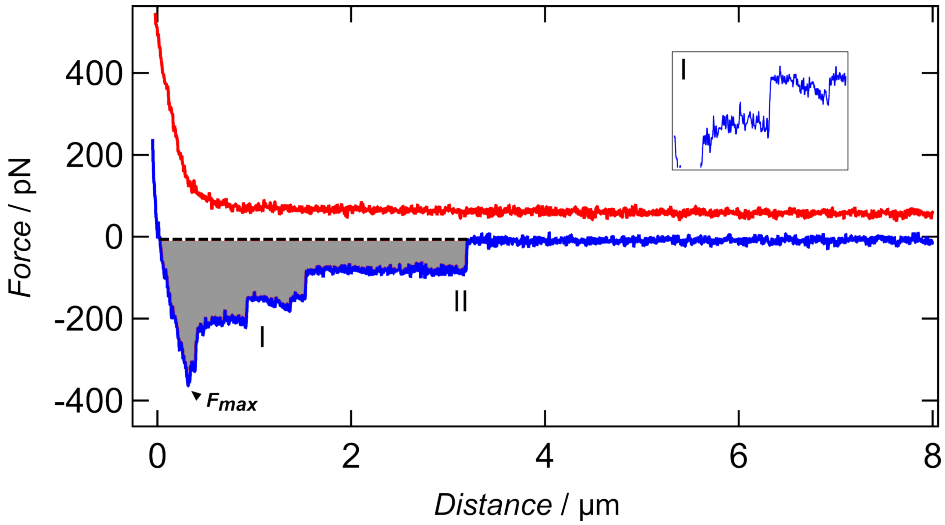

Figure 3-4 **Typical force distance curve** recorded with SCFS setup. Trace (red) and retrace (blue) curve with maximum adhesion force (F_{max}); work of adhesion (area between dashed line and retrace); single rupture events (I) and tether (II). (Set point 0.5 nN; velocity 5 µm/s; contact time 10 s)

Figure 3-4 shows a typical force distance curve recorded upon retraction of the cell from another cell displaying all relevant features that are usually observed. One important parameter is the maximum adhesion force (F_{max}) which is the largest adhesion force and represents the maximum strength of cell-cell or cell-substrate binding (Helenius et al., 2008, Friedrichs et al., 2013). It is dependent on many different properties of the cell, including tension from the cortex, cell elasticity, properties of the membrane, and receptor properties such as cooperativity and binding strength (Bershadsky et al., 2006, Puech et al., 2006).

During the retraction at larger distance from the surface, individual force steps can be observed. These force steps are originate either from cell receptors which are detached from the substrate (jumps (I)) or membrane tethers (plateau-like rupture (II)), which are pulled from the cell and also detach from the substrate if the lifetime of the bonds is exceeded.

For the rupture events where the cell receptors are detached from the substrate, the adhesive units (individual or small aggregates of receptors) are still connected to the cell cortex. They occur as jumps for single-molecule rupture events in the retrace curve (event I in Figure 3-4) (Taubenberger et al., 2007, Friedrichs et al., 2013). Tethers are membrane nanotubes which are formed due to applied force when the linkage between the cell receptor and the actomyosin cortex breaks.

Afterwards the receptor with the membrane is pulled from the cell surface due to the retraction of the cantilever until the bond breaks (Friedrichs et al., 2013, Benoit and Selhuber-Unkel, 2011). In force distance curves tether can be seen as plateaus of constant force followed by a step-like rupture force (see Figure 3-4; II). For a membrane tether the lipid composition of the cellular membrane and the mechanical properties of the cell cortex influence the force that is needed to exert a tether (Marcus et al., 2004, Evans and Calderwood, 2007, Helenius et al., 2008). After generating a tether, the force is largely independent from the tether length (Hochmuth et al., 1996, Benoit and Selhuber-Unkel, 2011).

Additionally, it is possible to calculate the work of adhesion from the force distance curve. It describes the energy dissipated during the detachment of the cell by integrating the area of the detachment of the retrace curve (indicated between dashed line and retrace Figure 3-4) and also serves to characterize the overall adhesion of the cell (Friedrichs et al., 2013).

After full retraction of the cantilever the cell is hold back for a certain amount of time for regeneration and is then brought back into contact to measure again the occurring interaction with the surface or cell. The retraction distances for a clear separation of cells in cell-cell experiments can be up to 100 µm (Puech et al., 2006, Friedrichs et al., 2013).

3.2.2 Experimental procedure

Single cell force spectroscopy measurements were carried out for chapter **4.1** (*p.* 67).

Some parts of this chapter has been published in Baronsky T, Dzementsei A, Oelkers M, Melchert J, Pieler T and Janshoff A, *Integr. Biol.,* **2016,** 8**,** 349-58; DOI: 10.1039/c5ib00291e.

For the actual measurement of the cellular adhesion between primordial germ cells (PGCs) and E-cadherin functionalized gold surfaces some preparation has to be done in the first place.

3.2.2.1 E-cadherin functionalization of gold surfaces

Gold-coated glass cover slips (150 nm gold on 20 nm chromium) were glued onto a petri dish serving as the substrate for the subsequent self-assembly steps. For this purpose, petri dish and cover slip were rinsed with isopropanol, dried, glued together and cured overnight. After annealing, the petri dish was rinsed with isopropanol, dried and stored. Formation of self-assembly monolayers functionalized with E-cadherin was achieved by following a protocol described in Fichtner et al (Fichtner et al., 2014). In brief, a mixture of benzylguanine thiol (BGT) and matrixthiol (MT) (1:100) at a total thiol concentration of 100 µM in isopropanol was incubated for 3 h onto the gold-coated glass cover slip. After incubation, the supernatant was removed and the petri dish with the cover slip was rinsed with pure isopropanol. Subsequently, the thiol-surface was exposed to 2 µM E-cadherin fusion proteins dissolved in HBS (1 mM EDTA, 10 mM HEPES, 150 mM NaCl, pH 7.4) for 2 hours at room temperature. The last step was to remove the supernatant E-cadherin solution by rinsing the surface with 1x DMEM containing 200 µg/mL Penicillin/Streptomycin, 5 µg/mL Amphotericin B, 15 mM HEPES.

The gold-coated glass cover slips and E-cadherin SNAP-*tag* fusion proteins were provided, from the Prof. Dr. Wedlich Lab (Karlsruhe Institute of Technology (KIT), DFG-Center for Functional Nanostructures, Karlsruhe, Germany).

3.2.2.2 Functionalization of the cantilever

For cell picking, poly-D-lysine coated silicon cantilevers (Arrow-TL2-50, Tipless Silicon SPM-Sensors, Nano World) with a nominal spring constant of 0.03 N/m were used. Before coating with poly-D-lysine, the cantilevers were first washed in a mixture of ethanol and ultra-pure water (1:1) and then in isopropanol both for 5 minutes and finally cleaned in argon plasma for 1 min. Afterwards, cantilevers were incubated in 100 µg/ml poly-D-lysine solution (1 mL; in 1x PBS^{--} (sterile)) for 15 min. Finally, they were washed in sterile ultra-pure water and stored at 2-8 °C. All steps were done at room temperature and the steps after the use of argon plasma were done under sterile conditions. The cantilevers were used maximum up to 2 weeks after functionalization. The functionalization of the cantilever was based on the protocol of Dzementsei et al., 2013.

3.2.2.3 Single cell force spectroscopy procedure

The primordial germ cells for each measurement were prepared and provided by Dr. Aliaksandr Dzementsei (*former:* Georg-August-University, Department of Developmental Biochemistry, Göttingen Center for Molecular Biosciences, Germany).

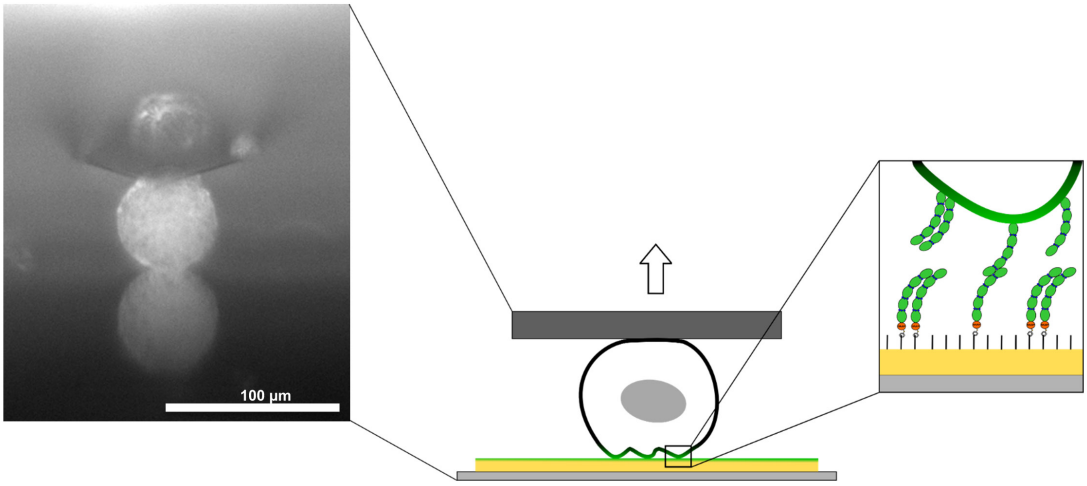

Figure 3-5 **Principle of the setup;** Bright-field side view image of a single cell attached to an atomic force microscope cantilever. The cell is brought into contact with a gold-coated glass cover slip functionalized with an E-cadherin monolayer. The scheme illustrates the setup in which the cell is pulled back from the E-cadherin layer by the AFM cantilever. The interaction between cell and E-cadherin layer is recorded by force distance curves. The E-cadherin is attached via SNAP-tag, which is covalently bound to the benzylguanine (BG) head groups of the thiols organized in a self-assembly monolayer (SAM) formed on the gold surface.

Single PGCs or the control somatic endodermal cells isolated either from stage 17–19 (early) or stage 28–30 (late) embryos were used. PGCs were fluorescently labelled by injection of GFP_DELE mRNA, where Dead End localization element (DELE) mediated PGC-specific expression. All measurements were performed using a Cellhesion200 AFM (JPK Instruments) mounted on top of an Olympus IX81 microscope. The used petri dishes were separated into two areas using a liquid-repellent slide marker pen (Super PAP Pen Liquid Blocker, mini) to investigate the interaction of either primordial germ cells or somatic cells with the E-cadherin layer. One area was coated with bovine serum albumin (BSA) (5% (w/v) in 1x PBS^{--}) for 1 h to avoid cell spreading and therefore facilitate picking of the cells, followed by 3x washing with 1x PBS^{--}. The E-cadherin layer was prepared in the other part of the petri dish (see section 3.2.2.1; *p.* 37). Up to 9 different spots on the E-cadherin layer were probed with 5 force curves using the

same cell on the cantilever. At least 5 cells were investigated per category. The whole measurement was performed in measurement buffer (DMEM) with 200 µg/mL Penicillin/Streptomycin, 5 µg/mL Amphotericin B, 15 mM HEPES at room temperature.

Figure 3-5 shows a scheme and sideview micrograph illustrating the measurement principle. A single primordial germ cell is brought into contact with an E-cadherin (extracellular domain (EC) 1-5) coated gold layer for a defined time and load force. After pressing the PGC onto the E-cadherin (EC 1-5) monolayer for a certain time the cell is detached and the resulting attractive forces between the cell and the E-cadherin layer are recorded as force distance curves. We have chosen only very short dwell times since we were mainly interested in mimicking the situation of cell locomotion where short contact times are expected. Moreover, longer dwell times result only in a larger width of the histograms (Dzementsei et al., 2013).

3.2.2.4 Settings and parameters

The cantilever spring constant was determined before each measurement using the thermal noise method (Hutter and Bechhoefer, 1993) which is implemented into the JPK software (section 3.1.1; *p.* 25).

For calibrating the cantilever following parameters were used:

	Set point	**Velocity**	**Contact time**	**Sample rate**
	1 - 2 V	5 µm/s	0 s	6 kHz

Table 3-3 Parameters for calibrating the cantilever for SCFS measurements

After calibrating the cantilever the cells (PGC/ somatic) were added to the petri dish and allowed to settle. Afterwards the calibrated and functionalized cantilever was used to pick one cell. Following parameters were used:

	Set point	Velocity	Contact time	Z-length
	0.5 - 1 nN	5 µm/s	10 - 30 s	80 µm

Table 3-4 Parameters for picking the cell

The cantilever with the picked cell is moved to the E-cadherin functionalized gold surface and pressed onto the surface. Up to 9 different spots on the E-cadherin layer were probed with 5 force curves using the same cell on the cantilever. Following parameters were used for the investigation of the E-cadherin interaction with the picked cell:

	Set point	Velocity	Contact time	Pause time	Z-length	Sample rate
	0.5 nN	5 µm/s	1 s	5 s	80 µm	2.48 / 6 kHz

Table 3-5 Parameters for SCFS measurements

3.2.2.5 Sideview imaging

Lateral images of the cantilever in contact with the surface were obtained by using the sideview-setup from JPK Instruments. Sample preparation and handling was done as described in (Gonnermann et al., 2015, JPK_Instruments, 2010).

3.2.2.6 Analysis of data

The recorded force distance curves were first edited with the JPK Data Processing software and afterwards analyzed with a home-made Matlab script. Each force distance curve were processed in the JPK Data Processing software through several steps which were already described in the AFM force spectroscopy section *3.1.3.3* (*p*. 30).

After executing these steps for each force distance curve the retrace/trace curve is saved as a text file (.txt).

Retrace curve:

The force distance curves were then imported into the home-made Matlab script (provided by Dr. Ingo Mey; Georg-August-University, Institute for Organic and Biomolecular Chemistry, Göttingen, Germany).

After smoothing the retrace curve following parameters were manually determined (Figure 3-6):

- work of detachment (blue area)
- maximum adhesion force (blue dot)
- force of single rupture events (green dots)
- tether force (red dots)

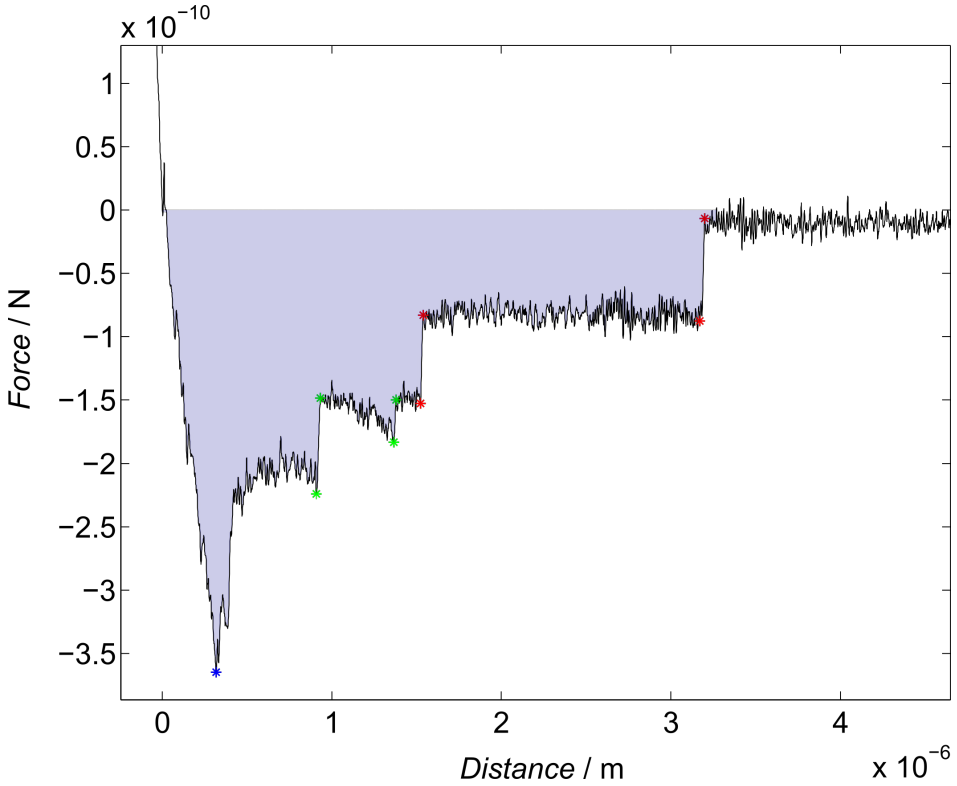

Figure 3-6 Force distance retrace curve after analyzing.

Trace curve:

Trace curves were analyzed for the cortex tension of the cell. The fact that the slope of the resulting force – compression curves is proportional to the cortical tension of the cell is used to measure the cortical tension of each cell type by parallel plate compression (Schafer et al., 2013).

Therefore all trace curves were edited in JPK Processing software as described before and open with a home-made matlab script (provided by Dr. Ingo Mey; Georg-August-University, Institute for Organic and Biomolecular Chemistry, Göttingen, Germany). For identifying the cortex tension an average curve per cell from trace force distance curves was generated (Figure 3-7). The average curve contained 3000 number of points and included the indentation area after the contact point of the trace curve.

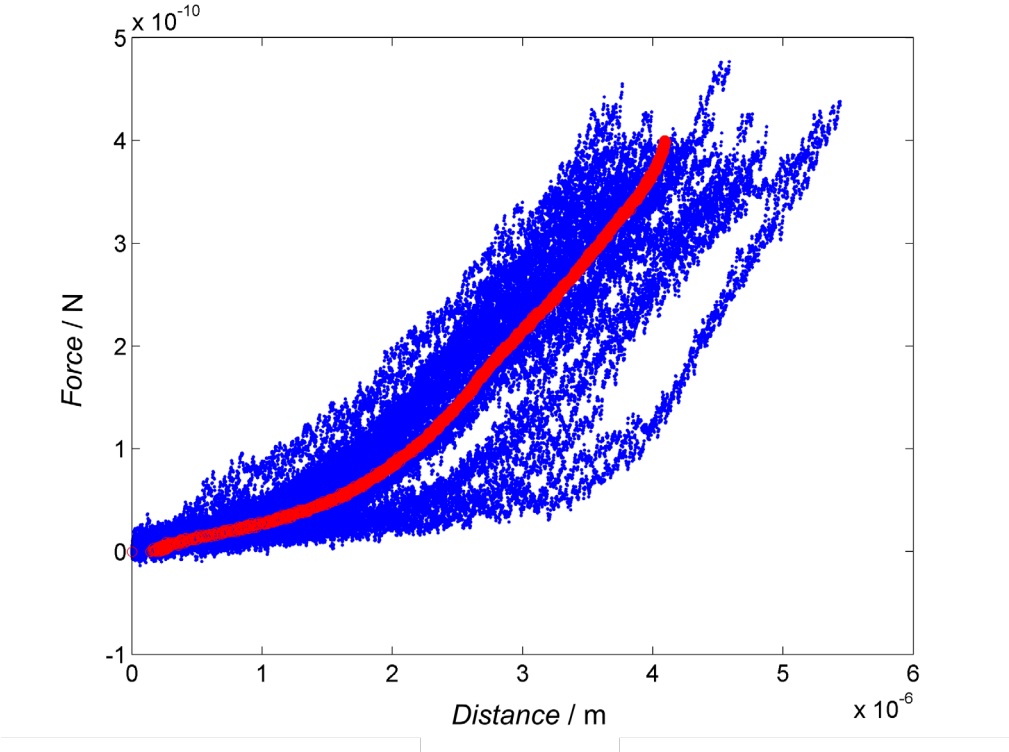

Figure 3-7 **Trace average SCFS** (red) generated from all traces curve from one cell (here somatic endodermal cell (*Xenopus laevis*)).

After generating the master curve for each cell, the slope of the master curve was fitted from contact point until the vertical deflection of 50 pN with a linear fit and the values were collected for each category.

The results were illustrated with the software IGOR. The criteria for the used box-whisker-plots: line denotes the median of the distribution, boxes comprise the 25th and 75th percentile, whisker tops and bottoms are drawn to the 10th and 90th percentiles, respectively.

3.3 Single molecule force spectroscopy

Single molecule force spectroscopy (SMFS) investigates the intermolecular forces between individual ligand-receptor pairs from biological systems. It is very close related to SCFS. In SMFS we gain knowledge on the single receptor level. As for the SCFS it is possible to investigate these forces on the single-molecule level with different techniques. The most common techniques are atomic force spectroscopy, optical tweezers and magnetic tweezers (Neuman and Nagy, 2008, Zlatanova et al., 2000).

In AFM-based SMFS the goal is to bind ligands to AFM cantilever tips, receptors to sample surfaces and investigate their interaction. The ligand is mostly a protein of interest, a specific antibody or an inhibitor. For the receptor it can be an immobilized protein on a substrate, artificial membranes or proteins expressed in membranes of living cells (Puntheeranurak et al., 2011).

Again as for the SCFS the advantage for AFM-based SMFS is the wide practical force range (10 pN to 10^4 pN), the simple and rapid sample preparation, the ability to work under near physioloigical conditions and therefore it is an ideal tool to investigate biological samples (Neuman and Nagy, 2008, Franz and Puech, 2008).

3.3.1 Setup

For the typical AFM-based setup the coated AFM cantilever is brought into contact with the surface, which is covered with the receptor. The cantilever stays for a certain time on the surface, to allow a formation of a single receptor-ligand complex before it is retracted again (Figure 3-8). During retraction the lifetime of the ligand-receptor bond is reduced through the exerted force until the interaction bond breaks at a critical force. These single rupture events are recorded in the force distance curves (Figure 3-9) through the deflection of the cantilever and can be used to quantify and categorize the ligand-receptor interaction of interest.

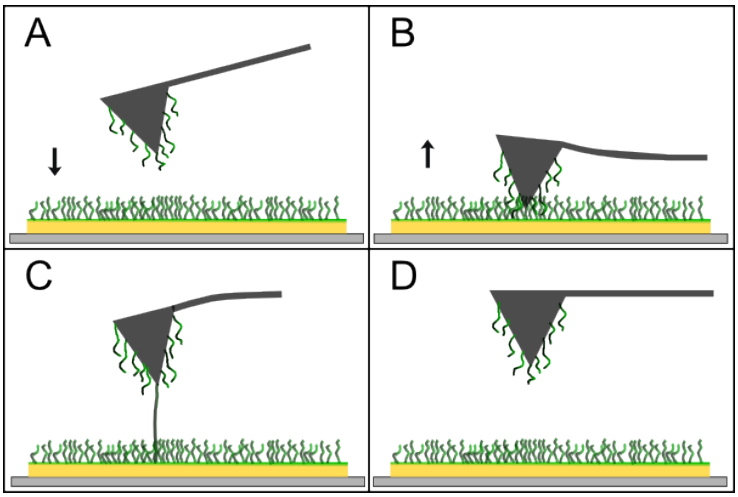

Figure 3-8 **SMFS cycle**: A) Cantilever functionalized with ligands is moved to the functionalized surface (receptors). B) It is pressed onto the surface to allow formation of a ligand-receptor complex. C) During retraction the bond gets elongated until it breaks which leads to a force signal in the force distance curve. D) After retraction of the cantilever the SMFS cycle starts again.

The crucial part in SMFS experiments is the connection of the ligand molecules to the AFM tip or the surface. The ligands have to be attached to the AFM tip very tightly and ideally at a low surface density. Additionally they should have enough mobility to interact with complementary molecules. To fulfil these conditions many coupling instructions have been designed over the last years (Puntheeranurak et al., 2011, Ebner et al., 2008).

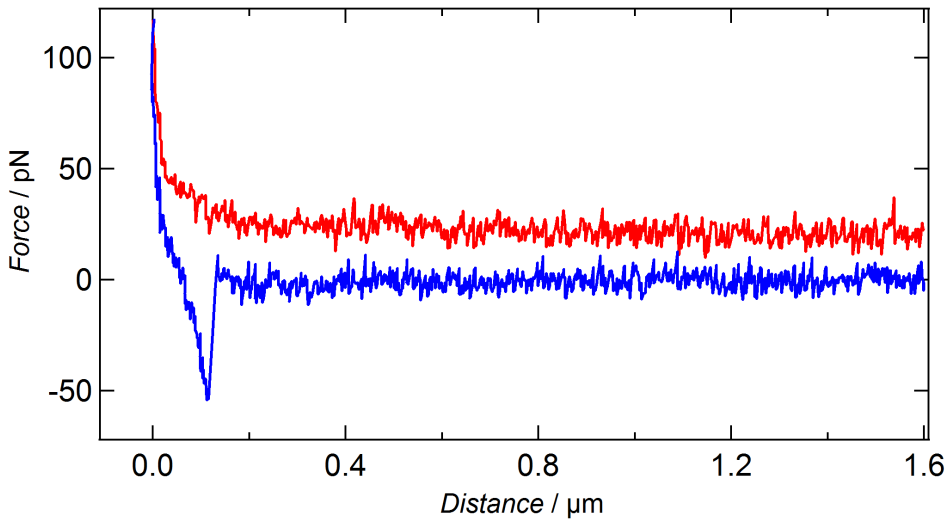

Figure 3-9 **Force distance curve for SMFS setup**. Trace (red) and retrace (blue) curve with one single rupture event of around 50 pN (Set point 0.1 nN; velocity 5 µm/s).

For this work the coupling of the E-cadherin to the cantilever was done by using the linkage between the gold surface and the Benzylguanine thiol (BGT).

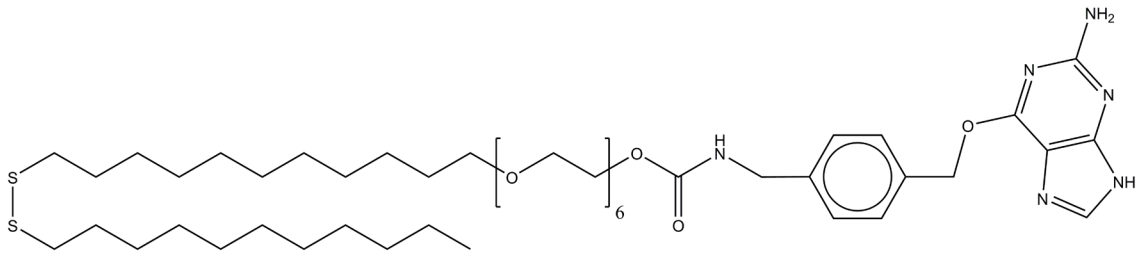

Figure 3-10 **Benzylguanine thiol (BGT)** ($C_{48}H_{82}N_6O_9S_2$)

Benzylguanine-thiol ($C_{48}H_{82}N_6O_9S_2$) (Figure 3-10) serves as a linker between cantilever and the single E-cadherin fusion protein. After cleavage of the disulfide bridge the benzylguanine binds with the thiol group directly to the gold surface of the cantilever. The E-cadherin fusion protein, with his five extracellular domains (EC 1-5) bind to a SNAP-tag, binds to the BG-thiol with his SNAP-*tag* on the BG head group by cleavage of the guanine (Engin et al., 2010). Additionally Methoxy terminal-EG3-thiol ($C_{18}H_{38}O_4S$) (Figure 3-11) is used which is shorter than the BG-thiol and binds also with the thiol group to the cantilever. It is used to passivate the remaining area of the cantilever so that no other discrete interactions with the cantilever tip can occur.

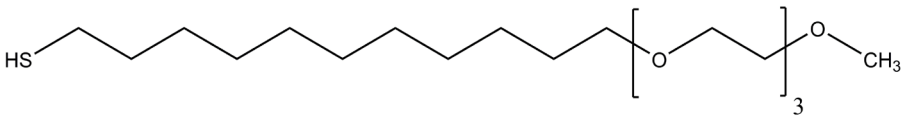

Figure 3-11 **Methoxy terminal (MeO)-EG3-thiol** ($C_{18}H_{38}O_4S$)

3.3.2 Experimental procedure

Single cell force spectroscopy measurements were carried out for chapter **4.1** (*p.* 67).

Some parts of this chapter has been published in Baronsky T, Dzementsei A, Oelkers M, Melchert J, Pieler T and Janshoff A, *Integr. Biol.,* **2016,** 8**,** 349-58; DOI: 10.1039/c5ib00291e.

There were two types of measurements. One SMFS setup investigated the interaction of E-cadherin with primordial germ cells of *Xenopus laevis* at different stages. Here the AFM cantilever was coated with E-cadherin-EC 1-5 and brought into contact with the cells. The second SMFS setup served as control for the SCFS measurements to confirm proper activity of the cadherins and successful surface functionalization. Here both, the AFM cantilever and the gold coated surface was functionalized with E-cadherin-EC 1-5 and the homophilic interaction was investigated.

For both setups the cantilever had to be prepared in first place. Additionally the gold coated surface had to be functionalized with E-cadherin fusion proteins for the second setup.

Single molecule force experiments were prepared and performed according to (Fichtner et al., 2014). Gold-coated glass cover slips and E-cadherin SNAP-*tag* fusion proteins were provided, as for the SCFS measurements, from the Prof. Dr. Wedlich Lab (Karlsruhe Institute of Technology (KIT), DFG-Center for Functional Nanostructures, Karlsruhe, Germany)

3.3.2.1 Functionalization of the cantilever

For SMFS measurements, gold vaporized silicon cantilevers (Bio-Lever, BL-RC150VB-C1, gold-coated on both sides) with a nominal spring constant of 0.006 N/m were used.

The cantilevers were first washed in isopropanol and then cleaned in argon plasma for 20 s. Subsequently they were immersed in thiol solution for 3 h (Benzylguanine thiol (BGT) and methoxy-terminal (MeO)-EG3-Thiol matrixthiol (MT) (1:100) at a total thiol concentration of 100 µM in isopropanol).

Prior to functionalization with E-cadherin molecules, cantilevers were rinsed after incubation of 3 h with pure isopropanol and dried carefully. Afterwards the cantilever was placed into the AFM setup and immersed into a drop of protein solution for 2 h at room temperature (ca. 80 µL) to allow binding of E-cadherins. The protein solution contained the protein E-cadherin-EC 1-5 (2 µM) in HBS (1 mM EDTA, 10 mM HEPES, 150 mM NaCl, pH 7.4). Finally the full functionalized cantilever with the AFM head was taken out of the protein solution and brought into the petri dish with PBS^{++} buffer for the experiment. Prior to the measurement the cantilever was washed again by taking it out of the buffer and dipping it in again for at least two times.

3.3.2.2 E-cadherin functionalization of gold surfaces

E-cadherin functionalization on gold surfaces was described before in the single cell force spectroscopy section and can be found in section *3.2.2.1* (*p*. 37).

3.3.2.3 Single molecule force spectroscopy procedure

The cantilever spring constant (nominal spring constant 0.006 N/m) was determined prior to each experiment by the thermal noise method (Hutter and Bechhoefer, 1993) as described in section 3.1.1 (*p.* 25).

Depending on the setup the cantilever was pushed on the E-cadherin functionalized gold surface or cells from *Xenopus laevis*.

For the investigation of E-cadherin interaction with cells from *Xenopus laevis* all measurements were performed using a NanoWizard II/III^{TM} AFM (JPK Instruments) mounted on top of an Olympus IX81 microscope in PBS with Ca^{2+} and Mg^{2+}-Ions (PBS^{++}) at room temperature. Alternatively, DMEM with 200 µg/mL Penicillin/Streptomycin, 5 µg/mL Amphotericin B and 15 mM HEPES was used.

At the beginning of the measurement the cells were added to the petri dish and allowed to settle. Afterwards force maps were performed on the settled cells with the E-cadherin functionalized cantilever. For a better adhesion of the cells to the surface, one measurement was performed with a functionalized poly-d-lysine petri dish (functionalization was adapted from 3.2.2.2; *p.* 37).

Control measurements for the SCFS measurements to confirm proper activity of the cadherins and successful surface functionalization a MFP-3D™ (Asylum Research) setup mounted on an inverted Olympus IX 51 microscope was used at room temperature in PBS^{++}. Force maps at different spots on the functionalized gold surface were performed to investigate the homophilic E-cadherin interaction.

3.3.2.4 Settings and parameters

For calibrating the cantilever following parameters were used:

	Set point	**Velocity**	**Contact time**	**Sample rate**
NW II / III	0.5 V	1 µm/s	0 s	2.48 kHz
MFP-3D	1 V	2 µm/s	0 s	2 kHz

Table 3-6 Parameters for calibrating the cantilever at SMFS measurements

The experiments were carried out by taking force maps on different spots on the cells or surface. Following parameters were used:

	Set point	**Velocity**	**Contact time**	**Sample rate**
NW II / III	0.1 nN	1 µm/s	0.5 / 1 / 3 / 5 / 10 s	2.48 kHz
MFP-3D	0.05 nN	1 µm/s	0 s	12.5 kHz

Table 3-7 Parameters for SMFS measurements

	Force map	
	Size	**Points**
NW II / III	10 x 10 µm^2 - 20 x 20 µm^2	5 x 5 - 15 x 15
MFP-3D	5 x 5 µm^2	10 x 10

Table 3-8 Parameters for Force maps at SMFS measurements

3.3.2.5 Analysis of data

The recorded force maps which were obtained from the Nano Wizard II/III were first edited with the JPK Data Processing software and afterwards analyzed with a home-made Matlab script. Each force distance curve were processed in the JPK Data Processing software through several steps which were already described in the AFM force spectroscopy section *3.1.3.3* (*p.* 30).

After executing these steps for each force distance curve the retrace/trace curve is saved as a text file (.txt).

The force curves obtained from the MFP-3D can be directly analyzed with the home-made Matlab script.

The retrace force distance curves were imported into the home-made matlab script (provided by Dr. Ingo Mey; Georg-August-University, Institute for Organic and Biomolecular Chemistry, Göttingen, Germany) and analyzed as for SCFS (see section 3.2.2.6; *p.* 40). The single rupture events were determined manually for each rupture event to calculate the rupture force.

The results were illustrated with the software IGOR. The criteria for the used box-whisker-plots: line denotes the median of the distribution, boxes comprise the 25th and 75th percentile, whisker tops and bottoms are drawn to the 10th and 90th percentiles, respectively.

3.4 Optical microscopy techniques

Fluorescence microscopy measurements were carried out for chapter **4.2** (*p.* 83).

3.4.1 Analyzing EMT with fluorescence microscopy

Here normal murine mammary gland epithelia (NMuMG) cells were fluorescently labeled for E-cadherin, F-actin and cell nucleus to observe the changes of these cell parts during the induced epithelial-mesenchymal transition (EMT). Immunostaining combined with fluorescence microscopy was carried out using a confocal laser scanning microscope (CLSM, Olympus Fluoview, FV1200).

NMuMGs were seeded on Ibidi^{TM} petri dishes. After 24 h the cells were treated with 10 ng/ml of TGF-ß1 for 48 h and compared to untreated reference samples. The medium was removed and the cells were fixed with cold 4 % paraformaldehyde (PFA) solution in PBS^{--} and an incubation time of 15 min. This was followed by washing the cells twice with 1 x PBS^{--} and permeabilizing them with a 1 x PBS^{--} solution containing 0.3 % Triton-X and 5 % BSA with an incubation time of 45 minutes. The containing BSA blocks unspecific binding sites. Afterwards the *blocking buffer* was removed and the respective fluorescence marker was used with a certain concentration. Between each labeling step the sample was washed 3 x with *washing buffer* (PBS^{--} supplemented with 0.1 % BSA) by shaking it for 5 minutes. Reaching the last labeling step the cells were washed 1 x PBS^{--} and stored in PBS^{--} at 2-8 °C.

<u>E-cadherin:</u>

Cells were incubated with a primary purified mouse anti-E-cadherin anti body (6 µg/mL in 1x PBS^{--} supplemented with 1 % BSA and 0.3 % Triton-X) for 1 h at room temperature and subsequently labeled with secondary antibody Alexa Fluor 488 goat-anti-mouse IgG (H+L) for 1 h (20 µg/mL in 1x PBS^{--} supplemented with 1 % BSA and 0.3 % Triton-X).

F-actin:

Staining was carried out with Alexa Fluor 546 phalloidin (diluted as recommended by the manufacturer, 2 µL methanolic stock solution with 200 µL PBS^- with 1 % BSA and 0.3 % Triton-X for each coverslip).

Cell nucleus:

For DNA staining 4'-6-diamidino-2-phenylindole (50 ng/ml in PBS^{--}, DAPI) was used with an incubation time of 20 minutes.

3.4.2 Analyzing EMT with metal induced energy transfer

3.4.2.1 Setup and procedure

For the MIET experiments a conventional home build confocal laser scanning microscope setup was used to measure fluorescence lifetime. It can be used to localize fluorescent molecules along one dimension with nanometer accuracy (see also chapter 4.2; *p.* 83). MIET uses the fact that the fluorescence lifetime is dependent on the distance between fluorophore and the used metal surface due to quenching effects. Therefore the measured fluorescence lifetime can be correlated to a fluorophore - sample distance, which has to be in a range of 100-200 nm (Chizhik et al., 2014). Therefore we modified our samples and used a thin semitransparent 20 nm gold film deposited on a glass cover slide and determined the fluorescence lifetime. Details about the setup can be found in the previous publication (Chizhik et al., 2014).

The acquired data was analyzed by Dr. Alexey Chizhik (Georg-August-University, III. Physical Institute, Göttingen, Germany).

3.4.2.2 Sample preparation

The sample preparation was based on the protocol of Chizhik et al., 2014.

The mouse mammary epithelial cell line NMuMG (ATCC, Manassas, VA), was cultured in regular culture medium ((DMEM) see section 3.5.2; *p.* 55) under standard conditions (37°C and 7.5 % CO_2).

To monitor the cell-substrate distance with MIET, NMuMGs were seeded on gold-coated glass bottom petri dishes (MatTek) in the culture medium for experiments ((DMEM^{++}) see section 3.5.2; *p.* 55)).

To induce the epithelial-mesenchymal transition (EMT) in NMuMGs, they were treated with recombinant human transforming growth factor – beta 1 (TGF-ß1) for a certain treatment time (0 h – 72 h). The TGF-ß1 addition always occurred at least 24 hours after seeding the cells onto the gold-coated glass bottom petri dish. TGF-ß1 was obtained from Life Technologies and used in a final concentration of 10 ng/mL diluted in culture medium DMEM^{++}.

For the measurement itself the plasma membrane of cells was stained by replacing the cell medium and incubating living cells with HEPES-buffered cell culture medium containing 5 µg/ml Cell Mask™ Deep Red Plasma Membrane Stain for 5 minutes at 37°C. Afterwards it was replaced with culture medium DMEM^{++}, which allowed the investigation of living cells up to one and a half hour after staining at 37°C, and measured at the MIET setup.

3.5 Cell culture

Cells were cultured by Angela Rübeling and Anja Herdlitschke (Georg-August-University, Institute for Organic and Biomolecular Chemistry, Göttingen, Germany). Preparation and passaging of cells were done under a sterile laminar flow (Safe 2020). Cells were cultured in a CO_2 incubator (Heracell 150i) at 37 °C and at 7.5 % CO_2 concentration in 25 cm^2 or 75 cm^2 culture flasks. Depending on the need the cells were passaged one or two times a week. For cell passage, cells were first trypsinated (Trypsin/EDTA 0.05%/0.02%) for approximately 1-2 minutes, added to stop solution (cell culture medium and fetal bovine serum), centrifuged (Heraeus Megafuge 16R; 1200 U/min for 3 minutes) and resuspended in cell culture medium again. For counting the cells a Neubauer cell counting chip was used (C-Chip, Neubauer Improved).

3.5.1 Cell line

NMuMG (normal murine mammary gland epithelial cell line) are cells from the breast epithelial tissue. The origin strain is NAMRU. The cells were obtained from ATCC, Manassas, VA, July 2009, passage 12.

3.5.2 Medium

Culture medium (DMEM):

Dulbecco's modified Eagles Medium (DMEM) with 4.5 g/l glucose, 10% fetal bovine serum (FBS) and 4 mM L-glutamine and 10 µg/ml insulin.

Medium for experiments ($DMEM^{++}$):

Regular culture medium supplemented with 15 mM HEPES, 5 µg/ml Amphotericin and 200 µg/ml Penicillin/Streptomycin.

Culture medium for SCFS (see chapter 3.2; *p.* 33) and SMFS (see chapter 3.3; *p.* 43):

Regular culture medium for experiments but without fetal bovine serum (FBS) to avoid clustering of the E-cadherin fusion proteins which were functionalized to the AFM cantilever or surface respectively.

3.6 Electric cell-substrate impedance sensing

3.6.1 Definition

Electric cell-substrate impedance sensing (ECIS) is an impedance-based, real time, non-invasive method to monitor the morphological changes of cells in tissue culture (Giaever and Keese, 1984). These include changes in cell-cell as well as cell-substrate interaction and cellular locomotion (Wegener et al., 2000, Lovelady et al., 2007, Tarantola et al., 2009, Lo et al., 1995, Giaever and Keese, 1991).

3.6.2 Setup

In this method cells were seeded on an array of small gold electrodes (250 µm diameter), which were evaporated on the bottom of tissue culture wells. The complex impedance *Z* of an alternating current (AC) between the small electrodes and a much larger counter electrode was measured. Cell culture medium dealt as the electrolyte. After the cells were attached and spread on the electrode, they altered the effective area available for current flow and therefore the impedance *Z* of the system increased depending on the AC-frequency. After this initial increase the impedance fluctuation can be monitored with time and analyzed to gain information on cell spreading and micromotion of the cells. (Giaever and Keese, 1991, Xiao et al., 2002).

Here any morphological changes of the cell, caused by the addition of compounds or changes in the physical environment can be detected by the ECIS method. It has been proofed as a useful tool for quantification of cell spreading and motility (Xiao et al., 2002, Keese et al., 2004, Smith et al., 1994, Lovelady et al., 2009, Schneider et al., 2011, Wegener et al., 2000).

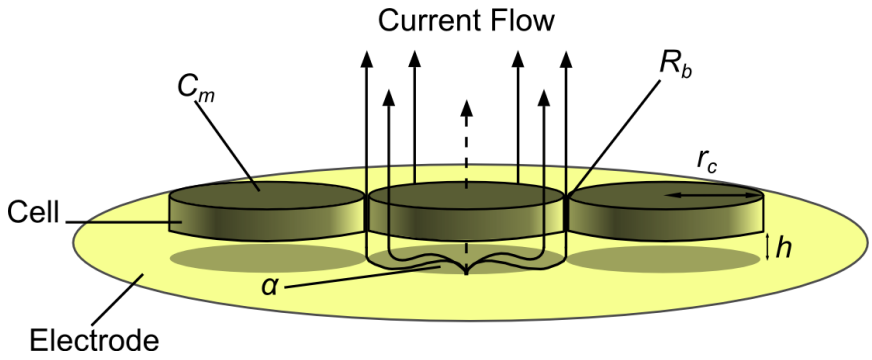

Figure 3-12 **Schematic of ECIS measurement** with the resistance α in the cleft between cells and substrate, the barrier resistance R_b between cells and the membrane capacity C_m. (Adapted from (Applied_BioPhysics)).

From the measured complex impedance spectrum additional parameters can be gained by using a model (Giaever and Keese, 1991, Lo and Ferrier, 1998) that provides information on the capacitance of the cell membrane (C_m), the barrier resistance between cells (R_b) and resistance in the cleft between cells and substrate (α) (Figure 3-12).

C_m can be obtained at high-frequency regime where it is dominating the impedance. R_b and α can be extracted at lower frequencies where the impedance is characterized by the current flow through the intercellular gaps and the cleft between cell and substrate (Figure 3-13) (Giaever and Keese, 1991).

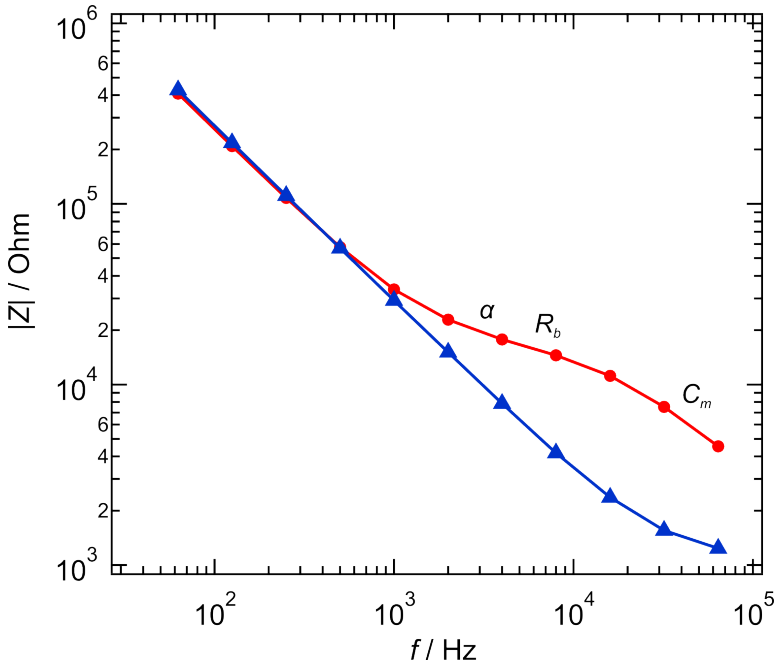

Figure 3-13 **Impedance spectrum** (log-log plot) of a cell-covered (red) and uncovered (blue) ECIS electrode.

3.6.3 Experimental procedure

ECIS measurements were carried out for chapter **4.2** (*p.* 83) to investigate the response of TGF-ß1 treatment on NMuMG and is based on the previous study of Schneider et al. (Schneider et al., 2011).

Measurements were accomplished by using an ECIS Zθ (Applied BioPhysics) combined with an incubator (37°C and 5 % CO_2). NMuMGs cells (either 100.000, 150.000 or 200.000 cells) were seeded onto gold electrodes of 8-well arrays (8W1E Ibidi^{TM}) in 300 µL culture medium DMEM^{++}. The arrays were placed in an incubator, connected to the ECIS instrument and 24 hours after starting the measurement, the cytokine TGF-β1 was added in fresh medium resulting in a final concentration of 5, 10 or 15 ng/ml.

3.6.3.1 Settings and parameters

To investigate the entire range of the impedance spectrum the impedance was measured with frequency sweeps ranging from 62,5 to 64.000 kHz.

3.6.3.2 Analysis of data

The measured data were analyzed using a home-made matlab script (provided by Dr. Jan Rother; Georg-August-University, Institute for Physical Chemistry, Göttingen, Germany) to gain the barrier resistance between cells (R_b), the resistance in the cleft between cells and substrate (α) and the membrane capacity (C_m). This was done by fitting an area contact model (Giaever and Keese, 1991, Lo and Ferrier, 1998) to the data.

The obtained values and the impedance spectra were illustrated with the software IGOR.

3.7 Rheology

3.7.1 Definition

Rheology deals with the study of deformation and flow of matter. The method looks deeper into the flow behavior of complex fluids like biological systems, polymers, suspensions, emulsions and other compounds. They do not follow Hooke's law of elasticity (see also (3-1)) which claims for the proportionality of the force to the deformation (3-5) (with τ for the force per unit area (stress), *G* the constant of proportionality and *γ* as the relative length change or deformation (strain) (Macosko, 1994)).

$$\tau = G\gamma \tag{3-5}$$

Neither they follow Newton's law of viscosity (3-6), which specifies the shear behavior for normal liquids (Morrison, 2001) and claims that the stress is proportional to the rate of straining

$$\tau = \eta\dot{\gamma} \qquad \dot{\gamma} = d\gamma/dt \tag{3-6}$$

with *η* as the Newtonian viscosity (Macosko, 1994). These complex materials exhibit both elastic and viscous responses to mechanical stress and therefore called viscoelastic. At fast deformation they exhibit solid-like behavior and at slow deformations more a fluid like behavior. Rheology attempts to quantify this dynamic viscoelasticity over a wide range of time and deformation scales (Chen et al., 2010, Picout and Ross-Murphy, 2003).

The measuring technology to identify rheological data is the rheometry. For purley elastic behavior stress and strain fluctuations are in phase, viscous components shift the fluctuations so that stress and strain are out of phase. Soft tissues often show viscoelastic response, which is nonlinear. So the samples stiffen with increasing strain (strain stiffening).

In the experiment the sample is deformed sinusoidally and the stress will also oscillate sinusoidally shifted by a phase angle δ with respect to the strain wave at the same frequency (ω) (Macosko, 1994, Hamley, 2008):

$$\gamma = \gamma_0 \sin(\omega t) \tag{3-7}$$

$$\tau = \tau_0 \sin(\omega t + \delta) \tag{3-8}$$

For analysing, *the stress* wave is decomposed into two waves of the same frequency. τ' is in phase with the strain wave (γ) and τ'' is 90° out of phase (cos ωt).

$$\tau = \tau' + \tau'' = \tau_0' \sin \omega t + \tau_0'' \cos \omega t \tag{3-9}$$

We can also write from the trigonometry

$$\tan \delta = \frac{\tau_0''}{\tau_0'} \tag{3-10}$$

From this decomposition we can gain the storage (elastic or in-phase) and loss (out-of-phase or viscous) moduli (*G'/ G''*):

$$G' = \frac{\tau_0'}{\gamma_0} \tag{3-11}$$

and

$$G'' = \frac{\tau_0''}{\gamma_0} \tag{3-12}$$

From equation (3-10) we can also bring the two moduli in relation:

$$\tan \delta = \frac{G''}{G'} \tag{3-13}$$

The loss modulus stands for the imaginary part and the storage modulus for the real part. Together they give the complex number *G** (Morrison, 2001, Picout and Ross-Murphy, 2003):

$$G^* = G' + iG'' \tag{3-14}$$

To overcome the imaginary unit *i*, the complex number *G** can also be written as:

$$|G^*| = \sqrt{\left(G'^2 + G''^2\right)} = \frac{\tau_0}{\gamma_0} \tag{3-15}$$

Nevertheless *G''* is physically not "imaginary" but rather describes the energy which is dissipated per cycle of deformation and per unit volume (Macosko, 1994).

3.7.2 Rheometer

The rheometer is used for rheology measurements and uses different geometries are to apply stress on the samples. By today cone and plate are probably the most popular rotational geometries for studying non-Newtonian effects by a constant rate of shear (Macosko, 1994). Here the sample is placed between a stationary plate and a rotating flat cone (Figure 3-14 (a)). The gap angle (φ) lays usually between 0.3° and 6° and the cone radius R_p is between 10 – 30 mm. With the distance *r* from the rotation axis the gap *h* increases linearly. The cone and plate geometry has the advantage that the shear rate remains constant and supplies homogenous shear conditions through the entire shear gap. It is used for rotational rheometers where the shear is generated between fixed and moving solid surfaces and the materials are characterized in steady or oscillatory shear flow (Bröckel et al., 2013). Apart from cone and plate also plate-plate geometry measurements are employed. Here the gap height (*H*) is adjustable and the sample is sheared by the rotation of one of the plates at angular velocity (ω) (Figure 3-14 (b)). The circumferential velocity v depends on the distance *r* from the rotational axis and the distance from the plate at rest *h* (Bröckel et al., 2013).

For investigating the complex fluids with a rheometer different types of setups are possible. One possible is to keep the stress constant and monitor the strain. The other way around is to held the strain constant and to monitor the decay of stress as a function of time. Or a dynamic measurement is possible were the applied

deformation is under steady state conditions. Here the strain is a function of time and the stress is monitored (Picout and Ross-Murphy, 2003, Hamley, 2008).

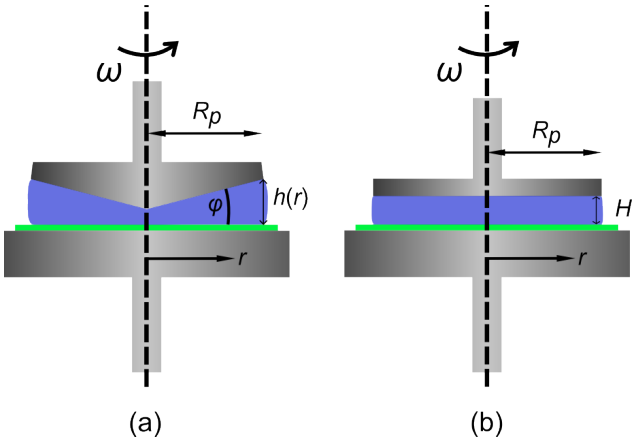

Figure 3-14 **Schematic of the two different geometries for a rheometer** (a) cone and plate geometry and (b) parallel-plate geometry. Adapted from (Bröckel et al., 2013).

3.7.3 Experimental procedure

Rheometer measurements were carried out for chapter **4.3** (*p.* 105).

For investigating the elastic properties of skin sample of DDR 2 deficient and wild type mice (C57BL/6) the samples had to be prepared in the first place. This was done by the working group of Dr. Missbach-Güntner (Göttingen University Medical School, Dept. of Diagnostic and Interventional Radiology). After preparation the glued macroscopic skin probes on cover slips (d = 25 mm; #1) were stored on ice. The measurements were performed with a rheometer (Physica MCR501, Anton Paar) with a parallel-plate systems geometrie (plate – plate) at room temperature. Samples were loaded into the plate rheometer, moistened with PBS^{--} and measured while exerting normal forces of 1 N and 5 N (Figure 3-15).

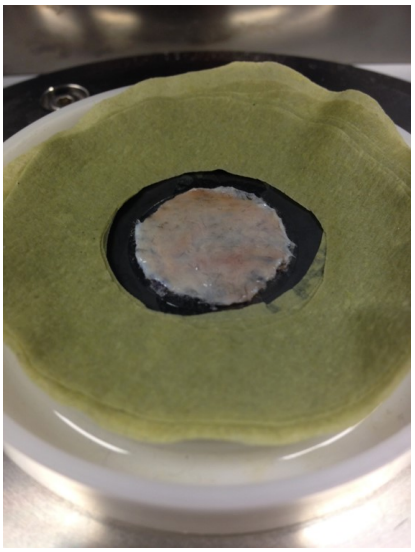

Figure 3-15 **Glued skin sample on cover slips** (d = 25 mm; #1) placed onto plate rheometer with moisten paper (green) to keep the humidity constant around the sample.

For time dependent experiments *G'* and *G''* were measured in dependency of the applied force for 5 minutes at 1 Hz Frequency (30 values per measurement). The frequency dependent measurement was done by a frequency sweep from 0.1 Hz to 100 Hz in 21 steps. Six different mouse skin probes were investigated per category.

3.7.3.1 Analysis of data

The obtained storage modulus (*G'*) and loss modulus (*G''*) are illustrated with the software IGOR. The criteria for the used box-whisker-plots: line denotes the median of the distribution, boxes comprise the 25th and 75th percentile, whisker tops and bottoms are drawn to the 10th and 90th percentiles, respectively.

4 Results and Discussion

4.1 Reduction in E-cadherin expression fosters migration of Xenopus laevis primordial germ cells

Most parts of this chapter are published in Baronsky T, Dzementsei A, Oelkers M, Melchert J, Pieler T and Janshoff A, *Integr. Biol.,* **2016,** 8**,** 349-58; DOI: 10.1039/c5ib00291e.

4.1.1 Introduction

In many species, specification of germ cells occurs in a region away from the site of gonad formation. During embryogenesis, germ cells actively migrate within the embryo, independent of the surrounding tissue. Transition of immobile cells to actively migrating ones correlates with a number of changes in cellular properties originating from a change in gene expression (Santos and Lehmann, 2004, Kunwar et al., 2006, Nakamura et al., 2010, Richardson and Lehmann, 2010).

In *Xenopus laevis*, primordial germ cells (PGCs) are progenitors to the germ cell lines during embryogenesis. Specification of these cells occurs due to the inheritance of maternal factors, including vegetally localized mRNAs and proteins (Heasman et al., 1984, Houston and King, 2000, Kloc et al., 2004). At early stages of embryogenesis, PGCs are tightly associated with their surrounding tissue, and together with somatic endodermal cells they are involuted within the embryo during gastrulation. At the neurula stage, PGCs are clustered within the endoderm, while at the tailbud stage (st.24-25) (Nieuwkoop and Faber, 1994) they initiate active migration within the embryo towards the prospective genital ridges (Nishiumi et al., 2005, Terayama et al., 2013). Although a number of factors were shown to contribute to active migration of PGCs in *X. laevis*, the molecular mechanism of this process remains largely unexplored (Dzementsei and Pieler, 2014).

In this study, we analyzed the role of E-cadherin in the context of active PGC migration in *X. laevis* embryos. We used single cell force and single molecule force spectroscopy in conjunction with cadherin-coated substrates to measure molecule-specific cellular adhesion down to single molecule level. We found that early pre-migratory PGCs display higher adhesion forces to covalently linked and density-controlled E-cadherin coated surfaces as compared to late migratory PGCs, suggesting that the capability to migrate is fostered by a decrease in E-cadherin mediated adhesion to adjacent cells.

4.1.2 Results

4.1.2.1 E-cadherin is expressed in the endoderm of X. laevis embryos

Previous immunostaining analysis of the E-cadherin distribution during *X. laevis* development had indicated that endodermal cells up to stage 20 express no or only very low levels of E-cadherin (Levi et al., 1991). Recent results had indicated that E-cadherin mRNA is present in somatic endodermal cells and PGCs at stages 17-19 and 28-30 (Dzementsei et al., 2013). The presence of E-cadherin protein in the endodermal explants, which includes both PGCs and somatic cells from stage 17-19 embryos, was quantified by Western Blot analysis (Figure 4-1). The specificity of the detected proteins was ensured by including controls with E-cadherin knockdown and detection of the closely related C-cadherin into the analysis. Several types of E-cadherin can be detected in *X. laevis* cells, including an E-cadherin precursor (~155 kDa), intact E-cadherin (~140 kDa), a degradation product (~116 kDa) and the trypsin resistant ectoplasmic domain (~100 kDa) (Choi and Gumbiner, 1989).

Each one of these proteins was detected in endodermal explants isolated from stage 17-19 *X. laevis* embryos, and their expression was significantly reduced upon E-cadherin knock-down via morpholino oligonucleotides (E-cad MO) (Figure 4-1 A). In contrast, C-cadherin expression was not affected by E-cad MO (Figure 4-1 B).

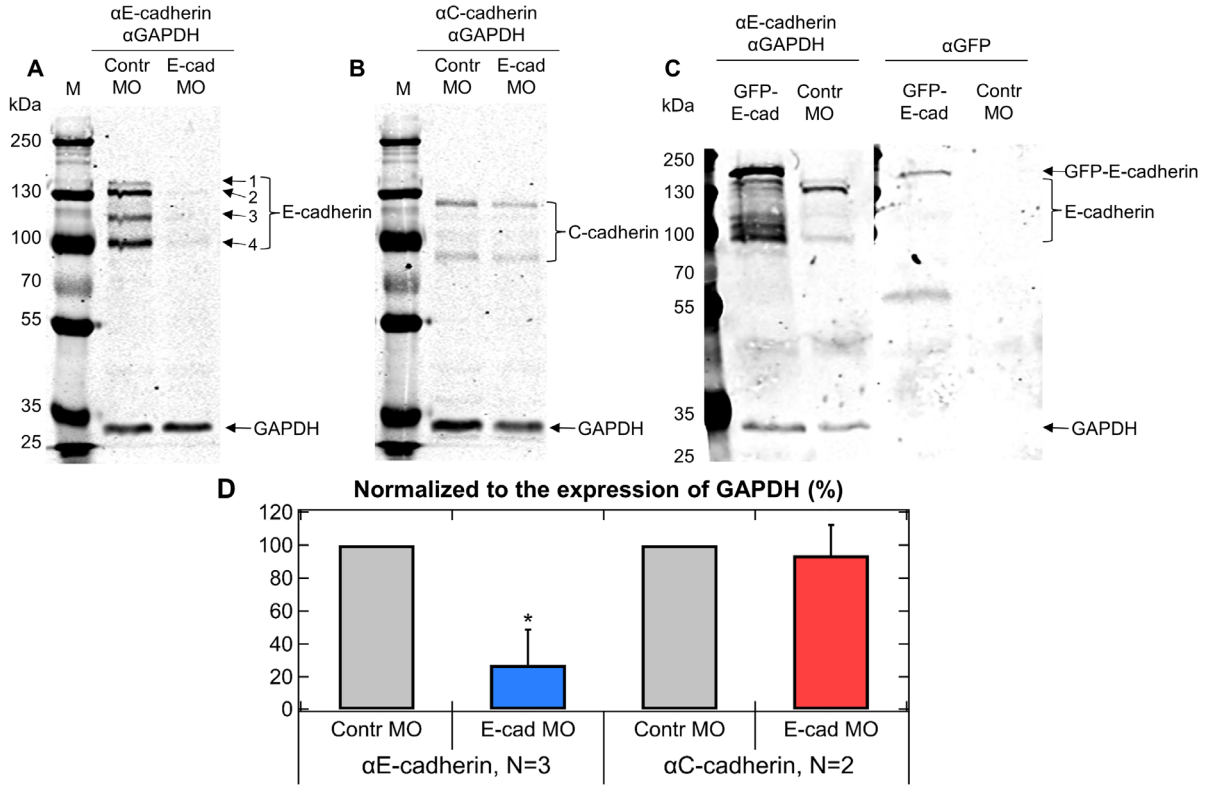

Figure 4-1 **E-cadherin is expressed in the endodermal cells of Xenopus laevis.** Embryos were injected at 2-cell stage with control morpholino oligonucleotides (Contr MO), E-cadherin morpholino oligonucleotides (E-cad MO) or GFP_E-cadherin_DELE mRNA (E-cad GFP). Endodermal explants were obtained from stage 17-19 embryos and used for Western Blot analysis. Expression of GAPDH was used as a positive control, M correspond to the marker lane. **(A)** Several bands correspond to different forms of E-cadherin[17]: 1 - E-cadherin precursor (155 kDa); 2 - intact E-cadherin (140 kDa); 3 - degradation product (116 kDa); 4 - trypsin-resistant ectoplasmic domain (100 kDa). **(B)** C-cadherin staining was used as a control for E-cad MO specificity. **(C)** GFP-tagged overexpressed E-cadherin can be detected in the endodermal explants. **(D)** Expression of E- and C-cadherin was normalized to the expression of GAPDH and quantified in E-cad MO injected embryos relative to Contr MO. N corresponds to the number of experiments. Error bars represent standard deviation. * - $p<0.05$ (Wilcoxon rank sum test). Injection of embryos and Western Blot analysis was carried out by Dr. Aliaksandr Dzementsei (former: Georg-August-University, Department of Developmental Biochemistry, Center for Molecular Biosciences, Germany).

4.1.2.2 Interference with endogenous E-cadherin expression leads to a decrease of PGC numbers at the tailbud stage

Maintenance of E-cadherin expression has been shown to be required for proper germ cell development and migration in several species, including *Drosophila*, zebrafish and mouse (Richardson and Lehmann, 2010). To elucidate whether E-cadherin is involved in PGC development in *X. laevis*, both knock-down and PGC-specific overexpression of E-cadherin were performed (Figure 4-2). PGC-specific

overexpression was achieved by the injection of chimeric mRNA, containing *X. laevis* E-cadherin ORF fused in frame to GFP ORF and Dead End localization element (DELE). GFP-tag was used to identify overexpressed E-cadherin (Figure 4-1), while DELE insured PGC-specific expression. In comparison to the control injection, embryos with overexpressed E-cadherin showed ~50 % reduction in the number of PGCs at the tail-bud stage (st.28-30). Similar results were obtained with E-cadherin knock-down via specific morpholino oligonucleotides (E-cad MO). In the latter case, however, knock-down was not specific to PGCs and led to defects in embryonic development and death of the embryos, especially during neurulation. This resulted in a low number of embryos, surviving until tail-bud stage. Decrease of PGC numbers upon both E-cadherin overexpression and knock-down was observed at tail-bud stage (st.28-30), but not at the neurula stage (st.17-19) of embryonic development.

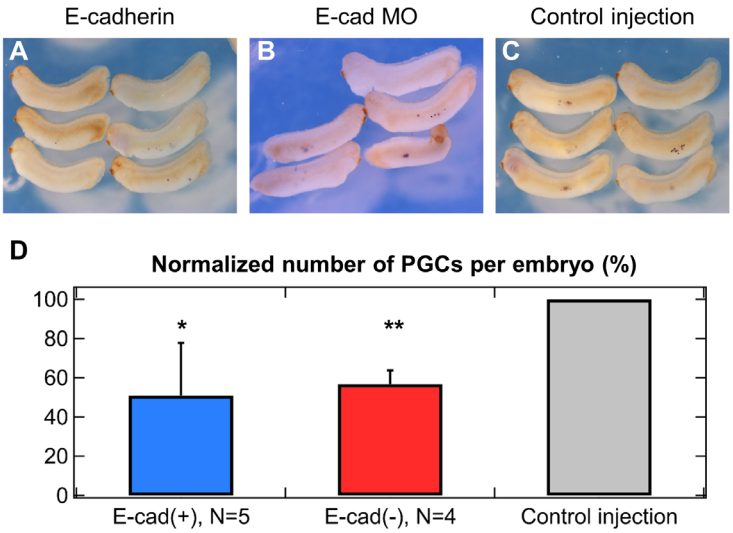

Figure 4-2 **Overexpression and knock-down of E-cadherin results in a decrease of PGC numbers**. Embryos were injected at the 2-cell stage with GFP_E-cadherin_DELE mRNA **(A)**, or E-cadherin morpholino oligonucleotides. **(B)**. For each experiment control injections with GFP_DELE mRNA **(C)** or control morpholino oligonucleotide were performed. **(A-C)** Embryos were fixed at stage 28-30 and used for whole mount in situ hybridisation with antisense Xpat RNA as a PGC marker. **(D)** Number of PGCs per embryo was calculated in each experiment and normalised to the control injection. N corresponds to the number of experiments. Error bars represent standard deviation. * - $p<0.05$; ** - $p<0.01$ (2-tailed paired t-test). Injection of embryos and analysis was carried out by Dr. Aliaksandr Dzementsei (former: Georg-August-University, Department of Developmental Biochemistry, Center for Molecular Biosciences, Germany).

4.1.2.3 Displaying the reduction of E-cadherin in response to SMFS

Previous studies had indicated that the E-cadherin mRNA level in late PGCs (but not in somatic endodermal cells) at the tail-bud stage (st. 28-30) decreases in comparison to the neurula stage (st.17-19) of *X. laevis* development (Dzementsei et al., 2013). Therefore, we decided to investigate the impact of expression level of E-cadherin on the repector-ligand interaction between PGCs at the two different stages and E-cadherin functionalized AFM tip by using single molecule force spectroscopy (SMFS). Additionally somatic endodermal cells served as control cells.

The SMFS measurements could not gain a significant number of rupture events indicative of E-cadherin specific interactions between the E-cadherin fusion protein and the PGCs or somatic endodermal cells respectively (Table 4-1).

	Pre-migratory			**Migratory**	
	Somatic	PGC		Somatic	PGC
Analyzed curves	602	452		585	516
E-cadherin specific interaction (> 20 pN)	2 %	3 %		5 %	5 %

Table 4-1 Overview of SMFS results between somatic endodermal cells (Somatic) and PGCs at the two different stages with contact time of 1 s.

Using the SMFS setup only few, mainly unspecific, interactions like van der Waals attraction and electrostatic interaction were observed with rupture forces below 20 pN. The gained number of E-cadherin specific rupture forces show additionally no difference between PGC and somatic at both stages. In the pre-migratory stage the force distance curves of somatic and PGCs cells reveal only 2 % and 3 % of E-cadherin specific unbinding events respectively. From pre-migratory to migratory state the number of *X. laevis* E-cadherin specific interactions in the force distance curves even increases to 5 % for PGC and somatic cells. We abandoned this strategy due to the low yield of force curves displaying rupture events that could be assigned unequivocally to E-cadherin specific interaction. Therefore we decided to change the setup from *single molecule* to *single cell*

force spectroscopy (Figure 4-3). By changing the setup the contact area was enlarged and thereby the number of interaction between cell and E-cadherin was increased.

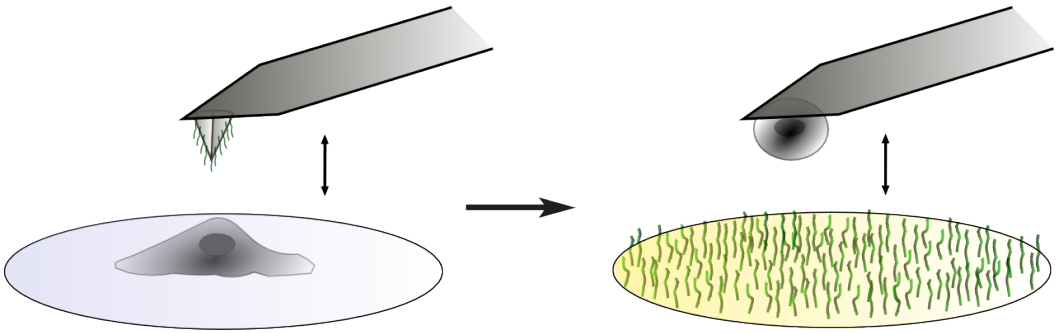

Figure 4-3 **Schematic overview** of changing the setup from SMFS to SCFS. In SMFS an E-cadherin (green rod-like structure) functionalized cantilever is lowered onto a cell. In SCFS the cell is attached to a cantilever a brought in contact with an E-cadherin functionalized surface.

4.1.2.4 E-cadherin-mediated adhesion is reduced in PGCs at the tail-bud stage

After changing the setup, we were able to investigate the impact of expression level of E-cadherin on the adhesion forces of PGCs and somatic endodermal cells.

The single cell force spectroscopy (SCFS) setup allows measuring the adhesive forces between PGCs and artificial E-cadherin (E1-5) layer down to molecular resolution. Using an E-cadherin functionalized substrate instead of living cells permits us to reduce complexity and to focus on a single dedicated non-covalent bond, in our case the homotypic E-cadherin interaction. The force distance curves (retraction curves) were analyzed with respect to the overall dynamic strength, i.e. the largest rupture force, and the occurrence and strength of small unbinding events that can be attributed to rupture of single non-covalent bonds formed between the E-cadherin on the cell's surface and that of the substrate, respectively. The maximum adhesion force represents the maximum dynamic strength of cell-substrate binding (Helenius et al., 2008) including all sources of attractive interactions between cell and surface. Besides specific interactions mediated by cadherins or other intercellular adhesion molecules (ICAMs), adhesion also compiles contributions from electrostatic interactions as well as attractive van der Waals forces partly counterbalanced by repulsive interactions

due to steric hindrance of repeller molecules and membrane undulations at low tension (Sackmann, 2015).

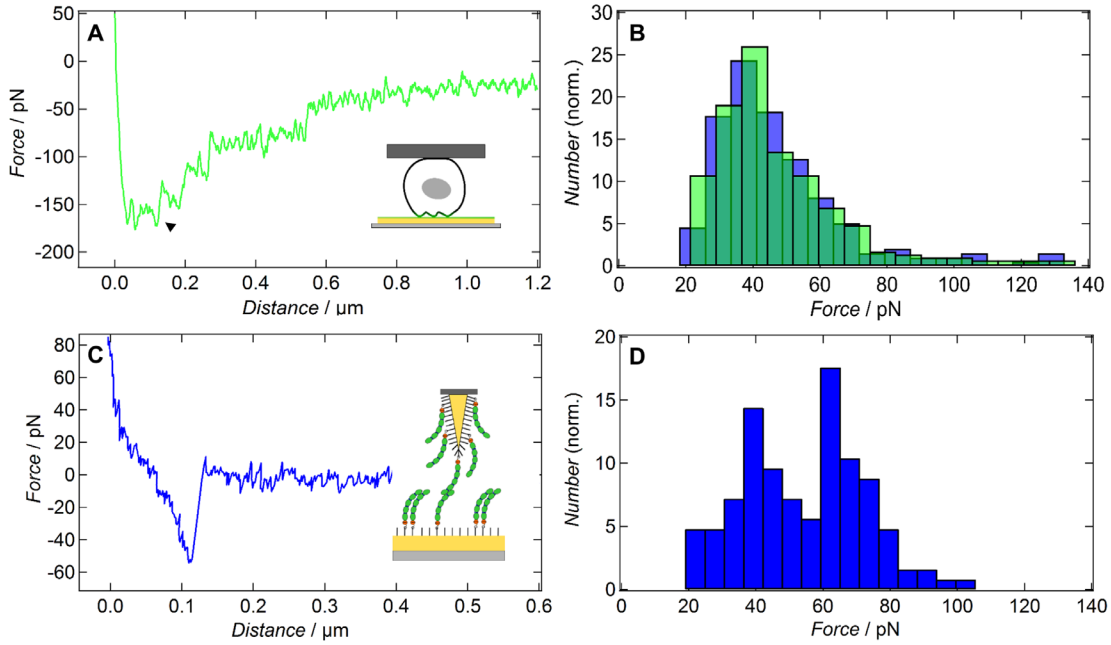

Figure 4-4 **Comparison SCFS vs SMFS**. **(A)** Typical AFM force distance curve of a primordial germ cell displaying the interaction with the E-cadherin (E1-5) layer. The arrow indicates a single rupture event (SRE) occurring during unbinding of the cell from the E-cadherin coated surface. **(B)** The rupture force histogram (normalized to the sum of 100) shows the distribution of the single rupture events of the PGCs isolated from embryos at stages 17–19 (pre-migratory PGCs/green/*n* (SRE) = 288/ *n* (cells) = 8) and stages 28–30 (migratory PGCs/purple/*n* (SRE) = 197/ *n* (cells) = 8). **(C)** Typical SMFS force distance curve shows the unbinding of E-cadherin trans-dimers between an AFM cantilever and the gold surface, which are both coated with E-cadherin (E1-5) monomers. **(D)** The rupture force histogram (normalized to the sum of 100) shows the distribution of the single rupture events of the SMFS experiments and reveals two major maxima indicating two types of bonds (*n* (SRE) = 125).

Figure 4-4 A illustrates a typical force distance curve recorded upon retraction of the cell from the E-cadherin coated surface displaying all relevant features that are usually observed. In addition to the maximal adhesion force measured close to the surface, single rupture events attributed to non-covalent molecular contacts, e.g. homotypic E-cadherin dimers, are also found. The maximum adhesion force sums up non-specific interactions and also the attractive forces exerted by E-cadherin clusters that are not resolved as individual rupture events. Besides, individual rupture events of E-cadherin dimers can frequently be assigned (black arrow Figure 4-4 A). At larger distance from the surface membrane, tethers are extracted from the cell that eventually detach from the substrate if the lifetime of the bonds is exceeded. The distribution of single

molecule forces obtained from rupture events with pre-migratory and migratory PGCs in contact with E-cadherin coated surface is exemplarily shown in Figure 4-4 B. Forces to separate E-cadherin dimers in between 20-80 pN are in very good accordance with previously published data (Leckband and de Rooij, 2014, Panorchan et al., 2006, Shi et al., 2010). Importantly, the histogram of rupture forces for migratory PGCs shows the same distribution as the pre-migratory PGCs with one maximum peak at 30 pN. This finding corresponds well with the assumption that differences in adhesion between the two types of PGCs are based on the number of expressed cadherins but not on alteration of the interaction force between two E-cadherins. We also carried out experiments with regular tip-carrying cantilevers equipped with E-cadherin as described recently (Fichtner et al., 2014). The data confirm that the maximum peak at 40 pN can indeed be attributed to specific E-cadherin unbinding events and that specific interactions are probed (Figure 4-4 C). The histograms for single molecule rupture events reveal the typical bimodal distribution for the unbinding force (Figure 4-4 D) of the homotypic E-cadherin bond as previously reported (Fichtner et al., 2014). The first maximum lies at 40 pN and the second centres around 65 pN. In comparison to the single cell experiments, the single molecule experiment shows one more maxima, the one at 65 pN, indicating a second type of bond for the E-cadherin interaction that is either not present in the cell-substrate experiments or obscured by a larger spread of loading rates due to the inherent softness of the cell (Panorchan et al., 2006).

In order to compare the adhesiveness between different cell types one can either count the number of single molecule rupture events per cell or measure the overall adhesion force. From a biophysical point of view, the latter strategy might be less molecule specific than counting the number of individual bonds but the overall adhesion force is more decisive for cell locomotion considering the general demands for directional and active cell migration. A certain amount of traction force is necessary for migration since PGCs cannot move without attachment, while on the other hand strong adhesion abolishes movement of cells.

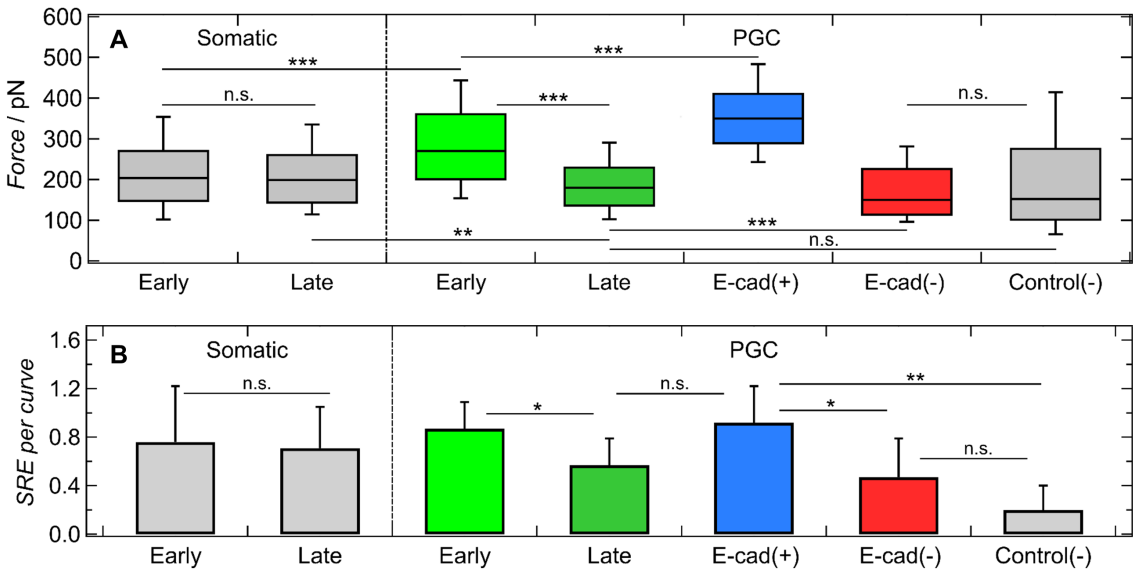

Figure 4-5 **E-cadherin interaction displayed through maximum adhesion force and single rupture events per curve. (A)** Maximum adhesion force of somatic endodermal cells and PGCs both isolated from embryos at stages 17–19 (**early**) and stages 28–30 (**late**). Additionally, the maximum adhesion force of PGCs with E-cadherin over expression (E-cad(+)), E-cadherin knock-down (E-cad(-)) and PGCs in contact with a thiol-monolayer without E-cadherin (Control(-)) is shown. Box-whisker-plots: line denotes the median of the distribution, boxes comprise the 25th and 75th percentile, whisker tops and bottoms are drawn to the 10th and 90th percentiles, respectively. Numbers of curves which were analyzed for each category: somatic endodermal cells early (n (curves) = 320); late (n (curves) = 312); PGC: early (n (curves) = 325); late (n (curves) = 344); E-cad(+) (n (curves) = 135); E-cad(-) (n (curves) = 328); Control(-) (n (curves) = 207) **(B)** Number of single rupture event (SRE) per curve (mean ± SEM) for the same categories as described in **(A)**. At least 5 cells were tested per category. P-values are calculated over the Wilcoxon rank sum test. Not significant (n.s.) - p>0.05; * - p<0.05; ** - p<0.01; *** - p<0.001.

Figure 4-5 A shows the maximum adhesion forces of all cell-substrate interactions measured in this study. The plot comprises somatic cells and PGCs harvested at different stages. We also investigated the adhesive behavior of E-cadherin knock-down (E-cad(-)) and PGCs isolated at the pre-migratory stage (st.17-19) of *X. laevis* overexpressing E-cadherin (E-cad(+)). As an additional control, the adhesion force between PGCs and the self-assembled thiol-monolayer on the gold surface in the absence of E-cadherin proteins (Control(-)) was analyzed. This control serves as a measure for the expected nonspecific adhesion comprising van der Waals attraction and electrostatic interaction between cell and the self-assembly layer on the gold surface. The box plots in Figure 4-5 A show that the adhesion force between early (st. 17-19) and late stage (st. 28-30) somatic endodermal cells remains at a constant level. Both

median values with 204 pN (early somatic cells) and 199 pN (late somatic cells) are essentially identical.

The primordial germ cells, however, change their adhesive behavior during the different stages of development (Figure 4-5 A). Between the early developmental stages 17-19 and the late stage 28-30 the overall adhesion between the cell and the E-cadherin layer is significantly reduced, in fact almost down to the level of non-specific adhesion (152 pN). The median value drops from 270 pN for the early PGCs to 180 pN for late PGCs in accordance with the transition to active migration.

In order to show that indeed E-cadherin is responsible for the drop in maximal adhesion forces we attached both E-cadherin deficient PGCs and PGCs overexpressing E-cadherin to the cantilever. E-cadherin knock-down with morpholino oligonucleotides (MO) resulted in a significant drop of the adhesion force to the level of nonspecific interactions between cells and the substrate (150 pN). In the case of PGCs overexpressing E-cadherin the adhesion force shows the largest values with median value of 350 pN.

Besides measuring the overall adhesion forces we also counted the number of single molecule rupture events (SRE) that match the force jumps found for E-cadherin-E-cadherin interactions in single molecule force spectroscopy experiment. These events are therefore indicative for the presence of E-cadherin molecules on the cell surface (Figure 4-5 B). We found essentially the same trend for SRE as for the maximum adhesion force. The number of single rupture events (SRE) per force curve remains constant for the somatic endodermal cells at the early and late stage. For the primordial germ cells the number of SRE drops from 0.87 at the early stage (st.17-19) to 0.57 at the late stage (st.28-30) and underlines the reduced number of E-cadherin contacts at the migratory stage. The highest value of SRE per curve is shown by the E-cadherin overexpressing PGCs with 0.92 (E-cad (+)). This means that on average in nearly every force distance curve at least one E-cadherin rupture event is identified. Note that in some force curves no single events were detected. For the E-Cadherin knock-down PGCs (E-cad (-)) the value is slightly below the one for late stage PGCs (0.47). The control cells in contact with only a self-assembled thiol-monolayer on the gold surface show the lowest number of SRE close to zero, as expected. The

values for the control and the knock-down PGCs show that the setup still detects some nonspecific unbinding events between the cell and the artificial system. But these nonspecific interactions occur in every category so that the observed differences are caused by the varying E-cadherin surface concentration and not by nonspecific binding forming the interaction baseline of the experiment.

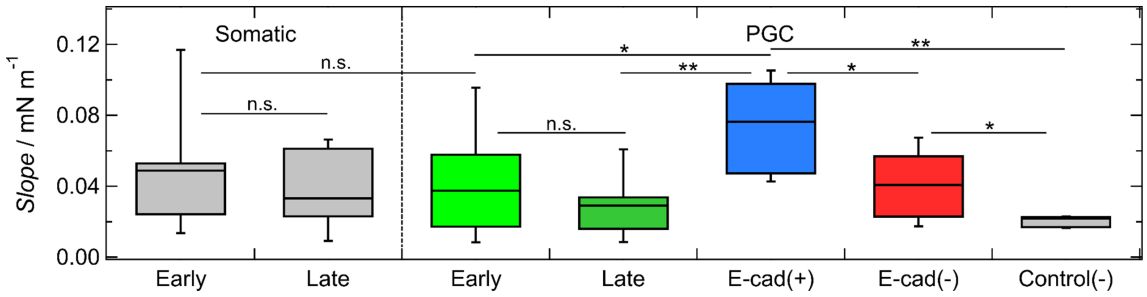

Figure 4-6 **Cortical tension.** Cortical tension shown through the slope of the trace curve (compression between parallel plates) as box-whisker-plots. Comparison between somatic endodermal cells and PGCs both isolated from embryos at stages 17–19 (**early**) and stages 28–30 (**late**) is shown. Additionally, the cortical tension of PGCs after E-cadherin over expression (E-cad (+)), E-cadherin knock-down (E-cad(-)) and PGCs in contact with a thiol-monolayer without E-cadherin (Control(-)) is shown. Box-whisker-plots: line represents the median of the distribution, boxes comprise the 25th and 75th percentile, whisker tops and bottoms are drawn to the 10th and 90th percentiles, respectively. P-values are calculated over T-Test/ Wilcoxon rank sum test. Not significant (n.s.) - $p>0.05$; * - $p<0.05$; ** - $p<0.01$; *** - $p<0.001$.

An important prerequisite for the validity of our approach is a maintained cortical tension and thereby conserved adhesion area regardless of the type of cell analyzed. A change in adhesion area is likely to occur if the cortical tension is altered by the treatment. Therefore, we measured the cortical tension of each cell type by parallel plate compression (Figure 4-6). The slope of the resulting force – compression curves is proportional to the cortical tension of cell (Schafer et al., 2013). A smaller stiffness of the cells would most likely result in a larger contact area and therefore generate larger adhesion forces. Except for the E-cad (+) PGCs, which were found to be slightly stiffer, we could not detect a systematic change of cortical tension in any of the categories that would explain our differences in cell adhesion. Therefore, it is safe to assume that the change in adhesion force is due to differences in the levels of E-cadherins on the cell surface and not due to an altered cell mechanics. In the case of E-cad (+) PGCs adhesion forces are even underestimated due to the larger stiffness, therefore we can safely assume that indeed E-cadherin overexpression is responsible for

the increase in interaction strength. A larger stiffness as observed for E-cadherin overexpressing cells most likely results from a larger cortical tension exerted by the contractile actomyosin cortex. Cells that overexpress E-cadherin are expected to recruit more actin to the plasma membrane attaching to the cytosolic adapter proteins and thereby generate a stronger and thicker cortex, which in turn produces an increased stiffness (Barry et al., 2014).

4.1.3 Discussion

Directional PGC migration is highly regulated both in time and space as it follows an intricate pathway in a varying environment. Most of our understanding of PGC migration comes from the model organisms *Drosophila melanogaster*, zebrafish, *Xenopus laevis* and mice. The dynamic changes associated with germ cell migration in *Xenopus* have been classified systematically (Terayama et al., 2013). Migration of PGCs within the endoderm is coupled to changes with respect to their locomotive and adhesive properties. Prior to the onset of active migration (before stage 25) isolated PGCs show only few protrusions and assume a predominately spherical morphology, similar to somatic endodermal cells. At stage 28 PGCs acquire an elongated shape and start displaying migratory activity. PGCs show a high level of cellular dynamics at stage 33/34 by formation of numerous bleb-like protrusions fostering migratory activity that switches between locomotive and pausing phases. Later, locomotion activity is reduced at stage 41 and subsequent migration of the PGCs to the gonads takes place via the dorsal mesentery. This mesentery is formed by two sheets of splanchnic mesoderm that surround the gut. As these sheets converge at the dorsal crest of the endoderm, PGCs can exit the endoderm and eventually incorporate into the dorsal mesentery (stage 45).

A number of germ cell specific proteins have been identified such as XDead end (Horvay et al., 2006) and XDAZL (Houston et al., 1998). XDead and XDAZL are mRNAs encoding RNA binding proteins that are required for dorsal migration since knockdown results in PGCs that are unable to disperse (Houston and King, 2000, Horvay et al., 2006). Therefore, it is assumed that these two proteins are functionally linked to each other as well as to the regulation of adhesive

properties. A more recent study has provided further insight into the role of Dead end in the context of bleb-based motility of zebrafish PGCs (Goudarzi et al., 2012). Messenger RNAs encoding myosin light chain kinase as well as transcriptional repressor Zeb1 were identified as putative Dead end targets. Zeb1 could be responsible for the downregulation of E-cadherin, as observed during the transition of zebrafish PGCs to their active migratory state (Blaser et al., 2005). Regulation of cellular adhesion is known to play an important role in the context of germ cell migration in different animal species (Richardson and Lehmann, 2010). Previously, we found that *X. laevis* PGCs isolated from the tail-bud stage (st.28-30) show a decrease in E-cadherin mRNA levels in contrast to somatic endodermal cells and PGCs from the neurula stage (st.17-19) (Dzementsei et al., 2013). Moreover, a newly established “under-agarose” cell migration assay was employed to study PGC migration in vitro. PGCs isolated from tailbud stage embryos were placed underneath a layer of agarose on top of bovine serum albumin (BSA)-coated culture dishes to prevent non-specific binding of the cells. The agarose gel on top created a confined environment, which allowed the cells to generate sufficient traction force. Under these conditions, cells migrate actively by producing blebs. The observation that isolated PGCs are able to migrate under these conditions, suggests that they do not require specific cell-cell or extracellular matrix adhesion for motility. This finding is in accordance with our observation that late PGCs essentially display very low E-cadherin mediated interactions. We recently carried out single-cell force spectroscopy (SCFS) to investigate whether cell-cell adhesion is diminished during the transition of Xenopus PGCs to active migration. We found that cell-cell adhesion between migratory PGCs and somatic cells is significantly decreased, as compared to the interactions of PGCs in an earlier state. These experiments suggested that PGCs reduce their adhesiveness to the surrounding somatic cells during development. But in this previous work we could not assign this to the reduced E-cadherin expression. Studies on zebrafish PGCs showed that reduced intercellular adhesion via E-cadherin is important for proper PGC migration (Blaser et al., 2005, Goudarzi et al., 2012, Kardash et al., 2010). Down-regulation of E-cadherin is also known to result in increased migratory behavior of germ cells in Drosophila melanogaster, (Kunwar et al., 2008) while other cell adhesion molecules such as integrins and selectins are known to be involved in the

interactions of mouse PGCs with their surrounding during migration (De Felici, 2000). Altogether, data from different model organisms indicate that lowering of cell adhesion fosters PGC motility. This has also been confirmed by our own qPCR data with *Xenopus* PGCs suggesting that the loss of adhesiveness to the surrounding endodermal somatic cells is mainly due to down-regulation of specific cell adhesion molecules such as E-cadherin (Dzementsei et al., 2013). Interestingly, somatic cells retain a similar level of mRNA encoding E-cadherin within the same period of development.

In this study, we quantified the adhesion of PGCs and somatic cells harvested at different stages to E-cadherin coated surfaces to elucidate the role of E-cadherin in migration of PGCs in *X. laevis* embryos. The setup allows us to focus on a particular molecule without interference from other cell adhesion molecules (CAMs). It is clear that besides CAM-CAM recognition, cellular adhesion also results from a competition between attractive van der Waals interactions and electrostatic repulsive mediated by, for instance, charged (glyco)lipids. In our SCFS experiment not only molecular recognition events between E-cadherin molecules on the cell surface and on the substrate are monitored but also non-specific interactions that appear as a background force. We found that the base level of the interaction was about 150 pN adhesion force. At the other end of the scale overexpression of E-cadherin produces adhesion forces higher than 300 pN for the same dwell time and even slightly elevated cortical tension. In between these two limit we find a significant difference between actively migrating PGCs with low adhesion force and pre-migratory ones that show essentially the identical adhesion force as found for somatic cells. Knock-down of E-cadherin with morpholino oligonucleotides shows only a negligible further decrease in adhesion as compared to late PGCs, suggesting that the number of E-cadherin molecules on the cell's surface is already extremely low. This kind of comparison is possible since the cells display essentially unaltered cortical tension ensuring a constant adhesion area that would otherwise impact the measured force. Importantly, the forces found in our experiments are similar to those probing PGCs and adherent somatic ones, (Dzementsei et al., 2013) where late PGC also display smaller unbinding forces (< 290 pN) compared to early ones (> 320 pN). Taken together, our approach using defined substrates functionalized with E-cadherin produces more significant results with a smaller spread than cell-cell experiments, which is

certainly due to the smaller background noise from other ICAMs and a more broadly varying adhesion area if two soft cells were brought into contact (Dzementsei et al., 2013).

Besides the maximum adhesion force that comprises individual molecule pairs as well as clusters and non-specific interactions, we also counted the number of individual rupture events in every force curve. The events were classified as rupture of homotypic E-cadherin bonds based on a comparison with single molecule force spectroscopy experiments. Here, the picture is consistent with the maximum adhesion force. We found a decreasing number of single rupture events for late PGCs in comparison to early ones. While almost every force curve also shows single rupture events, the number is almost cut into half for late PGCs. Altogether, our study confirms that downregulation of E-cadherin is a key step on active migration of primordial germ cells in *X. laevis* embryos. The necessary traction force to accomplish a directed motion is therefore most prominently provided by non-specific van der Waals forces rather than specialized molecules. It has been proposed that an independent migration mechanism, referred to as 'chimneying' in resemblance of a common climbing technique to conquer rock clefts, can account for 3D migration of cells (Paluch and Raz, 2013). Chimneying can be accomplished in the absence of specific adhesion as shown, for instance, by leukocytes, which can migrate by squeezing and exerting pushing forces perpendicular to the cell boundary (Lammermann et al., 2008). Yip et al. (Yip et al., 2015) showed that chimneying requires a balance between intracellular pressure and membrane cortex strength. Traction is mainly achieved by pushing against the wall. Pushing forces that originate from actin polymerizing against the sides of a cell embedded in confinement also allow for directional cell migration (Hawkins et al., 2009). It has been suggested that cortical flow of actin coupled to friction arising from both nonspecific and specific interactions with the substrate could move cells in confinement forward (Hawkins et al., 2011). Previously, reproducible PGC migration for late stage PGCs was achieved using a so-called "under-agarose" migration assay. There we found that blebbing is strongly enhanced in these migratory PGCs, which together with a reduced adhesiveness allows the cells to propel forward to their destination. Our electric impedance measurements with both early and late single isolated PGCs also suggest that internal cell contractility is not directly coupled to cell-cell adhesion

(Dzementsei et al., 2013). Similar findings have been reported for zebrafish PGCs (Blaser et al., 2005, Kardash et al., 2010, Goudarzi et al., 2012). In conclusion, we claim that a decrease of the E-cadherin expression level is required to change PGCs from a sessile to an actively migrating state. A change of a few tens of Piconewtons decides whether a cell moves or stays in place.

4.2 Dynamics and mechanics of epithelial-mesenchymal transition

The metal induced energy transfer (MIET) measurements for this chapter were done in cooperation with Dr. Alexey Chizhik (Georg-August-University, III. Physical Institute, Göttingen, Germany). He analyzed the acquired data and calculated the three-dimensional reconstruction of the basal cell membrane.

4.2.1 Introduction

The observation that epithelial cells can transit into mesenchymal cell is commonly described as the epithelial-mesenchymal transition (EMT) and occurs in many biological processes (Lamouille et al., 2014, Kalluri and Weinberg, 2009). EMT for epithelial cells is characterized by loss of cell junctions and apical-basal polarity, reorganization of their cytoskeleton, change of cell shape and gene expression, which enhance migratory capacity, invasiveness and resistance to apoptosis (Lamouille et al., 2014, Kalluri and Weinberg, 2009, Kalluri, 2009, Thiery et al., 2009, Thiery and Sleeman, 2006).

In the context of epithelial-mesenchymal transition and its consequential changes in cellular mechanics and dynamics we wanted to look deeper in the morphological change of the cell itself. Through the multiple biochemical changes within the transition, the alteration of cellular dynamics in cell-substrate as well as cell-cell contacts are crucial. To globally determine these variations, over the entire EMT, we wanted to monitor all stages of the EMT of normal murine mammary gland epithelia (NMuMG) cells, which are commonly used as *in vitro* model for EMT (Gal et al., 2008, Shirakihara et al., 2007, Netherton and Bonni, 2010).

For visualizing the EMT the recently newly developed metal induced energy transfer (MIET) nanoscopy (Chizhik et al., 2014) was used. Through a z-resolution of a few nanometers it allows to visualize and quantify the distance between the cell and the substrate precisely at the subcellular level (see chapter 3.4.2 *p.* 52). Additionally the cellular dynamics of the EMT such as global changes

in cell-cell as well as cell-substrate contacts were measured by electric cell-substrate impedance sensing (ECIS) (Schneider et al., 2011) (see chapter 3.6 *p.* 57). To trigger EMT the well-known cytokine transforming growth factor-ß1 (TGF-ß1) (see chapter 2.2.3; *p.* 17) was used.

The MIET measurements showed an altering average cell membrane-metal surface distance during the EMT. The NMuMGs first lifted up from the surface and after reaching the final mesenchymal state the cell-substrate distance dropped down to the same level as found for the initial epithelial state and remained constant. ECIS measurements also revealed a change in the impedance signal after addition of TGF-ß1 to the NMuMGs. The resonance to the cytokine was for the most part consistently with the MIET measurements.

4.2.2 Results

4.2.2.1 Effect of TGF-ß1 on cell morphology and principles of MIET

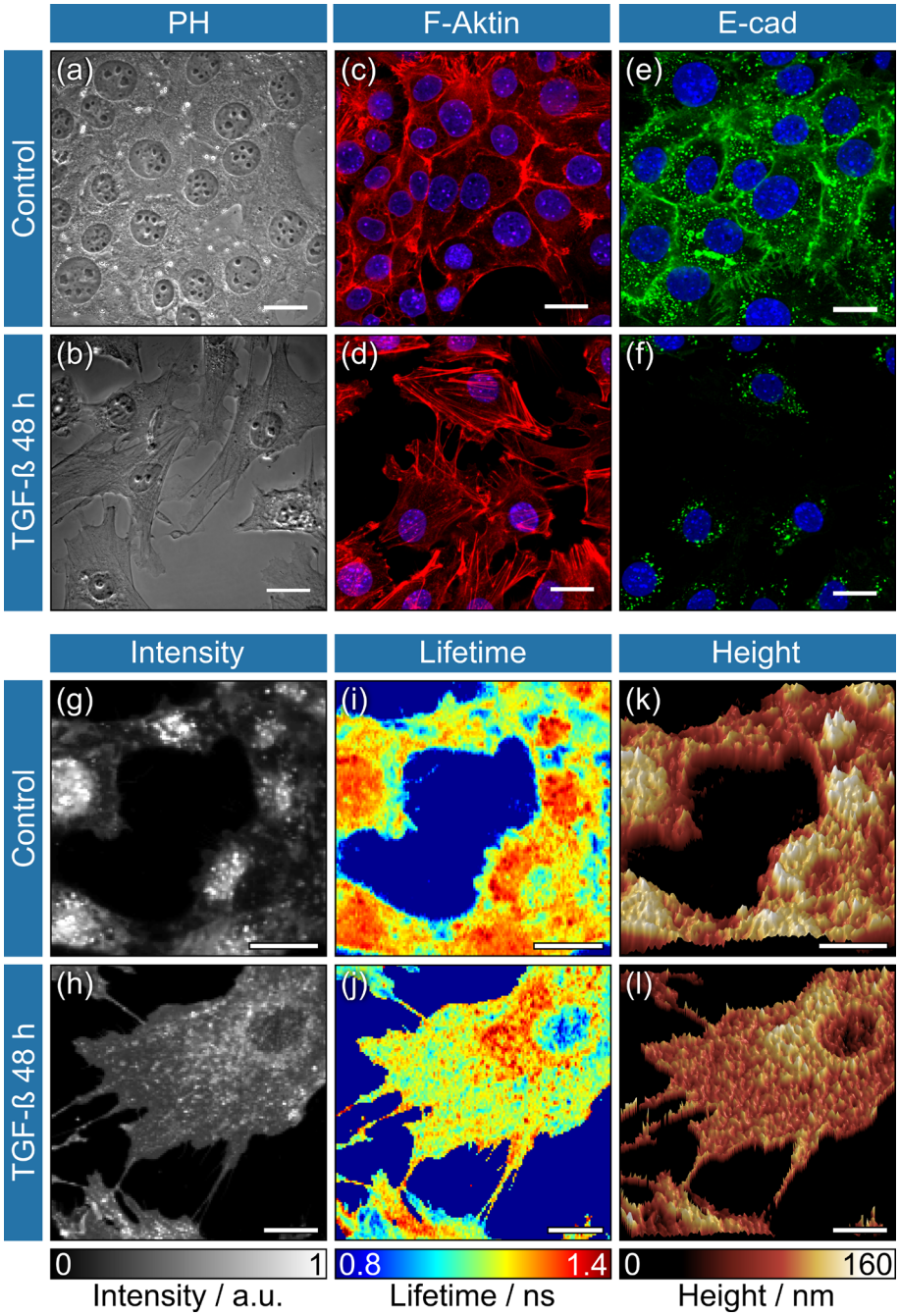

Figure 4-7 **TGF-β1 induced shape changes of NMuMG**. Phase contrast images (a-b) display NMuMGs without (control) and with TGF-β1 treatment (10 ng/ml) for 48 h. (c) and (d), display F-actin labeled in red (Alexa Phalloidin 546) and the nucleus in blue (DAPI). (e) and (f) show E-Cadherin labeled in green (Alexa Fluor 488) and the nucleus in blue (DAPI). Scale bars: 20 µm; **Fluorescence lifetime imaging and three-dimensional reconstruction of the basal cell membrane in response to TGF-ß1 treatment**. Simultaneously acquired fluorescence intensity (g-h) and lifetime (i-j) images of the basal membrane of living NMuMG cells grown on a gold-covered glass substrate. Three-dimensional profiles computed from fluorescence lifetime images from living NMuMG cells (k-l). NMuMGs without (control) and after TGF-β1 treatment (10 ng/ml) for 48 h. Scale bars: 20 µm.

Aim was to gain insight in the alteration of cellular dynamics in cell-substrate contact during the EMT by measuring the cell-substrate distance of epithelial NMuMGs cell with metal-induced energy transfer (MIET) nanoscopy. Before measuring the changing cell-substrate distance we proved that the addition of TGF-ß1 induced the change of the cells phenotype from epithelial to mesenchymal.

Figure 4-7 illustrates the morphological changes of the NMuMG cell line in response to cytokine TGF-ß1 exposure using phase contrast microscopy, fluorescence microscopy and the recently newly introduced MIET nanoscopy. The phase contrast images in Figure 4-7 (a) and (b) show nicely how the NMuMGs transformed from an epithelial ordered cell layer to individual elongated mesenchymal-like cells. After 48 h of TGF-ß1 treatment the NMuMGs are also significant larger compared to untreated cells. The fluorescence images reveal, that the F-actin (red) is reorganized to well defined stress fibers, which cross the entire cell (Figure 4-7 (c) and (d)). This typical change of F-actin-organization for EMT has been shown before (Haynes et al., 2011, Shankar and Nabi, 2015) and proves that the NMuMGs undergo the EMT. Fluorescently labeled E-cadherin indicates a reduction of E-cadherin expression in the NMuMGs in the response of the TGF-ß1 treatment (Figure 4-7 (e) and (f)), which also is a hallmark of this transition (Lamouille et al., 2014). After 48 h of TGF-ß1 treatment the amount of E-cadherin is significantly reduced and delocalizes in the cells. As an adhesion molecule, E-cadherin is down regulated during the EMT like other epithelial markers, e.g. ZO-1. E-cadherin is prevalent at adherens junctions and involved in many morphoregulatory processes, e.g. establishment of tissue boundaries or cell differentiation (Leckband and de Rooij, 2014, van Roy and Berx, 2008). These images in Figure 4-7 serve as an additional proof that the used cytokine TGF-ß1 induced EMT in NMuMGs cells and that after 48 h TGF-ß1 treatment the cells act like mesenchymal cells.

Image (g) - (l) on Figure 4-7 show the principles of nanoscopy MIET. Metal-induced energy transfer can be used to localize fluorescent molecules along one dimension with nanometer accuracy. The method uses the fact that the energy transfer rate from excited fluorescent molecules is dependent on the distance to the metal layer (Chizhik et al., 2014). Therefore the fluorescence lifetime as a function of the distance to the metal surface was determined. A thin

semitransparent 20 nm gold film deposited on a glass cover slide was used. To map the distance between cell and surface, the cell was stained with a membrane-staining fluorophore (Cell Mask Deep Red MM part) and detected by the fluorescence lifetime. Details about the setup can be found in the study of Chizhik et al., 2014.

Figure 4-7 (g) – (j) show examples of collected fluorescence intensity and lifetime images of the basal membrane of NMuMGs cells, respectively. We used the lifetime information for reconstructing a three-dimensional map of the basal membrane presented in Figure 4-7 (k) and (l). Details about the computation of the local height of the basal membrane above the surface can be found in the previous study (Chizhik et al., 2014). Figure 4-7 (g)/(i)/(k) shows untreated NMuMGs as a developing epithelial layer and (h)/(j)/(l) represent one transformed large cell treated with TGF-ß1 over 48 h.

After proving the EMT induction by administration of TGF-ß1 on NMuMGs and the principles of MIET we investigated the transition in response to TGF-ß1 treatment on different time scales and compared to untreated samples.

In Figure 4-8 we show the epithelial-mesenchymal transition at different stages using MIET. The reconstructed three-dimensional structures of the basal membrane were taken at 0/12/24/48/72 h after treatment of TGF-ß1 ((a)-(e)).

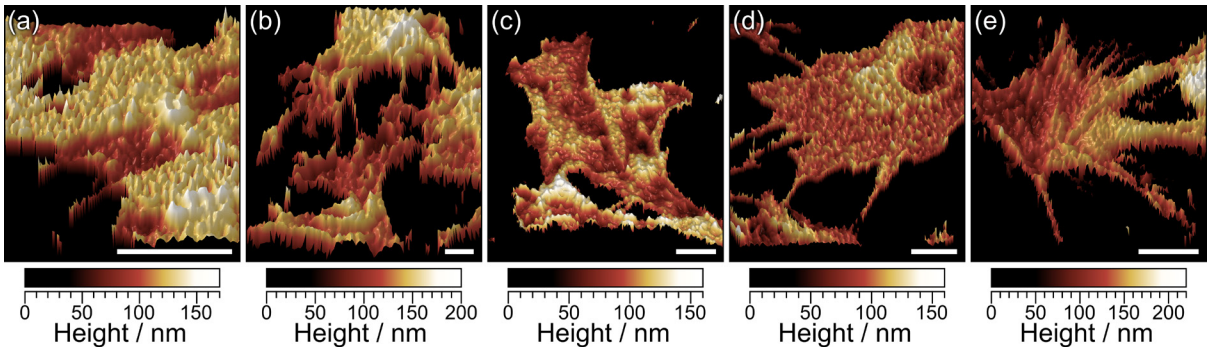

Figure 4-8 **Three-dimensional reconstruction of the basal cell membrane at different stages of EMT.** Three-dimensional profiles computed from fluorescence lifetime images of NMuMG cells recorded at 0 h (a), 12 h (b), 24 h (c), 48 h (d), 72 h (e) TGF-ß1 treatment (10 ng/ml); Scale bars: 20 µm.

Figure 4-8 illustrates the time dependence size changing of the single NMuMGs cells. In response to EMT the NMuMGs changes from an epithelial ordered cell layer (a) to single cells with increasing cell size ((d) and (e)). The single cells with mesenchymal character exhibit a more homogenous distance to the surface ((d) and (e)) comparing to the epithelial cell layer at the beginning of the EMT ((a) and (b)).

4.2.2.2 Cell membrane-substrate distance during EMT

The average cell membrane-substrate distance between untreated and TGF-ß1 treated NMuMGs are taking together in Figure 4-9. For every time point we measured the fluorescence lifetime from 10-30 cells. The colored area around the data points indicate the standard error of mean (SEM). Untreated cells maintain a constant average cell membrane – substrate distance of around 120 nm, the variation of the distance between cell membrane and substrate is only around 10 nm over the entire time. TGF-ß1 treated cells, in contrast, show an altering average cell membrane-substrate distance during the EMT. In the first hours of the transition the NMuMGs lift up from the surface. The average distance rises from around 120 nm up to 156 nm. After reaching the peak of 156 nm at around 5 h TGF-ß1 treatment, the cell membrane – substrate distance decreases again over the next 14 h. At around 18-20 h of TGF-ß1 treatment the same level of untreated cells is reached. After 48 h TGF-ß1 treatment the NMuMGs are still at the same cell-substrate distance as untreated cells. The results show that the cells are changing the distance to the substrate only during the EMT itself. After reaching the final mesenchymal state the cell-substrate distance stays constant and at the same level as found for the epithelial state.

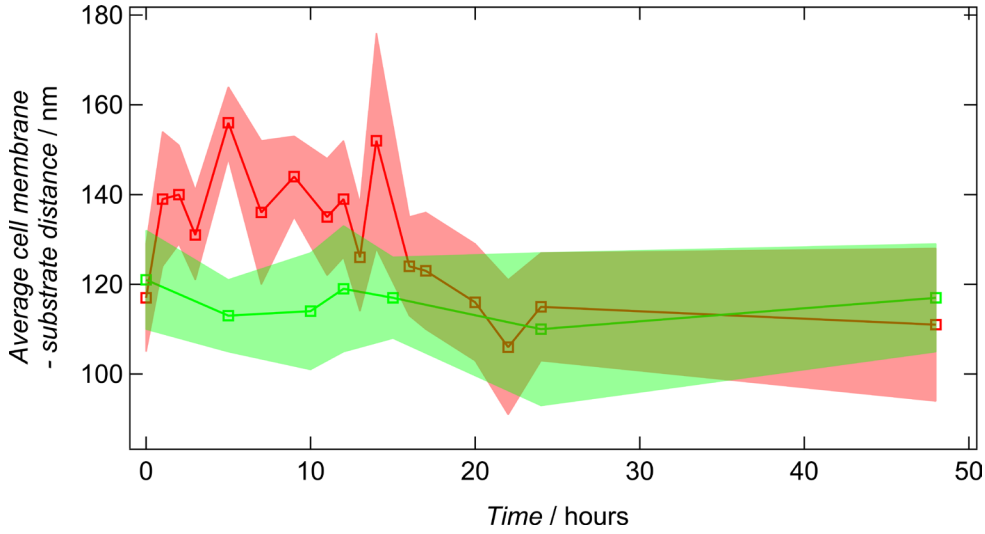

Figure 4-9 **Average cell membrane - substrate distance (nm) between untreated (green) and TGF-ß1 treated (red) NMuMGs.** Standard Error of Mean (SEM) is illustrated as colored area around the data points.

These findings are valid for single cells and also non confluent NMuMG cell layers. As the EMT occurs in nature only in fully polarized epithelial cell-layer (Polyak and Weinberg, 2009) we also measured the effect of TGF-ß1 on confluent NMuMG cell layers right after TGF-ß addition, 12 h and 24 h. We could demonstrate that the cells show the same general behavior as single cells and reveal the same distance between cell membrane and surface during the same time course (Figure 4-10).

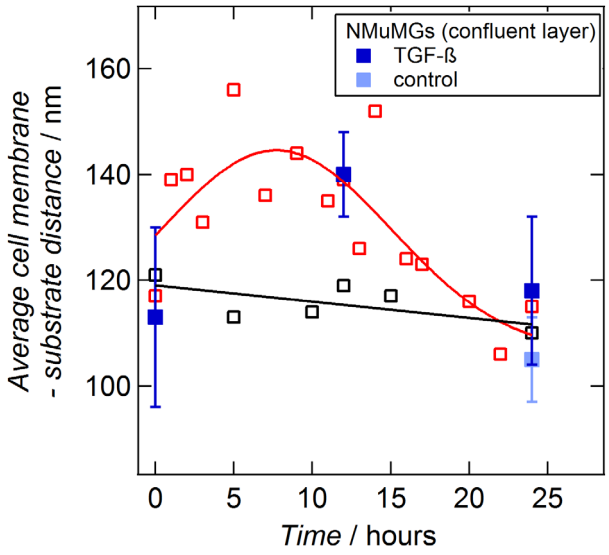

Figure 4-10 **Average cell membrane - substrate distance (nm) between untreated and TGF-ß1 treated single NMuMGs and cell layer.** Untreated cells (black) with linear fit and TGF-ß1 treated cells (red) with Gaussian fit. Confluent cell layer with SEM at 0/12/24 h TGF-treatment (dark blue) and without TGF-ß1 treatment (control; bright blue).

MIET imaging can also be used to monitor the cell motility by using time-elapsed imaging of the cell–substrate distance. With this opportunity we followed the motion of NMuMGs cells over the surface with an axial resolution of 3 nm over the first six hours of TGF treatment where the initial and strongest changes in cell-substrate distances appeared. Therefore, we took a fluorescence intensity image nearly every minute to monitor the beginning of EMT as highly time resolved as possible. The result is shown in Figure 4-11. Each dotted line represents one cell analyzed over time. The colors indicate the different measurements over maximal 1.5 hours. In some samples we were able to investigate up to two cells simultaneously which results in two dotted-lines in the plot. Figure 4-11 shows that in the very first hour the cell lifts up from the surface. Starting from 110 nm the cell goes up to 145 nm, afterwards the other cells fluctuate at this height for the next 5 h and then move again to the surface.

We visualized the rise of the cell membrane – substrate distance by showing examples of reconstructed three-dimensional structures of the cells basal membrane at different time spots (I-IV) with the same height scale. These 3D constructions underline the observed changes in cell – surface height and show clearly how the cell is detaching from the surface.

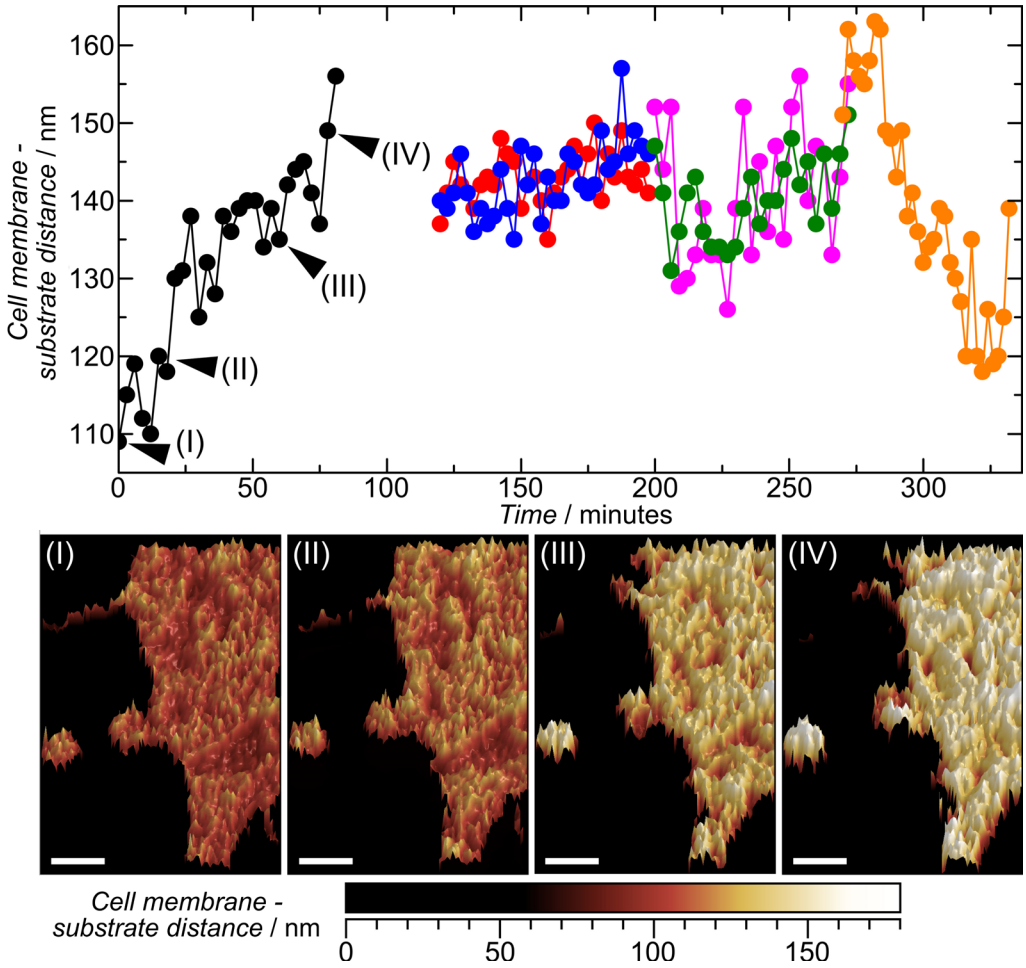

Figure 4-11 **Time-elapsed imaging of the cell membrane – substrate distance.** Cell membrane – substrate distance (nm) over the first six hours TGF-ß1 treatment (10 ng/ml). Each dotted line represents one cell, which was analyzed over time. 0-80 min (black), 120-200 min (blue/red), 200-270 min (green/pink), 270-330 min (orange). **Three-dimensional reconstruction of the basal cell membrane.** Three-dimensional profiles, computed from fluorescence lifetime images of NMuMG cell at four different time points (I-IV) at the same cell membrane-metal surface distance scale; Scale bars: 20 µm.

In order to confirm that these results rely on the EMT, we also made different time series of fluorescence intensity images of untreated cells. These time series reveal a constant cell membrane – substrate distance of around 120 nm over the full measuring time on different time slots (Figure 4-12).

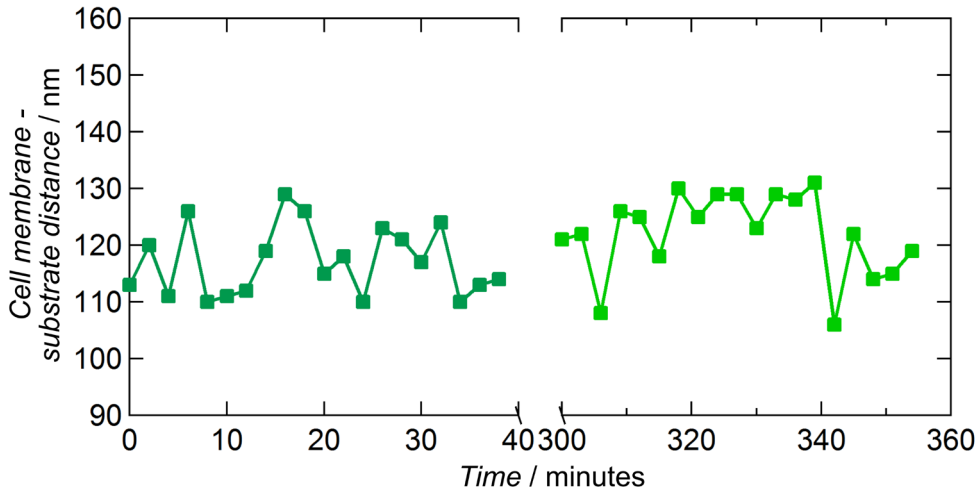

Figure 4-12 **Time-elapsed imaging of the cell membrane – substrate distance**. Cell membrane – substrate distance (nm) at different time slots of untreated NMuMG cells. Each dotted line stays for one cell, which was analyzed over the time. Timescale indicate minutes after changing the cell culture medium to mimic the TGF-ß1 addition.

This supports that the changes in the time series of TGF-ß1 treated NMuMGs are caused by the onset EMT and does not originate from the measurement itself.

4.2.2.3 Dynamic changes in focal adhesion

In the time series of the cell membrane – metal surface distance over the first 6 h of the EMT fluctuation of the adhesion by building and dissolving focal adhesion points could be observed. We illustrate these observation by showing the time evolution of cross sections of the basal cell membrane during a time period of 0-1.5 h TGF-ß1 treatment.

Figure 4-13 reveal that at 60 µm distance the focal adhesion (black arrow) is dissolved over time and at around 10 µm a new focal adhesion point is formed (red arrow). This reveals that MIET is capable for investigating these dynamics in cellular adhesion and give us an insight in the fluctuation of adhesion points.

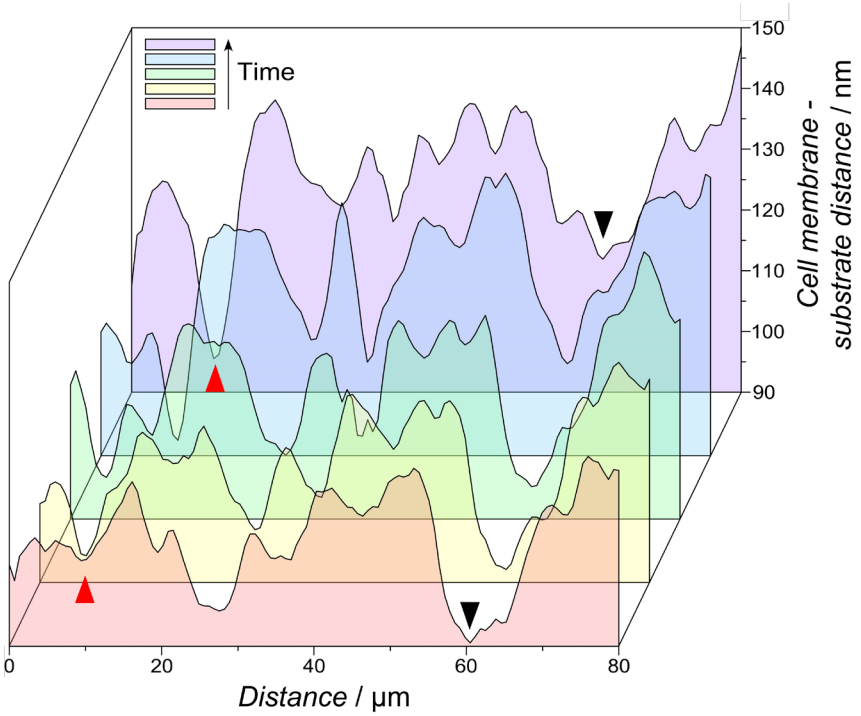

Figure 4-13 **Cross sections of basal cell membrane.** Cross sections were taken in dependence of the distance to the metal surface at different time points from the measurement 0-80 min TGF-ß1 (black dotted line *Figure 4-11*). The red arrow indicates building of adhesion spot and the black arrow indicates dissolving of adhesion spot.

4.2.2.4 Impact of TGF-ß1 on NMuMG cells measured by ECIS

In addition to MIET, the cellular dynamics during EMT such as changes in cell-cell as well as cell-substrate contacts were analyzed by electric cell-substrate impedance sensing (ECIS) (see chapter 3.6 *p.* 57). Therefore, the EMT process was followed by monitoring the impedance of NMuMG cells as a function of time in order to capture the dynamic structural alterations of the transition without interference from staining. The time period of interest was the first 24 h after exposure of TGF-ß1. In this time range the MIET measurements revealed that the NMuMGs lifted up from the surface and afterwards reduced the cell-substrate distance to the same level of untreated cells.

Fluctuations of the impedance signal reflect temporal changes in cell-substrate and cell-cell contacts since the signal depends on the current flow underneath and through adherent cells and in between cells and substrate (Schneider et al., 2011). To illustrate the progress of a time resolved impedance signal with and without the addition of TGF-ß1 on epithelial NMuMG cell layer, an example is shown in Figure 4-14.

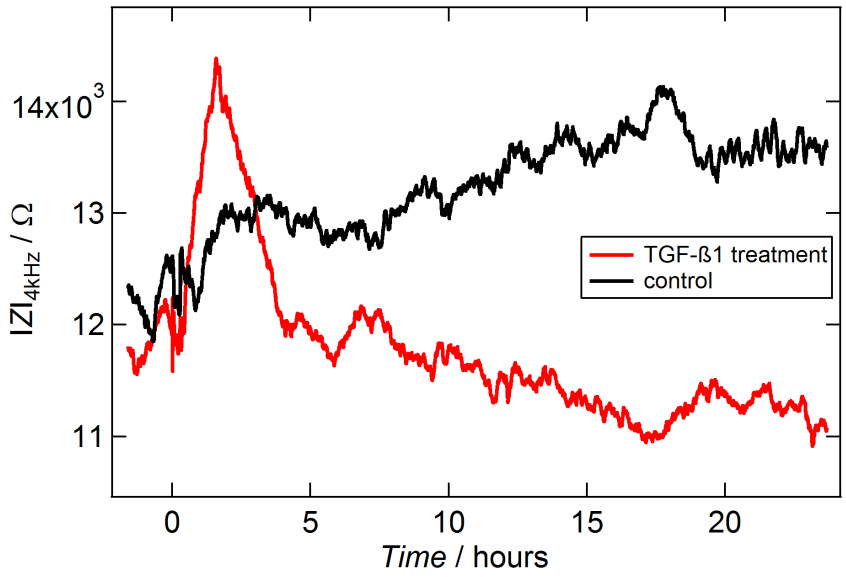

Figure 4-14 **Time resolved absolute impedance (|*Z*|) spectrum for at 4 kHz for NMuMG cells** (150.000 cells per chamber) after the addition of 0 ng/ml (control; black) and 15 ng/ml TGF-ß1 (red) (t=0) for 24 h.

In the response of TGF-ß1 addition the impedance shows a clear peak at 1.5 h (Figure 4-14) of TGF-ß1 exposure. Until this time point the impedance for control cells, where only cell culture medium was added at t = 0 h, increases about 7 % and stays at this level for the next 6 h. After the peak the impedance for TGF-ß1 treated NMuMGs decreases (between 7.5 h and 17.5 h) with a slope of -82 Ω/h. In the same time interval the impedance for control cells increases with a slope of 90 Ω/h. The first peak followed by a continuous decrease of the impedance could be found for all impedance measurements in response to the TGF-ß1 addition. From 17.5 h to 24 h the impedance for TGF-ß1 treated cells largely fluctuates while |*Z*| of the control cells remains constant after 19 h until the end of measurement.

Changes in the impedance signal can be attributed to morphological/adhesive alterations of cells (Arndt et al., 2004, De Blasio et al., 2004). Looking at the impedance, one can say that NMuMGs undergo the strongest morphological/adhesive changes in response to TGF-ß1 in the first 5 h of exposure. Here the biggest changes in impedance could be detected. For control cells we can see that the impedance remains not constant until 19 h after addition of cell culture medium. From the literature it is known that the impedance remains constant when the NMuMGs are fully spread over the gold electrode and reach

a confluent monolayer of cells (Giaever and Keese, 1993). So it seems that the control cells in Figure 4-14 reach the full confluent monolayer after 19 h of the experiment. The changes in impedance could also come from the micromotion from a constant movement of the monolayer, which additionally can cause fluctuations in the curve of impedance (Giaever and Keese, 1991).

To address the changes associated with TGF-ß treatment in the context of an equivalent mode, ECIS also allows to gain various cell-specific parameters like the barrier resistance between cells (R_b), resistance in the cleft between cells and substrate (α) and the capacitance of the cell membrane (C_m) simultaneously. Therefore, frequency sweeps of the impedance were recorded and an area contact model, which was first developed by Giaver and Keese (Giaever and Keese, 1991, Lo and Ferrier, 1998), was used to obtain the before mentioned parameters.

The exposure of NMuMG cells to TGF-ß1 resulted in a lower barrier resistance than found for untreated cells. An example can be found in Figure 4-15. This example represents the general response of R_b to TGF-ß1 addition. Here, R_b is normalized to the value before the addition of TGF-ß1 (or normal cell culture medium for untreated cells). The barrier resistance between cells originates from the cell-cell contacts, especially tight junctions (Schneider et al., 2011). Looking closer at Figure 4-15, we can observe that opposing to the overall behavior, the R_b value rises in the first hour about 37 %. The increase in barrier resistance suggests that the cell-cell contacts get tighter right after the addition. An initial drop of the signal can be observed before this rise. This drop of impedance is caused by the interruption of the equilibrium of the cellular system due to the addition of cytokine/cell medium (Schneider et al., 2011). One can also see this effect in the progress of α and C_m. Nevertheless, after the first hour R_b gets strongly reduced in the next 3 h and then continuously decreases over the rest of the measurement to values 40 % lower than before the addition of TGF-ß1. The decreasing barrier resistance can be attributed to the loss of cell-cell contacts during EMT.

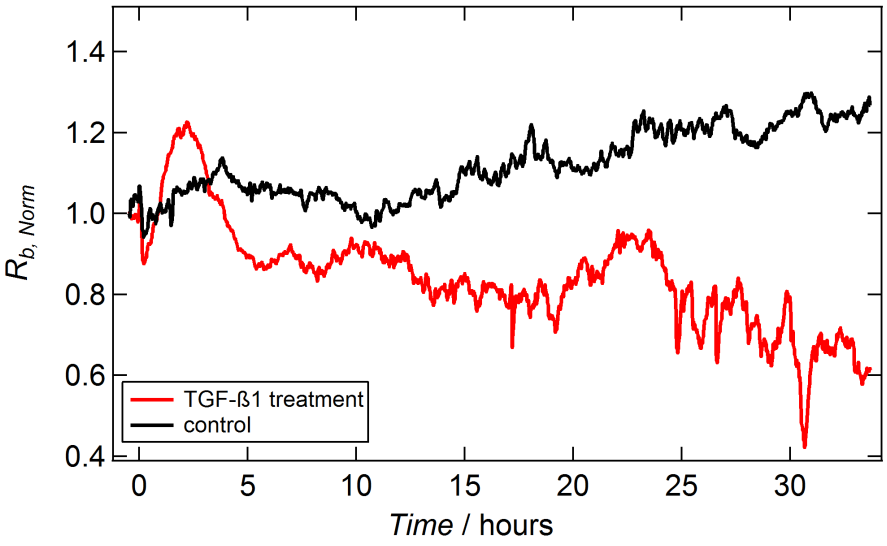

Figure 4-15 **Time resolved progress of the normalized barrier resistance between cells for NMuMG cells** (150.000 cells per chamber) after the addition of 0 ng/ml (control; black) and 10 ng/ml TGF-ß1 (red) (t=0). R_b is normalized to the R_b value before the addition of TGF-ß1/cell culture medium.

In the absence of TGF-ß1 the barrier resistance for control cells in Figure 4-15 first fluctuates within 10 % around a base level. At around 11 h it starts to increase continuously until the end of the measurement to around 25 % higher values. This increase shows that due to the formation of a full cell monolayer the cells exhibit a stronger cell-cell contact. The time point roughly 11 h after addition can be seen as a turning point where the data traces of R_b for TGF-ß1 treated and untreated cells move apart.

Looking at the resistance in the cleft between cells and substrate (α) in response to TGF-ß1 treatment an example is illustrated in Figure 4-16. The progress of α is also normalized to the value before the addition of TGF-ß1 (or normal cell culture medium for untreated cells). The characteristic steps in Figure 4-16 represent the general response of α to TGF-ß1 addition in ECIS measurements. One key step is that, after the cellular system reaches the equilibrium again, α exhibits a first peak after TGF-ß1 exposure. In Figure 4-16 the peak is at around 2 h after addition (highlighted in Box I; Figure 4-16) and is similar to the value of α found for control cells. For control cells this peak could not be observed. In other ECIS measurements for TGF-ß1 treated NMuMGs it could be seen that the first peak of α is bigger and reaches higher values than untreated cells. However, the subsequent, strong decrease of α to a minimum and the following increase are

other characteristic steps. In Figure 4-16 the value for α decreases about 17 % to its minimum at around 3 h after TGF-ß addition. The increase of α can be seen from around 5 h until 17 h of TGF-ß1 treatment, were α reaches the same values as before the decrease. Additionally, at 17 h after TGF-ß addition, one can see that α for treated cells reaches almost the same values as for untreated cells and then fluctuate at this level.

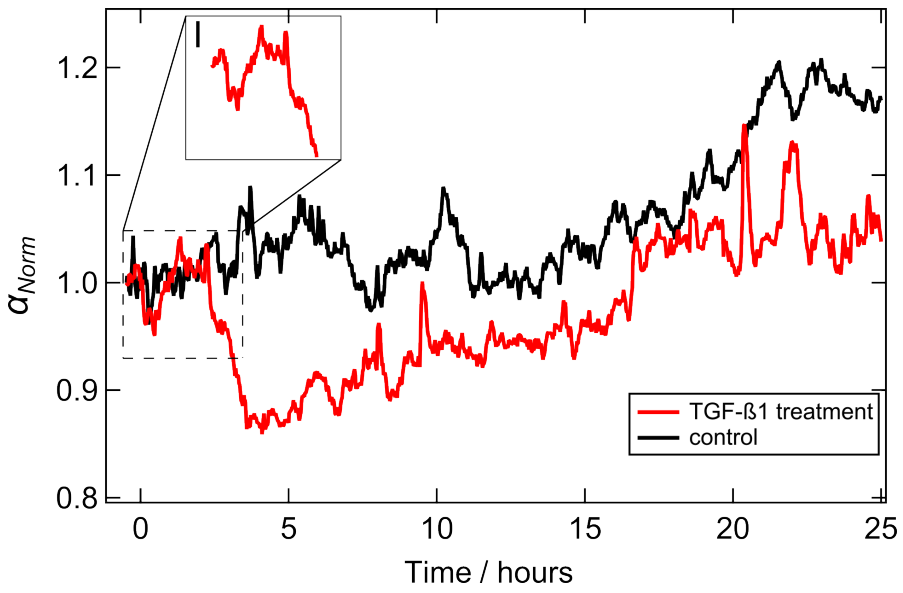

Figure 4-16 **Time resolved progress of the normalized resistance in the cleft between cells and substrate for NMuMG cells** (150.000 cells per chamber) after the addition of 0 ng/ml (control; black) and 10 ng/ml TGF-ß1 (red) (t=0). α is normalized to the α value before the addition of TGF-ß1/cell culture medium.

The decrease of α to a minimum and the following increase to nearly the values found for control cells is in a good accordance to the findings of MIET measurements. In contrast, the initial increase of α is not reflected in the MIET experiments.

A decreasing resistance corresponds to an increasing distance between cells and surface (Lo and Ferrier, 1998). This means that the NMuMGs increase the distance between themselves and surface and afterwards they decrease it again to the initial level which is close to α of untreated cells. This behavior fits to the observation from the MIET method. Also the time range for the changes in cell-substrate distance is nearly the same for both methods. In both methods the peak of cell-surface height can be found at around 5 h after TGF-ß1 addition. Also the

time range for the reduced cell-substrate distance until to the level of untreated cells lays at around 17-20 h after TGF-ß1 exposure. However, the first increase after half hour exposure of TGF-ß1 suggests that the cells move down to the substrate, this could not be observed with MIET.

For untreated cells α reveals a constant base level. However, in the course of the measurement α increases to higher values. The increase of 20 % for α can be found in Figure 4-16 between 14 h and 21 h. The first constant base level for α followed by a continuous increase could be found for all measurements. The increase of α leads to a reduced height between cell and surface and could not be found in the MIET experiments.

Looking at the membrane capacity (C_m), a general steeper decrease for TGF-ß1 treated NMuMGs than for untreated cells can be observed over the entire measurement. Figure 4-17 shows an example for the progress of C_m of TGF-ß1 treated and untreated (control) NMuMGs. The membrane capacity for TGF-ß treated cells first decreases in the same manner as the control cells but at 5.5 h it reveals a significant steeper decrease to values 25 % lower than before the addition of TGF-ß1. The significantly reduced membrane capacity during EMT could be caused by stress fiber formation and a concomitant decrease of membrane area due to morphological changes (Lo et al., 1995, Schneider et al., 2011). The membrane capacity for untreated cells is less reduced after 5.5 h and reaches a constant base level for C_m at around 15 h after the beginning of the experiment. The values for C_m at this point are around 10 % lower than at the beginning of the measurement.

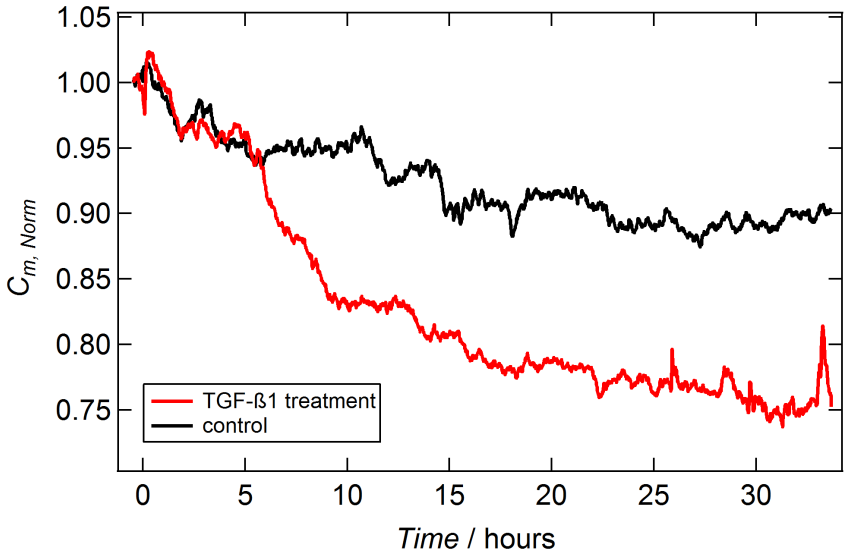

Figure 4-17 **Time resolved progress of the normalized capacitance of the cell membrane for NMuMG cells** (150.000 cells per chamber) after the addition of 0 ng/ml (control; black) and 10 ng/ml TGF-ß1 (red) (t=0). C_m is normalized to the C_m value before the addition of TGF-ß1/cell culture medium.

4.2.3 Discussion

The obtained data reveal that the metal induced energy transfer (MIET) nanoscopy is a very good method to gain knowledge of the precise cell–substrate distance as a function of time and location with matchless resolution. With MIET the different states of the epithelial-mesenchymal transition of normal murine mammary gland epithelia (NMuMG) cells could be identified.

MIET relates to the method of Förster resonance energy transfer (FRET) (Forster, 1948) and measures the energy transfer efficiency from donor molecule to metal surface plasmons. This enables to localize emitters with nanometer lateral accuracy over an axial distance range of more than 100 nm. This is an order of magnitude larger than for conventional FRET (Clegg, 1995, Wu and Brand, 1994). Additionally it does not need any hardware modification to a conventional fluorescence-lifetime imaging microscope (FLIM) (Berndt et al., 2010) and makes it therefore a reasonable alternative tool to FRET and also other recently developed super-resolution imaging techniques (Hell and Wichmann, 1994, Rust et al., 2006, Betzig et al., 2006, Gould et al., 2008).

Epithelial-mesenchymal transition has been reported as an important biological process which occurs in development, tumor progression and nonmalignant degenerative disorders (Zavadil and Bottinger, 2005). The focus of this work laid on the progress of cellular adhesion to the surface during EMT. How does the adhesion between cell and surface alter in response of dynamic morphological changes and directional motility?

The results showed that the cells changed the distance to the substrate only during the EMT itself. It seems that through the initial changes, like increase of the actin contractility, dissolving cell-cell contacts or elongation of cell shape (Lamouille et al., 2014, Kalluri and Weinberg, 2009), the cells have to lift up from the surface to improve motility. This lift up gives us new insight into the cellular adhesion during EMT. After reaching a maximum of an average cell membrane substrate distance of 156 nm, the cells approximately regain the initial cell substrate distance of untreated NMuMGs over the next 15 hours and stayed at this height. This finding showed that after the EMT the mesenchymal like cells are not closer to the surface than epithelial NMuMGs. The NMuMGs exhibit only one preferred distance to the surface, independent from the phenotype. Only for the transition itself the cells change their favored height distance to the surface.

Additionally, a time dependent size change of single NMuMG cells could be observed. NMuMG increased their cell size and exhibited a more homogenous distance to the surface in response to EMT. The variance of the cell – surface distance at the mesenchymal state was smaller than at the epithelial state. By losing cell-cell contacts and changing from an epithelial ordered cell layer to single cells it seems that the overall distance of the basal membrane to the metal surface appears more consistent.

MIET also serves as an alternative tool for analyzing the changes in focal adhesions. Focal adhesions are the linkage between cell and the surface using a complex intracellular connection of integrin and F-actin cytoskeleton that both respond to and transmit mechanical forces (Grashoff et al., 2010). Since focal adhesion components play a central part in the regulation of adhesive processes (Geiger and Bershadsky, 2001, Wozniak et al., 2004, Wehrle-Haller and Imhof, 2002) the analysis of the dynamics of focal adhesions brings another benefit to this method. It was possible to reveal the time dependent dynamics in cellular

adhesion by displaying the dissolution and formation of adhesion points through cross sections. The information was directly gained out of the experiment and did not need any additional modification of the cells.

The fact of no modification of single cell adhesion compounds apart from staining the cellular membrane, to receive the information about the dynamics of focal adhesions, states another advantage compared to other methods. For the total internal reflection fluorescence (TIRF) microscopy (Axelrod et al., 2002), for example, single compounds of the cellular adhesion like integrin, paxilin, vinculin or actin (Case and Waterman, 2015) has to be fluorescently label for analyzing the fluctuation of focal adhesions.

The method ECIS was used to support the findings from MIET measurements. With ECIS the global changes in cellular dynamics such as cell-substrate and cell-cell contacts were analyzed. This was done by measuring the complex impedance *Z* between small electrodes, cultured with cells, and a larger counter electrode with cell culture medium as an electrolyte (Giaever and Keese, 1991, Xiao et al., 2002) without interference from staining. The measurements revealed that NMuMGs exhibit the strongest morphological/ adhesive changes after administration of TGF-ß1 in the first 5 h of exposure. In this time range the impedance signal showed the biggest changes. Compared to MIET the initial and strongest changes in cell-substrate distances appeared also in the first 5-6 h of TGF treatment. Here the cells lifted up from the surface to an average height of 156 nm.

The barrier resistance between cells (R_b) and the membrane capacity (C_m) revealed the loss of cell-cell contacts and the formation of stress fibers with a concomitant decrease of membrane area due to morphological changes in response of TGF-ß1 addition and thereby underline the effect of EMT. The findings for R_b and C_m are in good accordance to previous studies from Schneider et al., 2011. Here also R_b and C_m decrease to lower values for NMuMGs in the response of TGF-ß1 treatment compared to untreated cells.

The parameter α allows to analyze globally the height changes between cells and substrate for the analyzed cell layer cultured on the gold electrode. A decreasing resistance stands for an increasing distance between cells and surface since α is reciprocal proportional to the height between cells and surface (Lo and Ferrier,

1998). The progress of *α* leads to the conclusion that the NMuMGs first rose their distance to the surface and afterwards decreased it again to the initial level which is close to the value of untreated cells. This supports the findings from the MIET measurement. In MIET the NMuMGs also started to lift up from the surface and then moved to the surface until they finally reached the height of untreated cells again. The peak of the cell-surface height laid in both methods at around 5 h after TGF-ß1 exposure. Also the time range for the reduced cell-substrate distance is nearly the same for both methods. Both revealed that the NMuMGs with TGF-ß1 reached the same distance as before the initial rise at around 17-20 h after TGF-ß1 exposure. The similar findings in both methods underline the observed effects and reveal that ECIS and MIET can be combine for analyzing biological processes. ECIS reveals the cellular changes on a global level for a cell layer and MIET allow to analyze single cells down to structures as small as single focal adhesions.

However, apart from the similarities, there are also discrepancies in the gained data. In some measurements, *α* revealed a significant rise after the first 0.5 h after exposure of TGF-ß1 which resulted in higher values than before the addition. This indicates that the distance between cells and substrate is first reduced before it starts to increase again. Such a tendency for the first hour could not be observed out of MIET. The time-elapsed imaging experiments of the cell–substrate distance showed that after the first 20 minutes exposure of TGF-ß1 the cells already started to lift up from the surface. Certainly, this effect in *α* could only be observed for some measurements. In most cases the increase of *α* at the beginning of the measurement did not lead to significant higher values than before the addition of TGF-ß1 (see Figure 4-16, *p.* 97) and could be declared as normal fluctuation of *α*. Apart from this *α* rose to higher values for untreated cells in the course of the measurement. This decrease of cell distance to the substrate could not be seen in MIET measurements. Untreated cells exhibited a constant cell-surface distance in MIET measurements over the entire analyzed time range.

Taking everything together, the results obtained from ECIS measurements support the main findings gained from MIET nanoscopy. The main findings are that the cells lift up from the surface for the EMT itself, that they lose their cell-cell contacts and undergo morphological changes in response to the added TGF-ß1. For the MIET nanoscopy it could be shown that it has the advantage to

monitor and quantify all stages of the EMT as a function of time and location by investigating the distance between cell and substrate. This gives a better understanding of the dynamics during EMT like the change of cell shape or reorganization of the cytoskeleton. Furthermore, it also reveals information about the dynamics of focal adhesion clusters. Taking this into account, MIET is a suitable tool for illustrating and quantifying cellular adhesion and locomotion to receive a deeper understanding of fundamental biological processes.

4.3 Influence of lacking discoidin domain receptor 2 in mice on mechanical properties of the ECM

4.3.1 Introduction

In cancer development the surrounding microenvironment of cancer cells play an important role. The extracellular matrix (ECM) is a major component of this microenvironment. It consists of a complex network of macromolecules and has very distinct biochemical, biomechanical and physical properties (Lu et al., 2012, Pupa et al., 2002, Bosman and Stamenkovic, 2003). This work looked closer at the mechanical properties of the ECM. In this context one member of the family of Discoidin Domain Receptors (DDRs), which are part of the receptor tyrosine kinases (RTKs), was used to vary the properties of the ECM.

DDR2 has a functional relevance for reconstruction of the ECM, it is expressed for example in the stroma of fibroblasts and activates matrix metalloprotease (MMP) (Labrador et al., 2001, Vogel et al., 2006). Knock out of DDR2 (DDR2 -/-) in the mouse delays healing of epidermal wounds significantly (Olaso et al., 2011b, Vogel et al., 2006). Additionally, experiments from the working group of Dr. Missbach-Güntner (Göttingen University Medical School, Dept. of Diagnostic and Interventional Radiology) and other studies (Olaso et al., 2011a) showed an increased collagen deposition on DDR2 -/- mice. Also the skin from the knock out mice are thicker compared to the wild type.

This chapter deals with the question if the knock out from DDR2 in mice also cause alteration of the stiffness of the dermal skin comparing to the wild type mice. The rigidity of the skin was determined with atomic force microscopy (AFM) and rheometry. Both methods showed that the dermal skin and therefore the ECM of DDR -/- is significant stiffer compared to wild type.

4.3.2 Results

4.3.2.1 Determination of ECM stiffness with AFM

To determine the different stiffnesses in the ECM between DDR2 -/- and wild type mice, skin samples were investigated with the AFM. Therefore, 30 µm thick native skin cross sections were prepared and analyzed through force spectroscopy. The Young's modulus *E* of the skin samples were determined from the force distance curves fitted with the Hertzian model (see also 3.1.3; *p*. 29). It serves as a degree of rigidity and can be used to compare between DDR2 -/- and wild type mice skin. For the measurement itself only dermis without hair or root of a hair were analyzed (Figure 4-18) to ensure that only the stiffness of the dermis matrix is measured.

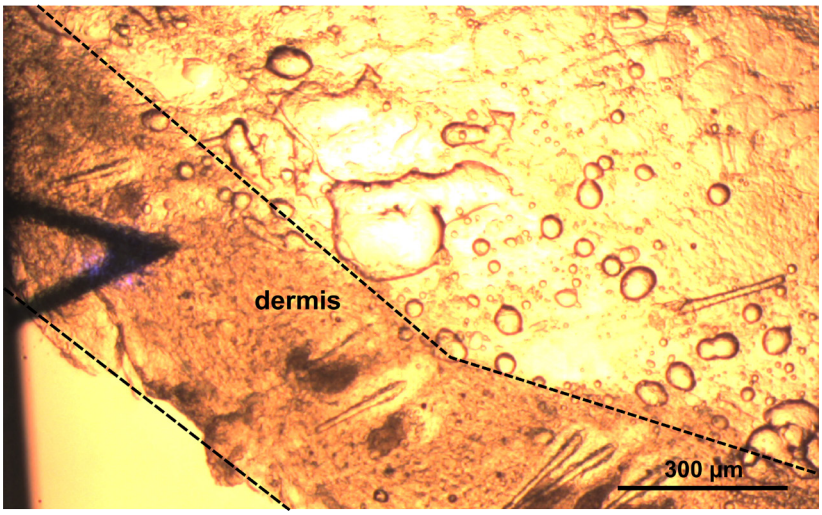

Figure 4-18 **Light microscopy picture of a measured native mice skin** (wild type) with the AFM cantilever. Only the dermis from the skin cross sections were measured (indicated area with dotted line).

The obtained elastic moduli of the wild type and DDR2 -/- dermis are shown in Figure 4-19.

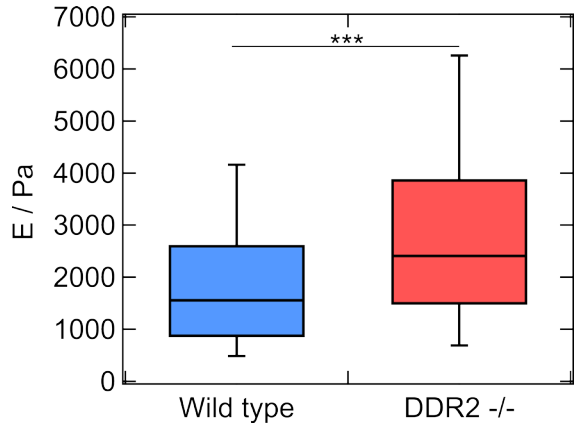

Figure 4-19 **Comparison of ECM stiffness** between wild type mice n (skin samples) = 3 and DDR2 -/- n (skin samples) = 4 showing Young's modules *E*. Box-whisker-plots: line represents the median of the distribution, boxes comprise the 25th and 75th percentile, whisker tops and bottoms are drawn to the 10th and 90th percentiles, respectively. P-values are calculated with Wilcoxon rank sum test. *** - p<0.001.

According to the Young's modulus *E* in Figure 4-19, the DDR2 knock out mice possess a significant stiffer dermis comparing to the wild type. Wilcoxon rank sum test underlines the significant difference between these two categories (*p-value* = 0). Looking at the median values from the box plots, we can see that the Young's modulus of DDR2 -/- with 2410 Pa, is around 900 Pa higher compared to the wild type (1554 Pa). The mean values from Table 4-2 show the same tendency with a 1 kPa stiffer dermis of DDR2 -/- compared to the wild type dermis. The high standard error of mean (SEM) is caused by the diversity of the mice dermis of DDR2 -/- and wild type, which can be also seen in the followed histogram (Figure 4-20).

	Wild type		**DDR2 -/-**
Median value of E / Pa	2036 ± 1797		3077 ± 2562
Analyzed curves	2679		3471
Hertzian fit applicable	748 (28 %)		1116 (32 %)

Table 4-2 Median values and standard error of mean (SEM) of *E* for wild type and DDR2 -/- mice and the number of analyzed and usable force distance curves generated from the AFM indentation measurements.

However, it has to be mentioned that a certain amount of force distance curves couldn't be used for determining *E* and therefore 28 % (for the wild type) and 32 % (for DDR2 -/-) of the generated force distance curves could be taken into account. The reason for this fact is that for the fit itself only trace curves could be used which exhibit a smooth baseline and clear contact point. Since the measurements were conducted on wet skin samples with a low stiffness, a certain interaction between cantilever tip and sample was unavoidable. The disturbances in the non-contact regime leads to the difference of generated and used force curve. Nevertheless, the number of curves where the fit is reasonably high to justify the interpretation.

To get a deeper look at the distribution, Figure 4-20 illustrates the resulting elastic modulus *E* as a histogram. Here we can also see the clear shift to higher *E*-values from wild type (blue) to DDR2 -/- (red).

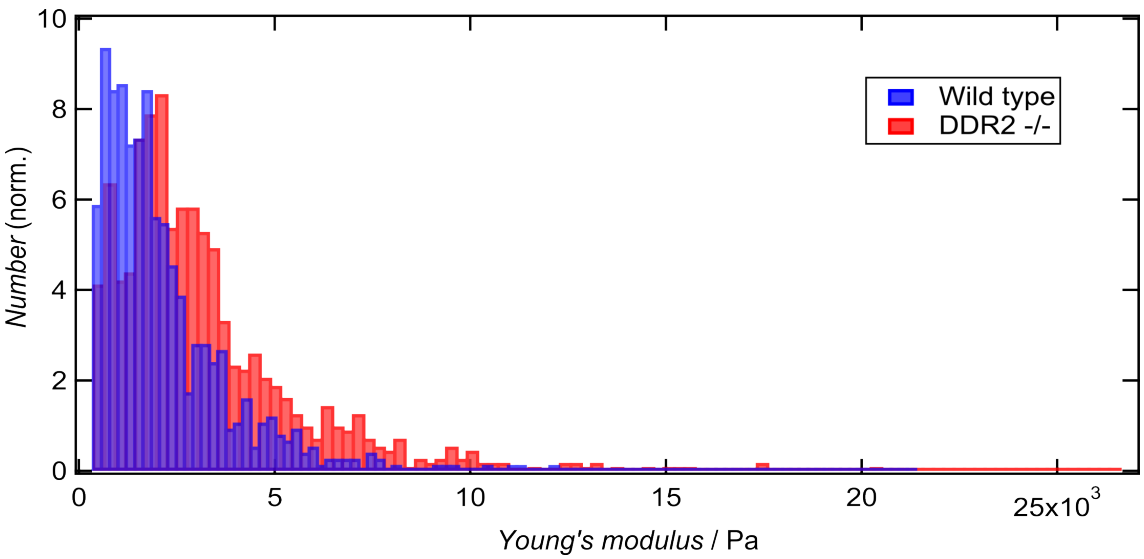

Figure 4-20 **Histogram of obtained Young's modulus *E***; wild type (red) and knock out DDR2 -/- (blue; semitransparent) mice. Histogram is normalized to the sum of 100.

The histogram shows that the Young's modulus for wild type dermis exhibit a maximum from 500 Pa to 1000 Pa. For DDR2 -/- dermis the histogram illustrates a maximum at around 2200 Pa with an additional peak in the regime of around 3000 to 3500 Pa (Figure 4-20). In summary one can say that both type of dermis exhibit a diversity in stiffness which is seen in the broad distribution of the elastic

modulus *E*. But still with this diversity the knock out DDR2 -/- mice display a more rigid dermis than the wild type.

With AFM it could be shown, that in response of the DDR2 knock out in mice the dermal matrix becomes stiffer. Since this evidence only refers to microscopic scale of several micrometer for cross sections of skin samples, this observation should be also confirm at macroscopic level. For this approach the entire skin sample was analyzed by using rheometry.

4.3.2.2 Determination of ECM stiffness with rheometry

Rheology deals with the study of deformation and flow of matter. In this work the deformation of mouse skin under different stress rates was studied to calculate its viscoelastic behavior (Chen et al., 2010). During rheology measurements with a rheometer we gather information about the mechanical response of the tissue represented by the storage modulus *G'* and the loss modulus *G''*. For a quantitative statement about the rigidity of the dermis *G'* is sufficient as it represents for elastic properties of the sample and is related to elastic energy storage by the material (Morrison, 2001, Bröckel et al., 2013).

For the measurements, the rheometer applied an initial force of 1 N and 5 N at 1 Hz frequency on the circular skin specimen and recorded *G'*/ *G''*. The two normal forces were used to investigate how the skin samples responded to low and high forces. First, the course of time of *G'*/ *G''* was analyzed (Figure 4-21; Figure 4-22).

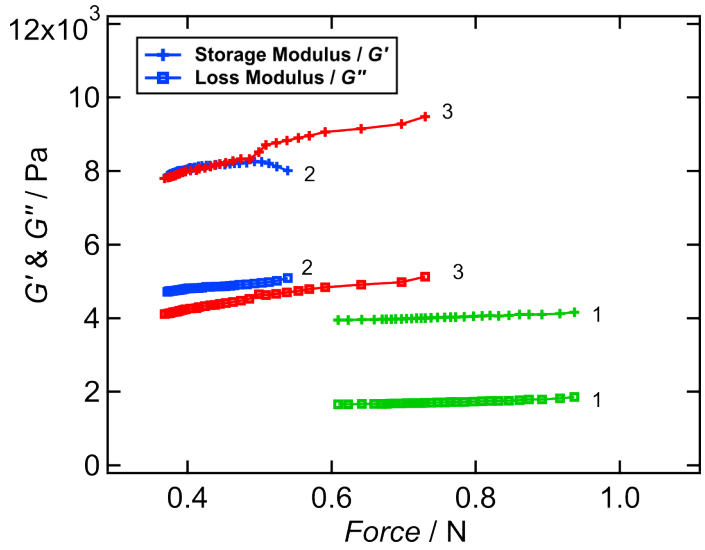

Figure 4-21 ***G'/G''*** **for wild type mice at pre-set 1 N normal force**: 5 minutes at 1 Hz frequency (30 values per measurement) for three different mouse skin samples (1 = green/ 2 = blue/ 3 = red).

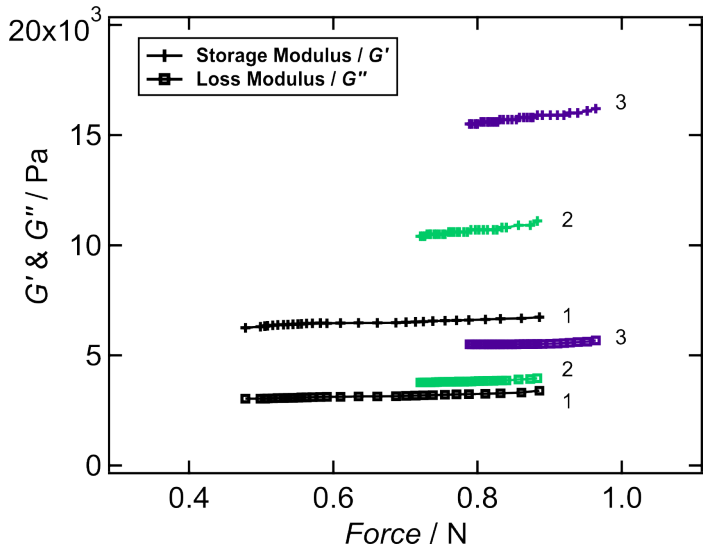

Figure 4-22 ***G'/G''*** **for DDR2 -/- mice at pre-set 1 N normal force**: 5 minutes at 1 Hz frequency (30 values per measurement) for three different mouse skin samples (1 = black/ 2 = green/ 3 = purple).

Both, Figure 4-21 and Figure 4-22 show the progress of the measured *G'* and *G''* which were measured for 5 minutes with applied force at 1 Hz frequency. Instead of showing the moduli of all six measured skin samples, the Figures illustrate only three measured skin samples for wild type and DDR 2 -/- for a better overview. During the five minutes of measurement the initial applied normal force of 1 N shows a decay for every skin sample. The decay for the wild-type mice samples

ranges from 23 % up to 50 % compared to the starting point of the measurement and 18 % - 46 % for the DDR -/-. For each measurement the applied force started at a value below the pre-set 1 N. The reason for this is that there was a small time gap between setting the applied force and starting the measurement itself, where the force already started to decline. The decay of the applied force during the measurement demonstrates the creep behavior of the tissue. Due to the viscous part of the biologically complex tissue, the sample starts to deform or move slowly under mechanical stresses which resulted in a reduced force on the sample (Morrison, 2001). Looking at the measured moduli one can say, that *G'* / *G''* generally exhibit constant values for 1 Hz frequency over the measured time. For *G'* only one skin sample revealed a decrease of more than 10 % compared to the starting point of the measurement. All other samples have a decay of less than 10 %. This indicates that the values in this force regime are relative force independent. Next, we see that also on the macroscopic level the values for the measured skin samples vary a lot. For wild type skin the values for *G'* range from 4 kPa to 24 kPa. The knock out skin reveals values for *G'* between 6 kPa and 50 kPa. Therefore, the diversity in DDR 2 -/- skin samples is stronger compared to the wild type. For the applied normal force of 5 N we can see the same behavior only at a higher Pascal regime (Figure 4-23 and Figure 4-24). During the measurements the applied force reveals a decay but the measured moduli exhibit a relative force independent behavior. Also for 5 N the measured values differ for the two types of dermis (*G'* (DDR2 -/-): 32 kPa to 81 kPa; *G'* (wt): 7 kPa to 52 kPa).

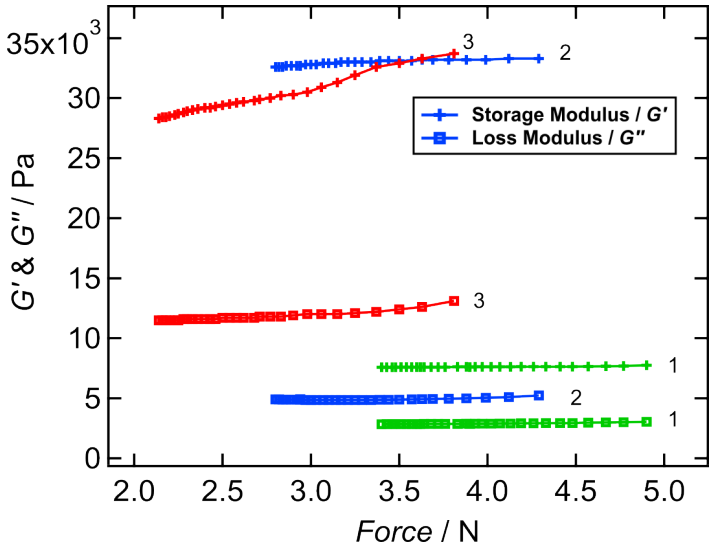

Figure 4-23 ***G'/G''*** **for wild type mice at pre-set 5 N normal force**: 5 minutes at 1 Hz frequency (30 values per measurement) for three different mouse skin samples (1 = green/ 2 = blue/ 3 = red).

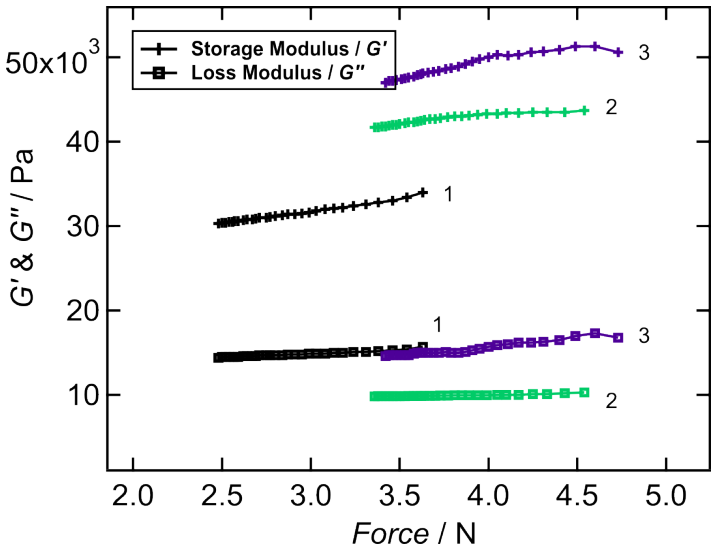

Figure 4-24 ***G'/G''*** **for DDR2 -/- mice at pre-set 5 N normal force**: 5 minutes at 1 Hz frequency (30 values per measurement) for three different mouse skin samples (1 = black/ 2 = green/ 3 = purple).

To characterize the frequency dependent viscoelastic behavior of DDR 2 -/- and wild type mice skin, the skin samples were analyzed by a frequency sweep from 0.1 Hz to 100 Hz in 21 steps. Here, also three of six measured skin samples were illustrated for each category (Figure 4-25; Figure 4-26; Figure 4-27; Figure 4-28).

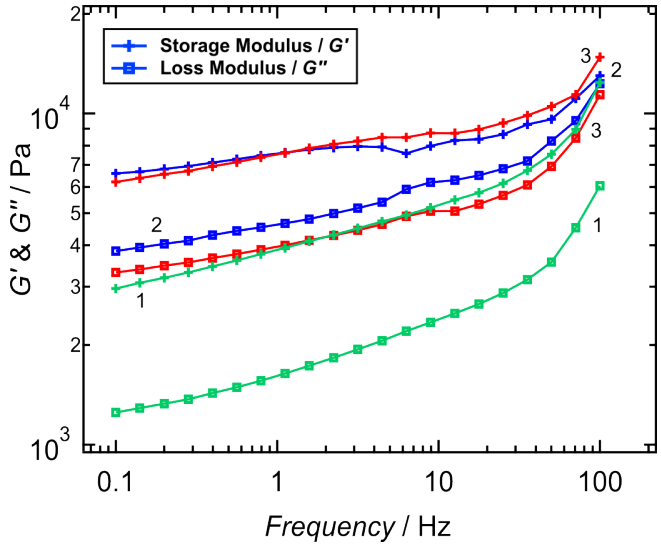

Figure 4-25 **Frequency sweep of *G'/G''* for wild type mice at 1 N normal force**: 0.1 Hz to 100 Hz in 21 steps for three different mouse skin samples (1 = green/ 2 = blue/ 3 = red).

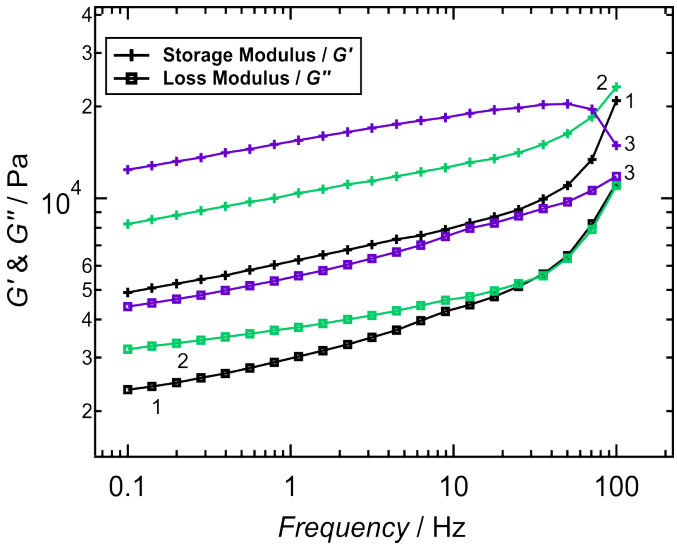

Figure 4-26 **Frequency sweep of *G'/G''* for DDR2 -/- mice at 1 N normal force**: 0.1 Hz to 100 Hz in 21 steps for three different mouse skin samples (1 = black/ 2 = green/ 3 = purple).

In all measurements the storage modulus (*G'*) reveals a higher value compared to the loss modulus (*G''*). The fact that *G'* is bigger than *G''* points out that the biologically complex skin acts more like a solid (Morrison, 2001). The frequency sweep gives us a fingerprint spectrum of the different mouse skin samples. For both applied forces (1 N and 5 N) we can observe that *G'* and *G''* exhibit no cross over area during the frequency sweep (Figure 4-25; Figure 4-26; Figure 4-27; Figure 4-28). Additionally, *G'* runs parallel to *G''* in response of the different

frequencies so that we can precise the previous term to the statement that the skin acts more like a solid gel system (Picout and Ross-Murphy, 2003).

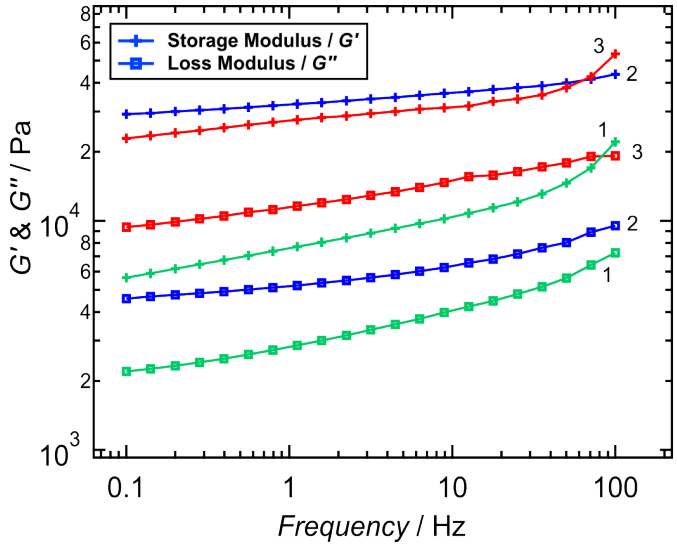

Figure 4-27 **Frequency sweep of *G'/G''* for wild type mice at 5 N normal force**: 0.1 Hz to 100 Hz in 21 steps for three different mouse skin samples (1 = green/ 2 = blue/ 3 = red).

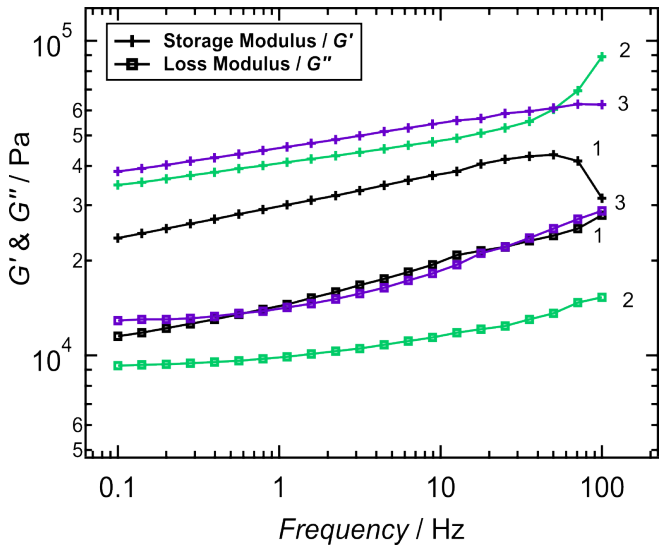

Figure 4-28 **Frequency sweep of *G'/G''* for DDR2 -/- mice at 5 N normal force**: 0.1 Hz to 100 Hz in 21 steps for three different mouse skin samples (1 = black/ 2 = green/ 3 = purple).

Apart from this, we can also conclude from the frequency sweep that all used skin samples exhibit a nonlinear viscoelastic response to the strain. With increasing frequency they stiffen which results in higher values for *G'* and *G''*. This strain stiffening is a common feature for soft tissues (Chen et al., 2010).

After analyzing the viscoelastic behavior by frequency sweeps the elastic response from DDR2 -/- skin to the wild type skin was investigated.

To compare the elastic behavior between the DDR2 -/- and wild type skin from the mice the elastic modulus *G'* of all measured skin samples was taken into account.

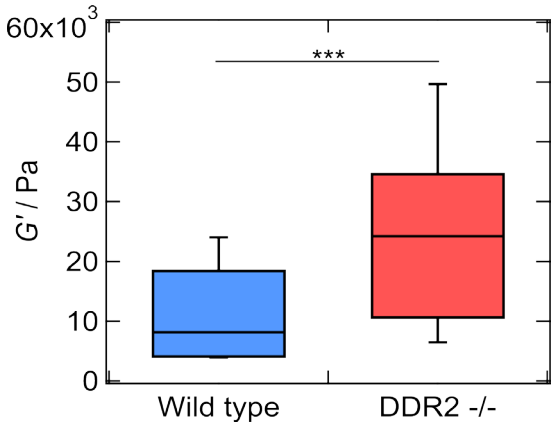

Figure 4-29 **Comparison of *G'*** between wild type mice n (skin samples) = 6 and DDR2 -/- n (skin samples) = 6 for a normal force of 1N. Box-whisker-plots: line represents the median of the distribution, boxes comprise the 25th and 75th percentile, whisker tops and bottoms are drawn to the 10th and 90th percentiles, respectively. P-values are calculated with Wilcoxon rank sum test. *** - p<0.001.

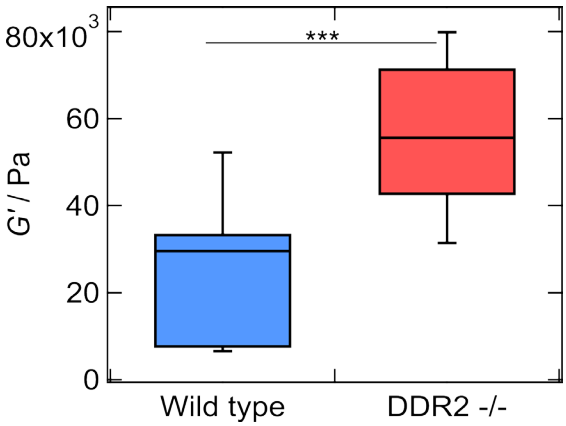

Figure 4-30 **Comparison of *G'*** between wild type mice n (skin samples) = 5 and DDR2 -/- n (skin samples) = 6 for a normal force of 5N. Box-whisker-plots: line represents the median of the distribution, boxes comprise the 25th and 75th percentile, whisker tops and bottoms are drawn to the 10th and 90th percentiles, respectively. P-values are calculated with Wilcoxon rank sum test. *** - p<0.001.

For both applied normal forces, the DDR2 -/- skin has a significant higher *G'* (each *p-value* = 0) than the wild type skin. Looking at the median values, we can see that *G'* for DDR2 -/- with 24 kPa, is three times higher as for the wild type with 8 kPa. For 5 N applied force *G'* for DDR2 -/- skin is with 56 kPa nearly twice as

high as for the wild type with 30 kPa. The mean values from Table 4-3 show for 1 N and 5 N applied force that the G' for DDR2 -/- skin is twice as high as for the wild type. These values show that also on the macroscopic scale the skin of DDR2 -/- mice is stiffer than the wild type skin and confirm the results from the AFM measurements (see section 4.3.2.1; *p.106*).

Force / N	**Mean value of *G'* / kPa**	
	Wild type	DDR2 -/-
1	11 ± 7	25 ± 15
5	26 ± 17	56 ± 17

Table 4-3 Mean values and standard error of mean (SEM) of *G'* for wild type and DDR2 -/- mice at normal force of 1 N and 5 N.

4.3.3 Discussion

Cellular migration is transmitted by adhesion to the extracellular matrix and is a product of the net force which is exerted from the actin-based machinery (Zaman et al., 2006). The mechanical properties of the extracellular matrix (ECM) influence the locomotion and adhesion of cells (Khatiwala et al., 2006). By looking at the interplay between ECM and cell, the cell surface receptors become important. Discoidin Domain Receptor 2 (DDR2) is part of the family of receptor tyrosine kinases and has a functional relevance for reconstruction of the ECM (Labrador et al., 2001, Vogel et al., 2006).

The group of Dr. Missbach-Güntner (Göttingen University Medical School, Dept. of Diagnostic and Interventional Radiology) investigate the effect of DDR2 on ECM in mice in the context of tumor invasion and metastasis. They and other authors (Olaso et al., 2011a) could show that the knock-out of DDR2 lead to an increased collagen deposition and a thicker skin. The mechanical changes on ECM are still unknown.

To validate that the DDR2-deficient mice is suitable for the analysis of matrix-tumor-interaction with altering ECM properties the changes in stiffness for the ECM has to be determined.

Therefore, to clarify if there is a difference in the rigidity of the wild type and DDR2 -/- mice dermis, the mechanics of different skin samples were analyzed with AFM and rheometry. Both methods could successfully determine that the stiffness of DDR 2 -/- skin is significant higher than the wild type skin.

Looking at the results one can see that both type of dermis exhibit a certain diversity in stiffness. In rheometry the broad distribution of values was observed between each sample whatever category. In AFM the diversity in the obtained values could be found between each skin sample for DDR2 -/- and wild type as well as within the sample itself. But still with this diversity is was possible to determine a significant difference in the rigidity of the dermis between wild type and knock out.

The Young's modulus *E* of the skin samples, which serves as a degree of rigidity, was measured with AFM. The moduli *G'* and *G''* were measured with rheometry. Where *G'* is the value of interest as it stands for the elastic response to the applied stress (Morrison, 2001, Bröckel et al., 2013). In both methods the DDR2 -/- mice skin showed higher values than the wild type skin, which is a direct statement for an increased stiffness of the dermis.

The combination of AFM and rheometry was used to cover a broad range of length scale. As AFM probed single focal spots of micrometer scale of the skin and rheometry investigated the entire skin at the macroscopic level of several centimeter. The fact that both methods revealed the same observation underlines the result of a stiffer rigidity in the dermis of DDR2 -/-.

These results nicely demonstrate that AFM and rheometry complement one another and can be combined to investigate the stiffness of biological samples over a wide range of magnitude. It is important to take only the qualitative tendency into account and not to compare the values itself from both methods. Both methods generate physical different parameters to judge the stiffness of the measured skin samples. Therefore it doesn't make sense to compare the values itself. Only the tendency within each method is relevant.

With the result of a differ rigidity of skin, the knock out mice can be taken as a valuable tool to analyze biological effects of altered stiffness. This model could trace how altering stiffness from the ECM influence cell functions like tumor progression. It could already be shown that the reconstructed ECM in DDR2 -/- mice caused a significant delay of healing of epidermal wounds through hindered fibroblast migration (Olaso et al., 2011b, Vogel et al., 2006). Based on this results it is interesting to look how the invasive behavior of tumor cells and the tumor progression itself are influenced through a stiffer surrounding microenvironment by using the model of DDR2 -/- mice. It is well documented that the invasive potential of tumor cells directly matters on the capability of adhesion to the ECM (Crowe and Shuler, 1999, Vogel et al., 2006, Pathak and Kumar, 2011). Therefore this new knowledge would serve for a continuative analysis of tumor cell – ECM interaction.

5 Conclusion

I investigated with this work the cellular locomotion and adhesion in the context of different substrate properties to establish a better understanding of the response of cells to their environment. The two phenomena of cellular locomotion and adhesion are tightly coupled and key factors for a cell's life (Ladoux and Nicolas, 2012). I examined these two phenomena in the context of three different biological processes.

First process, the active migration of single *Xenopus* PGCs at early embryonic stages was investigated with respect to of E-cadherin mediated adhesion. It was found that in zebrafish the E-cadherin play a special role for the changes in the migratory behavior (Richardson and Lehmann, 2010, Kardash et al., 2010). But the role of E-cadherin in the process of active migration in *Xenopus* PGCs so far remained unclear. The study of Dzementsei et al., already indicated a down-regulation of E-cadherin in response to the migration but only quantified it by qPCR analysis from isolated PGCs (Dzementsei et al., 2013). From the research of this thesis, it is possible to conclude that PGCs indeed exhibit a reduced E-cadherin expression through migration by using SCFS. The work revealed that the adhesion force between migratory PGCs and E-cadherin-coated surfaces is significantly reduced compared to non-migratory PGCs. Additionally, it could be shown that in the migratory phase still a certain amount of E-cadherin remains since the adhesion force did not reach the exact level of E-cadherin knock down PGCs. In view of the role in active migration this work claims that in *Xenopus* PGCs the E-cadherin also plays an important role for the changes in the migratory behavior. The decrease of E-cadherin is required to change PGCs from their passive to the actively migrating state, in order to enhance the turnover of adhesion contacts.

Secondly, this work went into the matter of how the adhesion between NMuMGs and surface alter during epithelial-mesenchymal transition (EMT). In EMT the cells change from an epithelial to a mesenchymal phenotype to start migration individually. With the help of MIET and ECIS it has been demonstrated, that the cells changed the distance to the substrate only in the first 24 h of the transition. The new gained insight into the cellular adhesion during EMT is that the NMuMGs

lift of from the surface to accomplish the transition. Additionally it could be seen that the cells exhibit the same distance to the surface independently of the phenotype and only for the transition itself, the cells change their favored height above the surface. The used ECIS method investigates the globally dynamic changes of cell-substrate and cell-cell contacts by looking on an entire cell layer for a long time period (up to 3 days). MIET instead with the high spacial resolution investigates more the dynamic changes of cell-substrate on small cell aggregates and also single cells for a shorter time range (up to 1.5 h). Apart from this, ECIS data also provides additional information for the barrier resistance between cells and the membrane capacity, which is a good enhancement to MIET. These characteristics lead to a reasonable combination of MIET and ECIS to complement one another. For the newly developed MIET one can say that it is a suitable tool for illustrating and quantifying cellular adhesion and locomotion to receive a deeper understanding of fundamental biological processes.

The last project of this thesis was to investigate the interplay between extracellular matrix (ECM) and cellular adhesion and migration. The working group of Dr. Missbach-Güntner (Göttingen University Medical School, Dept. of Diagnostic and Interventional Radiology) investigate the effect of DDR2 on ECM in mice in the context of tumor invasion and metastasis. However, the mechanical changes of the ECM were still unknown. With the used methods of AFM and rheometry, it can be concluded that after knock out of the DDR2, the dermis of mice becomes significantly stiffer compared to the wild type. This fact conclude that the DDR2-deficient mice could be used as a model for the analysis of tumor progression in ECM of different stiffnesses. With this model one can investigate if the invasive behavior of tumor cells and the tumor progression itself are influenced by a stiffer surrounding microenvironment. This new knowledge could help to accomplish a better understanding of the response of a cancer cell on its environment. The results additionally prove that also AFM and rheometry complement one another and can be well combined to investigate the stiffness of biological samples over a wide range of sizes.

Summing up the results, it can be concluded that this work helps to gain new insights in three different processes with the connecting elements of cellular locomotion and adhesion. The dependency between matrix stiffness and cell surface receptors, the regulation in cell contacts or the distance to the surface

influence cellular migration and adhesion. Furthermore, it could be shown that the combination of AFM with rheometry and MIET with ECIS helps to enlarge the parameter space of cells interacting with their environment.

6 References

APPLIED_BIOPHYSICS. *ECIS Model* [Online]. Available: http://www.biophysics.com/ecismodel.php 2016].

ARNDT, S., SEEBACH, J., PSATHAKI, K., GALLA, H. J. & WEGENER, J. 2004. Bioelectrical impedance assay to monitor changes in cell shape during apoptosis. *Biosens Bioelectron,* 19**,** 583-94.

AXELROD, D., HELLEN, E. H. & FULBRIGHT, R. M. 2002. Total Internal Reflection Fluorescence. *In:* LAKOWICZ, J. R. (ed.) *Topics in Fluorescence Spectroscopy.* Boston, MA: Springer US.

BAJPAI, S., FENG, Y., KRISHNAMURTHY, R., LONGMORE, G. D. & WIRTZ, D. 2009. Loss of alpha-catenin decreases the strength of single E-cadherin bonds between human cancer cells. *J Biol Chem,* 284**,** 18252-9.

BARRY, A. K., TABDILI, H., MUHAMED, I., WU, J., SHASHIKANTH, N., GOMEZ, G. A., YAP, A. S., GOTTARDI, C. J., DE ROOIJ, J., WANG, N. & LECKBAND, D. E. 2014. alpha-catenin cytomechanics--role in cadherin-dependent adhesion and mechanotransduction. *J Cell Sci,* 127**,** 1779-91.

BENOIT, M., GABRIEL, D., GERISCH, G. & GAUB, H. E. 2000. Discrete interactions in cell adhesion measured by single-molecule force spectroscopy. *Nat Cell Biol,* 2**,** 313-7.

BENOIT, M. & SELHUBER-UNKEL, C. 2011. Measuring cell adhesion forces: theory and principles. *Methods Mol Biol,* 736**,** 355-77.

BERNDT, M., LORENZ, M., ENDERLEIN, J. & DIEZ, S. 2010. Axial nanometer distances measured by fluorescence lifetime imaging microscopy. *Nano Lett,* 10**,** 1497-500.

BERSHADSKY, A., KOZLOV, M. & GEIGER, B. 2006. Adhesion-mediated mechanosensitivity: a time to experiment, and a time to theorize. *Curr Opin Cell Biol,* 18**,** 472-81.

BETZIG, E., PATTERSON, G. H., SOUGRAT, R., LINDWASSER, O. W., OLENYCH, S., BONIFACINO, J. S., DAVIDSON, M. W., LIPPINCOTT-SCHWARTZ, J. & HESS, H. F. 2006. Imaging intracellular fluorescent proteins at nanometer resolution. *Science,* 313**,** 1642-5.

BINNIG, G., QUATE, C. F. & GERBER, C. 1986. Atomic force microscope. *Phys Rev Lett,* 56**,** 930-933.

BINNIG, G. & ROHRER, H. 1983. Scanning Tunneling Microscopy. *Helvetica Physica Acta,* 56**,** 481-482.

BLASER, H., EISENBEISS, S., NEUMANN, M., REICHMAN-FRIED, M., THISSE, B., THISSE, C. & RAZ, E. 2005. Transition from non-motile behaviour to directed migration during early PGC development in zebrafish. *J Cell Sci,* 118**,** 4027-38.

BORZA, C. M. & POZZI, A. 2014. Discoidin domain receptors in disease. *Matrix Biol,* 34**,** 185-92.

BOSMAN, F. T. & STAMENKOVIC, I. 2003. Functional structure and composition of the extracellular matrix. *J Pathol,* 200**,** 423-8.

BOUDOU, T., OHAYON, J., PICART, C. & TRACQUI, P. 2006. An extended relationship for the characterization of Young's modulus and Poisson's ratio of tunable polyacrylamide gels. *Biorheology,* 43**,** 721-8.

BRÖCKEL, U., MEIER, W. & WAGNER, G. 2013. Product design and engineering formulation of gels and pastes.

BUTT, H. J., CAPPELLA, B. & KAPPL, M. 2005. Force measurements with the atomic force microscope: Technique, interpretation and applications. *Surface Science Reports,* 59**,** 1-152.

CASE, L. B. & WATERMAN, C. M. 2015. Integration of actin dynamics and cell adhesion by a three-dimensional, mechanosensitive molecular clutch. *Nat Cell Biol,* 17**,** 955-63.

CHEN, D. T. N., WEN, Q., JANMEY, P. A., CROCKER, J. C. & YODH, A. G. 2010. Rheology of Soft Materials. *Annual Review of Condensed Matter Physics, Vol 1,* 1**,** 301-322.

CHIZHIK, A. I., ROTHER, J., GREGOR, I., JANSHOFF, A. & ENDERLEIN, J. 2014. Metal-induced energy transfer for live cell nanoscopy. *Nature Photonics,* 8**,** 124-127.

CHOI, Y. S. & GUMBINER, B. 1989. Expression of cell adhesion molecule E-cadherin in Xenopus embryos begins at gastrulation and predominates in the ectoderm. *The Journal of Cell Biology,* 108**,** 2449-2458.

CLEGG, R. M. 1995. Fluorescence resonance energy transfer. *Curr Opin Biotechnol,* 6**,** 103-10.

CONACCI-SORRELL, M., ZHURINSKY, J. & BEN-ZE'EV, A. 2002. The cadherin-catenin adhesion system in signaling and cancer. *J Clin Invest,* 109**,** 987-91.

CROWE, D. L. & SHULER, C. F. 1999. Regulation of tumor cell invasion by extracellular matrix. *Histol Histopathol,* 14**,** 665-71.

DE BLASIO, B. F., ROTTINGEN, J. A., SAND, K. L., GIAEVER, I. & IVERSEN, J. G. 2004. Global, synchronous oscillations in cytosolic calcium and adherence in bradykinin-stimulated Madin-Darby canine kidney cells. *Acta Physiol Scand,* 180**,** 335-46.

DE FELICI, M. 2000. Regulation of primordial germ cell development in the mouse. *Int J Dev Biol,* 44**,** 575-80.

DEGUCHI, S., OHASHI, T. & SATO, M. 2006. Tensile properties of single stress fibers isolated from cultured vascular smooth muscle cells. *J Biomech,* 39**,** 2603-10.

DZEMENTSEI, A. & PIELER, T. 2014. Primordial Germ Cell Migration. *Xenopus Development.* John Wiley & Sons, Inc.

DZEMENTSEI, A., SCHNEIDER, D., JANSHOFF, A. & PIELER, T. 2013. Migratory and adhesive properties of Xenopus laevis primordial germ cells in vitro. *Biol Open,* 2**,** 1279-87.

EBNER, A., WILDLING, L., ZHU, R., RANKL, C., HASELGRUBLER, T., HINTERDORFER, P. & GRUBER, H. J. 2008. Functionalization of probe tips and supports for single-molecule recognition force microscopy. *Top Curr Chem,* 285**,** 29-76.

EGEBLAD, M., RASCH, M. G. & WEAVER, V. M. 2010. Dynamic interplay between the collagen scaffold and tumor evolution. *Current Opinion in Cell Biology,* 22**,** 697-706.

ENGIN, S., TROUILLET, V., FRANZ, C. M., WELLE, A., BRUNS, M. & WEDLICH, D. 2010. Benzylguanine thiol self-assembled monolayers for the immobilization of SNAP-tag proteins on microcontact-printed surface structures. *Langmuir,* 26**,** 6097-101.

EVANS, E., RITCHIE, K. & MERKEL, R. 1995. Sensitive force technique to probe molecular adhesion and structural linkages at biological interfaces. *Biophys J,* 68**,** 2580-7.

EVANS, E. A. & CALDERWOOD, D. A. 2007. Forces and bond dynamics in cell adhesion. *Science,* 316**,** 1148-53.

FICHTNER, D., LORENZ, B., ENGIN, S., DEICHMANN, C., OELKERS, M., JANSHOFF, A., MENKE, A., WEDLICH, D. & FRANZ, C. M. 2014. Covalent and density-controlled surface immobilization of E-cadherin for adhesion force spectroscopy. *PLoS One,* 9**,** e93123.

FORSTER, T. 1948. *Zwischenmolekulare Energiewanderung Und Fluoreszenz. *Annalen Der Physik,* 2**,** 55-75.

FOTIADIS, D., SCHEURING, S., MULLER, S. A., ENGEL, A. & MULLER, D. J. 2002. Imaging and manipulation of biological structures with the AFM. *Micron,* 33**,** 385-97.

FRANZ, C. M. & PUECH, P. H. 2008. Atomic Force Microscopy: A Versatile Tool for Studying Cell Morphology, Adhesion and Mechanics. *Cellular and Molecular Bioengineering,* 1**,** 289-300.

FRIEDRICHS, J., LEGATE, K. R., SCHUBERT, R., BHARADWAJ, M., WERNER, C., MULLER, D. J. & BENOIT, M. 2013. A practical guide to quantify cell adhesion using single-cell force spectroscopy. *Methods,* 60**,** 169-78.

GAL, A., SJOBLOM, T., FEDOROVA, L., IMREH, S., BEUG, H. & MOUSTAKAS, A. 2008. Sustained TGF beta exposure suppresses Smad and non-Smad signalling in mammary epithelial cells, leading to EMT and inhibition of growth arrest and apoptosis. *Oncogene,* 27**,** 1218-30.

GEIGER, B. & BERSHADSKY, A. 2001. Assembly and mechanosensory function of focal contacts. *Curr Opin Cell Biol,* 13**,** 584-92.

GIAEVER, I. & KEESE, C. R. 1991. Micromotion of mammalian cells measured electrically. *Proc Natl Acad Sci U S A,* 88**,** 7896-900.

GIAEVER, I. & KEESE, C. R. 1993. A morphological biosensor for mammalian cells. *Nature,* 366**,** 591-2.

GONNERMANN, C., HUANG, C., BECKER, S. F., STAMOV, D. R., WEDLICH, D., KASHEF, J. & FRANZ, C. M. 2015. Quantitating membrane bleb stiffness using AFM force spectroscopy and an optical sideview setup. *Integr Biol (Camb),* 7**,** 356-63.

GOODING, J. M., YAP, K. L. & IKURA, M. 2004. The cadherin-catenin complex as a focal point of cell adhesion and signalling: new insights from three-dimensional structures. *Bioessays,* 26**,** 497-511.

GOUDARZI, M., BANISCH, T. U., MOBIN, M. B., MAGHELLI, N., TARBASHEVICH, K., STRATE, I., VAN DEN BERG, J., BLASER, H., BANDEMER, S., PALUCH, E., BAKKERS, J., TOLIC-NORRELYKKE, I. M. & RAZ, E. 2012. Identification and regulation of a molecular module for bleb-based cell motility. *Dev Cell,* 23**,** 210-8.

GOULD, T. J., GUNEWARDENE, M. S., GUDHETI, M. V., VERKHUSHA, V. V., YIN, S. R., GOSSE, J. A. & HESS, S. T. 2008. Nanoscale imaging of molecular positions and anisotropies. *Nat Methods,* 5**,** 1027-30.

GRASHOFF, C., HOFFMAN, B. D., BRENNER, M. D., ZHOU, R., PARSONS, M., YANG, M. T., MCLEAN, M. A., SLIGAR, S. G., CHEN, C. S., HA, T. & SCHWARTZ, M. A. 2010. Measuring mechanical tension across vinculin reveals regulation of focal adhesion dynamics. *Nature,* 466**,** 263-6.

GREGORY, P. A., BRACKEN, C. P., SMITH, E., BERT, A. G., WRIGHT, J. A., ROSLAN, S., MORRIS, M., WYATT, L., FARSHID, G., LIM, Y. Y., LINDEMAN, G. J., SHANNON, M. F., DREW, P. A., KHEW-GOODALL, Y. & GOODALL, G. J. 2011. An autocrine TGF-beta/ZEB/miR-200 signaling network regulates establishment and maintenance of epithelial-mesenchymal transition. *Mol Biol Cell,* 22**,** 1686-98.

HAMLEY, I. W. 2008. *Introduction to soft-matter : synthetic and biological self-assembling materials,* Chichester, John Wiley & Sons.

HAUSSINGER, D., AHRENS, T., SASS, H. J., PERTZ, O., ENGEL, J. & GRZESIEK, S. 2002. Calcium-dependent homoassociation of E-cadherin by NMR spectroscopy: changes in mobility, conformation and mapping of contact regions. *J Mol Biol,* 324**,** 823-39.

HAWKINS, R. J., PIEL, M., FAURE-ANDRE, G., LENNON-DUMENIL, A. M., JOANNY, J. F., PROST, J. & VOITURIEZ, R. 2009. Pushing off the walls: a mechanism of cell motility in confinement. *Phys Rev Lett,* 102**,** 058103.

HAWKINS, R. J., POINCLOUX, R., BENICHOU, O., PIEL, M., CHAVRIER, P. & VOITURIEZ, R. 2011. Spontaneous contractility-mediated cortical flow generates cell migration in three-dimensional environments. *Biophys J,* 101**,** 1041-5.

HAYNES, J., SRIVASTAVA, J., MADSON, N., WITTMANN, T. & BARBER, D. L. 2011. Dynamic actin remodeling during epithelial-mesenchymal transition depends on increased moesin expression. *Mol Biol Cell,* 22**,** 4750-64.

HEASMAN, J., QUARMBY, J. & WYLIE, C. C. 1984. The mitochondrial cloud of Xenopus oocytes: the source of germinal granule material. *Dev Biol,* 105**,** 458-69.

HELENIUS, J., HEISENBERG, C. P., GAUB, H. E. & MULLER, D. J. 2008. Single-cell force spectroscopy. *J Cell Sci,* 121**,** 1785-91.

HELL, S. W. & WICHMANN, J. 1994. Breaking the diffraction resolution limit by stimulated emission: stimulated-emission-depletion fluorescence microscopy. *Opt Lett,* 19**,** 780-2.

HERTZ, H. 1881. Über die Berührung fester elastischer Körper. *Journal für die reine und angewandte Mathematik,* 92**,** 156-171.

HOCHMUTH, F. M., SHAO, J. Y., DAI, J. & SHEETZ, M. P. 1996. Deformation and flow of membrane into tethers extracted from neuronal growth cones. *Biophys J,* 70**,** 358-69.

HOLTERMAN, J. & GROEN, P. 2013. *An Introduction to Piezoelectric Materials and Applications*, Stichting Applied Piezo.

HONG, S., TROYANOVSKY, R. B. & TROYANOVSKY, S. M. 2011. Cadherin exits the junction by switching its adhesive bond. *J Cell Biol,* 192**,** 1073-83.

HORVAY, K., CLAUSSEN, M., KATZER, M., LANDGREBE, J. & PIELER, T. 2006. Xenopus Dead end mRNA is a localized maternal determinant that serves a conserved function in germ cell development. *Dev Biol,* 291**,** 1-11.

HOUSTON, D. W. & KING, M. L. 2000. Germ plasm and molecular determinants of germ cell fate. *Curr Top Dev Biol,* 50**,** 155-81.

HOUSTON, D. W., ZHANG, J., MAINES, J. Z., WASSERMAN, S. A. & KING, M. L. 1998. A Xenopus DAZ-like gene encodes an RNA component of germ plasm and is a functional homologue of Drosophila boule. *Development,* 125**,** 171-80.

HUTTER, J. L. & BECHHOEFER, J. 1993. Calibration of Atomic-Force Microscope Tips. *Review of Scientific Instruments,* 64**,** 1868-1873.

JANSHOFF, A., NEITZERT, M., OBERDORFER, Y. & FUCHS, H. 2000. Force Spectroscopy of Molecular Systems-Single Molecule Spectroscopy of Polymers and Biomolecules. *Angew Chem Int Ed Engl,* 39**,** 3212-3237.

JEANES, A., GOTTARDI, C. J. & YAP, A. S. 2008. Cadherins and cancer: how does cadherin dysfunction promote tumor progression? *Oncogene,* 27**,** 6920-9.

JIAO, Y. & SCHAFFER, T. E. 2004. Accurate height and volume measurements on soft samples with the atomic force microscope. *Langmuir,* 20**,** 10038-45.

JOHNSON, K. L. 1985. Contact mechanics.

JPK_INSTRUMENTS 2010. *JPK SideView CantileverHolder User Manual*.

JPK_INSTRUMENTS 2015. *NanoWizard AFM Handbook*.

KALLURI, R. 2009. EMT: when epithelial cells decide to become mesenchymal-like cells. *J Clin Invest,* 119**,** 1417-9.

KALLURI, R. & WEINBERG, R. A. 2009. The basics of epithelial-mesenchymal transition. *J Clin Invest,* 119**,** 1420-8.

KARDASH, E., REICHMAN-FRIED, M., MAITRE, J. L., BOLDAJIPOUR, B., PAPUSHEVA, E., MESSERSCHMIDT, E. M., HEISENBERG, C. P. & RAZ, E. 2010. A role for Rho GTPases and cell-cell adhesion in single-cell motility in vivo. *Nat Cell Biol,* 12**,** 47-53; sup pp 1-11.

KEESE, C. R., WEGENER, J., WALKER, S. R. & GIAEVER, I. 2004. Electrical wound-healing assay for cells in vitro. *Proc Natl Acad Sci U S A,* 101**,** 1554-9.

KELLER, R. 2005. Cell migration during gastrulation. *Curr Opin Cell Biol,* 17**,** 533-41.

KHATIWALA, C. B., PEYTON, S. R. & PUTNAM, A. J. 2006. Intrinsic mechanical properties of the extracellular matrix affect the behavior of pre-osteoblastic MC3T3-E1 cells. *Am J Physiol Cell Physiol,* 290**,** C1640-50.

KLOC, M., BILINSKI, S. & ETKIN, L. D. 2004. The Balbiani body and germ cell determinants: 150 years later. *Curr Top Dev Biol,* 59**,** 1-36.

KUNWAR, P. S., SANO, H., RENAULT, A. D., BARBOSA, V., FUSE, N. & LEHMANN, R. 2008. Tre1 GPCR initiates germ cell transepithelial migration by regulating Drosophila melanogaster E-cadherin. *J Cell Biol,* 183**,** 157-68.

KUNWAR, P. S., SIEKHAUS, D. E. & LEHMANN, R. 2006. In vivo migration: a germ cell perspective. *Annu Rev Cell Dev Biol,* 22**,** 237-65.

LABRADOR, J. P., AZCOITIA, V., TUCKERMANN, J., LIN, C., OLASO, E., MANES, S., BRUCKNER, K., GOERGEN, J. L., LEMKE, G., YANCOPOULOS, G., ANGEL, P., MARTINEZ, C. & KLEIN, R. 2001. The collagen receptor DDR2 regulates proliferation and its elimination leads to dwarfism. *EMBO Rep,* 2**,** 446-52.

LADOUX, B. & NICOLAS, A. 2012. Physically based principles of cell adhesion mechanosensitivity in tissues. *Rep Prog Phys,* 75**,** 116601.

LAMMERMANN, T., BADER, B. L., MONKLEY, S. J., WORBS, T., WEDLICH-SOLDNER, R., HIRSCH, K., KELLER, M., FORSTER, R., CRITCHLEY, D. R., FASSLER, R. & SIXT, M. 2008. Rapid leukocyte migration by integrin-independent flowing and squeezing. *Nature,* 453**,** 51-5.

LAMOUILLE, S., XU, J. & DERYNCK, R. 2014. Molecular mechanisms of epithelial-mesenchymal transition. *Nat Rev Mol Cell Biol,* 15**,** 178-96.

LAUFFENBURGER, D. A. & HORWITZ, A. F. 1996. Cell migration: a physically integrated molecular process. *Cell,* 84**,** 359-69.

LE CLAINCHE, C. & CARLIER, M. F. 2008. Regulation of actin assembly associated with protrusion and adhesion in cell migration. *Physiol Rev,* 88**,** 489-513.

LECKBAND, D. E. & DE ROOIJ, J. 2014. Cadherin adhesion and mechanotransduction. *Annu Rev Cell Dev Biol,* 30**,** 291-315.

LEE, C. K., WANG, Y. M., HUANG, L. S. & LIN, S. 2007. Atomic force microscopy: determination of unbinding force, off rate and energy barrier for protein-ligand interaction. *Micron,* 38**,** 446-61.

LEKKA, M., GIL, D., DABROS, W., JACZEWSKA, J., KULIK, A. J., LEKKI, J., STACHURA, Z., STACHURA, J. & LAIDLER, P. 2011. Characterization of N-cadherin unbinding properties in non-malignant (HCV29) and malignant (T24) bladder cells. *J Mol Recognit,* 24**,** 833-42.

LEVI, G., GUMBINER, B. & THIERY, J. P. 1991. The distribution of E-cadherin during Xenopus laevis development. *Development,* 111**,** 159-69.

LITVINOV, R. I., SHUMAN, H., BENNETT, J. S. & WEISEL, J. W. 2002. Binding strength and activation state of single fibrinogen-integrin pairs on living cells. *Proc Natl Acad Sci U S A,* 99**,** 7426-31.

LO, C. M. & FERRIER, J. 1998. Impedance analysis of fibroblastic cell layers measured by electric cell-substrate impedance sensing. *Physical Review E,* 57**,** 6982-6987.

LO, C. M., KEESE, C. R. & GIAEVER, I. 1995. Impedance analysis of MDCK cells measured by electric cell-substrate impedance sensing. *Biophys J,* 69**,** 2800-7.

LOCASCIO, A. & NIETO, M. A. 2001. Cell movements during vertebrate development: integrated tissue behaviour versus individual cell migration. *Curr Opin Genet Dev,* 11**,** 464-9.

LOVELADY, D. C., FRIEDMAN, J., PATEL, S., RABSON, D. A. & LO, C. M. 2009. Detecting effects of low levels of cytochalasin B in 3T3 fibroblast cultures by analysis of electrical noise obtained from cellular micromotion. *Biosens Bioelectron,* 24**,** 2250-4.

LU, L., OSWALD, S. J., NGU, H. & YIN, F. C. 2008. Mechanical properties of actin stress fibers in living cells. *Biophys J,* 95**,** 6060-71.

LU, P., WEAVER, V. M. & WERB, Z. 2012. The extracellular matrix: a dynamic niche in cancer progression. *J Cell Biol,* 196**,** 395-406.

LU, P. F., TAKAI, K., WEAVER, V. M. & WERB, Z. 2011. Extracellular Matrix Degradation and Remodeling in Development and Disease. *Cold Spring Harbor Perspectives in Biology,* 3.

MACOSKO, C. W. 1994. *Rheology : principles, measurements, and applications,* New York, VCH.

MAEYAMA, M., KOGA, H., SELVENDIRAN, K., YANAGIMOTO, C., HANADA, S., TANIGUCHI, E., KAWAGUCHI, T., HARADA, M., UENO, T. & SATA, M. 2008. Switching in discoid domain receptor expressions in SLUG-induced epithelial-mesenchymal transition. *Cancer,* 113**,** 2823-31.

MARASTONI, S., LIGRESTI, G., LORENZON, E., COLOMBATTI, A. & MONGIAT, M. 2008. Extracellular matrix: A matter of life and death. *Connective Tissue Research,* 49**,** 203-206.

MARCUS, W. D., MCEVER, R. P. & ZHU, C. 2004. Forces required to initiate membrane tether extrusion from cell surface depend on cell type but not on the surface molecule. *Mech Chem Biosyst,* 1**,** 245-51.

MARTIN, P. 1997. Wound healing--aiming for perfect skin regeneration. *Science,* 276**,** 75-81.

MORRISON, F. A. 2001. *Understanding rheology,* New York, Oxford University Press.

MULLER, W. A. 2003. Leukocyte-endothelial-cell interactions in leukocyte transmigration and the inflammatory response. *Trends Immunol,* 24**,** 327-34.

NAKAMURA, A., SHIRAE-KURABAYASHI, M. & HANYU-NAKAMURA, K. 2010. Repression of early zygotic transcription in the germline. *Curr Opin Cell Biol,* 22**,** 709-14.

NETHERTON, S. J. & BONNI, S. 2010. Suppression of TGFbeta-induced epithelial-mesenchymal transition like phenotype by a PIAS1 regulated sumoylation pathway in NMuMG epithelial cells. *PLoS One,* 5**,** e13971.

NEUMAN, K. C. & NAGY, A. 2008. Single-molecule force spectroscopy: optical tweezers, magnetic tweezers and atomic force microscopy. *Nat Methods,* 5**,** 491-505.

NIESSEN, C. M., LECKBAND, D. & YAP, A. S. 2011. Tissue organization by cadherin adhesion molecules: dynamic molecular and cellular mechanisms of morphogenetic regulation. *Physiol Rev,* 91**,** 691-731.

NIETO, M. A. 2002. The snail superfamily of zinc-finger transcription factors. *Nat Rev Mol Cell Biol,* 3**,** 155-66.

NIEUWKOOP, P. D. & FABER, J. 1994. *Normal table of Xenopus laevis (Daudin) : a systematical and chronological survey of the development from the fertilized egg till the end of metamorphosis,* New York, Garland Pub.

NISHIUMI, F., KOMIYA, T. & IKENISHI, K. 2005. The mode and molecular mechanisms of the migration of presumptive PGC in the endoderm cell mass of Xenopus embryos. *Dev Growth Differ,* 47**,** 37-48.

OLASO, E., ARTETA, B., BENEDICTO, A., CRENDE, O. & FRIEDMAN, S. L. 2011a. Loss of discoidin domain receptor 2 promotes hepatic fibrosis after chronic carbon tetrachloride through altered paracrine interactions between hepatic stellate cells and liver-associated macrophages. *Am J Pathol,* 179**,** 2894-904.

OLASO, E., LIN, H. C., WANG, L. H. & FRIEDMAN, S. L. 2011b. Impaired dermal wound healing in discoidin domain receptor 2-deficient mice associated with defective extracellular matrix remodeling. *Fibrogenesis Tissue Repair,* 4**,** 5.

OROZ, J., VALBUENA, A., VERA, A. M., MENDIETA, J., GOMEZ-PUERTAS, P. & CARRION-VAZQUEZ, M. 2011. Nanomechanics of the cadherin ectodomain: "canalization" by Ca2+ binding results in a new mechanical element. *J Biol Chem,* 286**,** 9405-18.

OZAWA, M. & KEMLER, R. 1998. Altered cell adhesion activity by pervanadate due to the dissociation of alpha-catenin from the E-cadherin.catenin complex. *J Biol Chem,* 273**,** 6166-70.

PALUCH, E. K. & RAZ, E. 2013. The role and regulation of blebs in cell migration. *Curr Opin Cell Biol,* 25**,** 582-90.

PANORCHAN, P., THOMPSON, M. S., DAVIS, K. J., TSENG, Y., KONSTANTOPOULOS, K. & WIRTZ, D. 2006. Single-molecule analysis of cadherin-mediated cell-cell adhesion. *J Cell Sci,* 119**,** 66-74.

PATHAK, A. & KUMAR, S. 2011. Biophysical regulation of tumor cell invasion: moving beyond matrix stiffness. *Integr Biol (Camb),* 3**,** 267-78.

PICOUT, D. R. & ROSS-MURPHY, S. B. 2003. Rheology of biopolymer solutions and gels. *ScientificWorldJournal,* 3**,** 105-21.

POLLARD, T. D., EARNSHAW, W. C., LIPPINCOTT-SCHWARTZ, J. & JOHNSON, G. T. 2008. Cell biology.

POLYAK, K. & WEINBERG, R. A. 2009. Transitions between epithelial and mesenchymal states: acquisition of malignant and stem cell traits. *Nat Rev Cancer,* 9**,** 265-73.

PUCHNER, E. M. & GAUB, H. E. 2009. Force and function: probing proteins with AFM-based force spectroscopy. *Curr Opin Struct Biol,* 19**,** 605-14.

PUECH, P. H., POOLE, K., KNEBEL, D. & MULLER, D. J. 2006. A new technical approach to quantify cell-cell adhesion forces by AFM. *Ultramicroscopy,* 106**,** 637-44.

PUNTHEERANURAK, T., NEUNDLINGER, I., KINNE, R. K. & HINTERDORFER, P. 2011. Single-molecule recognition force spectroscopy of transmembrane transporters on living cells. *Nat Protoc,* 6**,** 1443-52.

PUPA, S. M., MENARD, S., FORTI, S. & TAGLIABUE, E. 2002. New insights into the role of extracellular matrix during tumor onset and progression. *J Cell Physiol,* 192**,** 259-67.

RADMACHER, M. 1997. Measuring the elastic properties of biological samples with the AFM. *Ieee Engineering in Medicine and Biology Magazine,* 16**,** 47-57.

RASTALDI, M. P., FERRARIO, F., GIARDINO, L., DELL'ANTONIO, G., GRILLO, C., GRILLO, P., STRUTZ, F., MULLER, G. A., COLASANTI, G. & D'AMICO, G. 2002. Epithelial-mesenchymal transition of tubular epithelial cells in human renal biopsies. *Kidney Int,* 62**,** 137-46.

RICHARDSON, B. E. & LEHMANN, R. 2010. Mechanisms guiding primordial germ cell migration: strategies from different organisms. *Nat Rev Mol Cell Biol,* 11**,** 37-49.

RUST, M. J., BATES, M. & ZHUANG, X. W. 2006. Sub-diffraction-limit imaging by stochastic optical reconstruction microscopy (STORM). *Nature Methods,* 3**,** 793-795.

SACKMANN, E. 2015. How actin/myosin crosstalks guide the adhesion, locomotion and polarization of cells. *Biochimica Et Biophysica Acta-Molecular Cell Research,* 1853**,** 3132-3142.

SANTOS, A. C. & LEHMANN, R. 2004. Germ cell specification and migration in Drosophila and beyond. *Curr Biol,* 14**,** R578-89.

SCHAFER, E., KLIESCH, T. T. & JANSHOFF, A. 2013. Mechanical properties of giant liposomes compressed between two parallel plates: impact of artificial actin shells. *Langmuir,* 29**,** 10463-74.

SCHNEIDER, D., TARANTOLA, M. & JANSHOFF, A. 2011. Dynamics of TGF-beta induced epithelial-to-mesenchymal transition monitored by electric cell-substrate impedance sensing. *Biochim Biophys Acta,* 1813**,** 2099-107.

SHANKAR, J. & NABI, I. R. 2015. Actin cytoskeleton regulation of epithelial mesenchymal transition in metastatic cancer cells. *PLoS One,* 10**,** e0119954.

SHAPIRO, L., FANNON, A. M., KWONG, P. D., THOMPSON, A., LEHMANN, M. S., GRUBEL, G., LEGRAND, J. F., ALS-NIELSEN, J., COLMAN, D. R. & HENDRICKSON, W. A. 1995. Structural basis of cell-cell adhesion by cadherins. *Nature,* 374**,** 327-37.

SHI, Q., MARUTHAMUTHU, V., LI, F. & LECKBAND, D. 2010. Allosteric cross talk between cadherin extracellular domains. *Biophys J,* 99**,** 95-104.

SHIRAKIHARA, T., SAITOH, M. & MIYAZONO, K. 2007. Differential regulation of epithelial and mesenchymal markers by deltaEF1 proteins in epithelial mesenchymal transition induced by TGF-beta. *Mol Biol Cell,* 18**,** 3533-44.

SHRIVASTAVA, A., RADZIEJEWSKI, C., CAMPBELL, E., KOVAC, L., MCGLYNN, M., RYAN, T. E., DAVIS, S., GOLDFARB, M. P., GLASS, D. J., LEMKE, G. & YANCOPOULOS, G. D. 1997. An orphan receptor tyrosine kinase family whose members serve as nonintegrin collagen receptors. *Mol Cell,* 1**,** 25-34.

SIEMENS, H., JACKSTADT, R., HUNTEN, S., KALLER, M., MENSSEN, A., GOTZ, U. & HERMEKING, H. 2011. miR-34 and SNAIL form a double-negative feedback loop to regulate epithelial-mesenchymal transitions. *Cell Cycle,* 10**,** 4256-71.

SIVASANKAR, S. 2013. Tuning the kinetics of cadherin adhesion. *J Invest Dermatol,* 133**,** 2318-23.

SMITH, T. J., WANG, H. S., HOGG, M. G., HENRIKSON, R. C., KEESE, C. R. & GIAEVER, I. 1994. Prostaglandin E2 elicits a morphological change in cultured orbital fibroblasts from patients with Graves ophthalmopathy. *Proc Natl Acad Sci U S A,* 91**,** 5094-8.

SNEDDON, I. N. 1965. The relation between load and penetration in the axisymmetric boussinesq problem for a punch of arbitrary profile *Int. J. Engng Sci.,* 3**,** 47-57.

SON, H. & MOON, A. 2010. Epithelial-mesenchymal Transition and Cell Invasion. *Toxicol Res,* 26**,** 245-52.

SOOFI, S. S., LAST, J. A., LILIENSIEK, S. J., NEALEY, P. F. & MURPHY, C. J. 2009. The elastic modulus of Matrigel (TM) as determined by atomic force microscopy. *Journal of Structural Biology,* 167**,** 216-219.

STICKENS, D., BEHONICK, D. J., ORTEGA, N., HEYER, B., HARTENSTEIN, B., YU, Y., FOSANG, A. J., SCHORPP-KISTNER, M., ANGEL, P. & WERB, Z. 2004. Altered endochondral bone development in matrix metalloproteinase 13-deficient mice. *Development,* 131**,** 5883-95.

TAUBENBERGER, A., CISNEROS, D. A., FRIEDRICHS, J., PUECH, P. H., MULLER, D. J. & FRANZ, C. M. 2007. Revealing early steps of alpha2beta1 integrin-mediated adhesion to collagen type I by using single-cell force spectroscopy. *Mol Biol Cell,* 18**,** 1634-44.

TERAYAMA, K., KATAOKA, K., MORICHIKA, K., ORII, H., WATANABE, K. & MOCHII, M. 2013. Developmental regulation of locomotive activity in Xenopus primordial germ cells. *Dev Growth Differ,* 55**,** 217-28.

THEVENEAU, E. & MAYOR, R. 2013. Collective cell migration of epithelial and mesenchymal cells. *Cell Mol Life Sci,* 70**,** 3481-92.

THIERY, J. P., ACLOQUE, H., HUANG, R. Y. & NIETO, M. A. 2009. Epithelial-mesenchymal transitions in development and disease. *Cell,* 139**,** 871-90.

THIERY, J. P. & SLEEMAN, J. P. 2006. Complex networks orchestrate epithelial-mesenchymal transitions. *Nat Rev Mol Cell Biol,* 7**,** 131-42.

TIAN, X., LIU, Z., NIU, B., ZHANG, J., TAN, T. K., LEE, S. R., ZHAO, Y., HARRIS, D. C. & ZHENG, G. 2011. E-cadherin/beta-catenin complex and the epithelial barrier. *J Biomed Biotechnol,* 2011**,** 567305.

TSAI, J. H. & YANG, J. 2013. Epithelial-mesenchymal plasticity in carcinoma metastasis. *Genes Dev,* 27**,** 2192-206.

VAN ROY, F. & BERX, G. 2008. The cell-cell adhesion molecule E-cadherin. *Cell Mol Life Sci,* 65**,** 3756-88.

VOGEL, W. F., ABDULHUSSEIN, R. & FORD, C. E. 2006. Sensing extracellular matrix: an update on discoidin domain receptor function. *Cell Signal,* 18**,** 1108-16.

WALSH, L. A., NAWSHAD, A. & MEDICI, D. 2011. Discoidin domain receptor 2 is a critical regulator of epithelial-mesenchymal transition. *Matrix Biology,* 30**,** 243-247.

WEGENER, J., KEESE, C. R. & GIAEVER, I. 2000. Electric cell-substrate impedance sensing (ECIS) as a noninvasive means to monitor the kinetics of cell spreading to artificial surfaces. *Exp Cell Res,* 259**,** 158-66.

WEHRLE-HALLER, B. & IMHOF, B. 2002. The inner lives of focal adhesions. *Trends Cell Biol,* 12**,** 382-9.

WELLNER, U., SCHUBERT, J., BURK, U. C., SCHMALHOFER, O., ZHU, F., SONNTAG, A., WALDVOGEL, B., VANNIER, C., DARLING, D., ZUR HAUSEN, A., BRUNTON, V. G., MORTON, J., SANSOM, O., SCHULER, J., STEMMLER, M. P., HERZBERGER, C., HOPT, U., KECK, T., BRABLETZ, S. & BRABLETZ, T. 2009. The EMT-activator ZEB1 promotes tumorigenicity by repressing stemness-inhibiting microRNAs. *Nat Cell Biol,* 11**,** 1487-95.

WISEMAN, B. S., STERNLICHT, M. D., LUND, L. R., ALEXANDER, C. M., MOTT, J., BISSELL, M. J., SOLOWAY, P., ITOHARA, S. & WERB, Z. 2003. Site-specific inductive and inhibitory activities of MMP-2 and MMP-3 orchestrate mammary gland branching morphogenesis. *J Cell Biol,* 162**,** 1123-33.

WOZNIAK, M. A., MODZELEWSKA, K., KWONG, L. & KEELY, P. J. 2004. Focal adhesion regulation of cell behavior. *Biochim Biophys Acta,* 1692**,** 103-19.

WU, P. & BRAND, L. 1994. Resonance energy transfer: methods and applications. *Anal Biochem,* 218**,** 1-13.

XIAO, C., LACHANCE, B., SUNAHARA, G. & LUONG, J. H. 2002. An in-depth analysis of electric cell-substrate impedance sensing to study the attachment and spreading of mammalian cells. *Anal Chem,* 74**,** 1333-9.

XIE, L., LAW, B. K., AAKRE, M. E., EDGERTON, M., SHYR, Y., BHOWMICK, N. A. & MOSES, H. L. 2003. Transforming growth factor beta-regulated gene expression in a mouse mammary gland epithelial cell line. *Breast Cancer Res,* 5**,** R187-98.

XU, J., LAMOUILLE, S. & DERYNCK, R. 2009. TGF-beta-induced epithelial to mesenchymal transition. *Cell Res,* 19**,** 156-72.

YAMAGUCHI, H., WYCKOFF, J. & CONDEELIS, J. 2005. Cell migration in tumors. *Curr Opin Cell Biol,* 17**,** 559-64.

YILMAZ, M. & CHRISTOFORI, G. 2009. EMT, the cytoskeleton, and cancer cell invasion. *Cancer Metastasis Rev,* 28**,** 15-33.

YIP, A. K., CHIAM, K. H. & MATSUDAIRA, P. 2015. Traction stress analysis and modeling reveal that amoeboid migration in confined spaces is accompanied by expansive forces and requires the structural integrity of the membrane-cortex interactions. *Integr Biol (Camb),* 7**,** 1196-211.

YUE, J. & MULDER, K. M. 2001. Transforming growth factor-beta signal transduction in epithelial cells. *Pharmacol Ther,* 91**,** 1-34.

ZAMAN, M. H., TRAPANI, L. M., SIEMINSKI, A. L., MACKELLAR, D., GONG, H., KAMM, R. D., WELLS, A., LAUFFENBURGER, D. A. & MATSUDAIRA, P. 2006. Migration of tumor cells in 3D matrices is governed by matrix stiffness along with cell-matrix adhesion and proteolysis. *Proc Natl Acad Sci U S A,* 103**,** 10889-94.

ZAVADIL, J. & BOTTINGER, E. P. 2005. TGF-beta and epithelial-to-mesenchymal transitions. *Oncogene,* 24**,** 5764-74.

ZEISBERG, M. & NEILSON, E. G. 2009. Biomarkers for epithelial-mesenchymal transitions. *J Clin Invest,* 119**,** 1429-37.

ZHANG, J., TIAN, X. J., ZHANG, H., TENG, Y., LI, R., BAI, F., ELANKUMARAN, S. & XING, J. 2014. TGF-beta-induced epithelial-to-mesenchymal transition proceeds through stepwise activation of multiple feedback loops. *Sci Signal,* 7**,** ra91.

ZHANG, K., CORSA, C. A., PONIK, S. M., PRIOR, J. L., PIWNICA-WORMS, D., ELICEIRI, K. W., KEELY, P. J. & LONGMORE, G. D. 2013. The collagen receptor discoidin domain receptor 2 stabilizes SNAIL1 to facilitate breast cancer metastasis. *Nat Cell Biol,* 15**,** 677-87.

ZLATANOVA, J., LINDSAY, S. M. & LEUBA, S. H. 2000. Single molecule force spectroscopy in biology using the atomic force microscope. *Prog Biophys Mol Biol,* 74**,** 37-61.

7 List of figures

8 List of tables

9 List of materials

9.1 Chemicals

Alexa Fluor 488 goat-anti-mouse IgG (H+L)	Life Technologies, Darmstadt, Germany
Alexa Fluor 546 phalloidin	Life Technologies, Darmstadt, Germany
Amphotericin B	GE Healthcare, Freiburg, Germany
Anti-E-cadherin anti body	BD Biosciences, Heidelberg, Germany
Benzylguanine-thiol (BG) solution	Senso Path Technologies, Inc.; Bozeman, USA
BSA (Albumin IgG free)	Carl Roth GmbH, Karlsruhe, Germany
Cell Mask™; Deep Red Plasma Membrane Stain	Life Technologies, Darmstadt, Germany
DAPI	Life Technologies, Darmstadt, Germany
DMEM	Lonza, Basel, Switzerland
E-cadherin SNAP-*tag* fusion protein	Prof. Dr. Wedlich Lab (Karlsruhe Institute of Technology (KIT), DFG-Center for Functional Nanostructures, Karlsruhe, Germany
EDTA	Sigma-Aldrich, Munich, Germany
Ethanol	Sigma-Aldrich, Munich, Germany
FBS	BioWest, Nuaillé, France

HEPES	Biochrom AG, Berlin, Germany
Insulin	Sigma-Aldrich, Munich, Germany
Isopropanol	VWR Chemicals, Darmstadt, Germany
L-glutamine	Lonza, Basel, Switzerland
Methoxy terminal-EG3-thiol	Fraunhofer Instiut für Fertigungstechnik und angewandte Materialforschung, Dr. K. Rischka, Bremen, Germany
NaCl	PanReac AppliChem, Darmstadt, Germany
PBS^{--}	Biochrom AG, Berlin, Germany
PBS^{++}	Biochrom AG, Berlin, Germany
Penicillin/Streptomycin	GE Healthcare, Freiburg, Germany
PFA	Sigma-Aldrich, Munich, Germany
Poly-D-lysine	Sigma-Aldrich, Munich, Germany
TGF-ß1	Life Technologies, Darmstadt, Germany
Triton-X	Sigma-Aldrich, Munich, Germany
Trypsin/EDTA solution	Biochrom, Berlin, Germany
Ultra-pure water	MilliQ; Merck Millipore, Darmstadt, Germany

9.2 Devices and Materials

Software

Matlab	The MathWorks, Inc., Natick, MA, USA
IGOR	Wavemetrics, Lake Oswego, OR; USA
JPK Data Processing	JPK Instruments, Berlin, Germany

Atomic force spectroscopy

NanoWizard II™ AFM	JPK Instruments, Berlin, Germany
Olympus IX81 microscope	Olympus, Hamburg, Germany
MFP-3D™	Asylum Research, Santa Barbara, CA, USA
Olympus IX 51 microscope	Olympus, Hamburg, Germany
CP-PNPL-SiO-A cantilever	sQube, Bickenbach, Germany
CP-PNPL-Au-C-8 cantilever	sQube, Bickenbach, Germany
Microscope glass slides	Menzel-Gläser; Braunschweig, Germany

Single cell force spectroscopy

Cellhesion200 AFM	JPK Instruments, Berlin, Germany
Olympus IX81 microscope	Olympus, Hamburg, Germany
Arrow-TL2-50, Tipless Silicon SPM-Sensors, cantilever	Nano World
UHU endfest 300 glue	UHU, Bühl, Germany
Super PAP Pen Liquid Blocker, mini	Daido Sangyo Co., Ltd, Tokyo, Japan

Single molecule force spectroscopy

NanoWizard II/III™ AFM	JPK Instruments, Berlin, Germany
Olympus IX81 microscope	Olympus, Hamburg, Germany
MFP-3D™	Asylum Research, Santa Barbara, CA, USA
Olympus IX 51 microscope	Olympus, Hamburg, Germany
Bio-Lever BL-RC150VB-C1, cantilever	Olympus, Hamburg, Germany

Optical microscopy techniques

CLSM, Olympus Fluoview, FV1200	Olympus, Hamburg, Germany
Ibidi™ petri dishes	Ibidi, Martinsried, Germany
Sterile filter Minisart	Sartorius Stedim, Göttingen, Germany;

Analysing EMT with metal induced energy transfer

Home build CLSM setup	Georg-August-University, III. Physical Institute, Göttingen, Germany
MatTek petri dishes	Ashland, MA, USA

Cell culture

Safe 2020 sterile laminar flow	Thermo Scientific, Waltham, MA, USA
Heracell 150i, CO_2 incubator	Thermo Scientific, Waltham, MA, USA
Culture flasks	TPP, Trasadingen, Switzerland
Heraeus, Megafuge 16R, Centrifuge	Thermo Scientific, Waltham, MA, USA
C-Chip, Neubauer Improved	Digial Bio, Seoul, Korea

Electric cell-substrate impedance sensing

ECIS Zθ (Theta)	Applied BioPhysics, Troy, NY, USA
CO_2 Incubator	MMM Medcenter Einrichtungen GmbH, München, Germany
Gold electrodes of 8W1E arrays	Ibidi^{TM}, Martinsried, Germany

Rheometry

Physica MCR501 (plate rheometer)	Anton Paar, Graz, Austria
Cover slips	Menzel-Gläser; Braunschweig, Germany

Other

Petri dish	TPP, Trasadingen, Switzerland
Plasma Cleaner	Harrick Scientific Corp., Pleasantville NY, USA

10 List of abbreviations

ADP	adenosine diphosphate
AFM	atomic force microscopy
ATP	adenosine triphosphate
BGT	benzylguanine thiol
BSA	bovine serum albumin
C-cadherin	classical cadherin
CLSM	confocal laser scanning microscope
DAPI	4'-6-diamidino-2-phenylindole
DDR	discoidin domain receptor 2
DELE	Dead End localization element
DMEM	Dulbecco's modified eagle medium
E	Youngs's Modulus
EC	ectodomain/extracellular domain
E-cadherin	epithelial cadherin
ECIS	electric cell-substrate impedance sensing
ECM	extracellular matrix
EDTA	ethylenediaminetetraacetic acid
EMT	epithelial-mesenchymal transition
F-actin	actin filament
FBS	fetal bovine serum
FLIM	fluorescence lifetime imaging
F_{max}	maximum adhesion force
FRET	Förster resonance energy transfer
G'	storage modulus
G"	loss modulus
h	hour
HEPES	4-(2-hydroxyethyl)-1-piperazineethanesulfonic acid
ICAM	intercellular adhesion molecule
MDCK	Madin-Darby Canine Kidney Epithelial Cells
MET	mesenchymal-epithelial transition
MIET	metal induced energy transfer

MMP	matrix metalloprotease
MO	morpholino oligonucleotides
MT	matrix thiol
NaCl	sodium chloride
N-cadherin	neural cadherin
NMuMG	normal murine mammary gland epithelia
PBS	phosphate buffered saline
PFA	paraformaledhyde
PGC	primordial germ cell
pN	piconewton
qPCR	real-time quantitative polymerase chain reaction
RhoA	Ras homolog gene family, member A
RNA	ribonucleic acid
ROCK	Rho-associated protein kinase
RTK	receptor tyrosine kinase
SCFS	single cell force spectroscopy
SEM	standard error of mean
SMFS	single molecule force spectroscopy
SNAIL	Zinc finger protein SNAI1
SRE	single rupture event
STM	scanning tunneling microscope
TGF-ß1	transforming growth factor ß1
TIRF	total internal reflectance microscopy
ZEB	Zinc finger E-box-binding homeobox 1
v	Poisson’s ratio

11 Danksagung

An dieser Stelle möchte ich mich bei allen Menschen herzlich bedanken, die mich während meiner Doktorarbeit unterstützt haben.

Mein besonderer Dank gilt Herrn Prof. Dr. Andreas Janshoff für die Möglichkeit bei ihm diese Doktorarbeit durchzuführen, die interessante Themenstellung und die Diskussionen und Anregungen - nicht zu vergessen die tollen Fußball-diskussionsrunden.

Den Mitgliedern des Thesis Komitees Herrn Prof. Dr. Tomas Pieler und Herrn Prof. Dr. Andras Wodarz danke ich für die Unterstützung meiner Arbeit und die hilfreichen Diskussionen während der Treffen.

Dr. Aliaksandr Dzementsei und Prof. Dr. Tomas Pieler danke ich für die gute Kooperation, Dr. Alexey Chizhik für die tolle Kooperation und seine Unterstützung bei der Auswertung der MIET Daten, sowie Dr. Jeannine Missbach-Güntner für das interessante Thema unserer Kooperation.

Für ihre Herzlichkeit, die Bereitstellung der Zellen und die bereitwillige Erfüllung von Sonderwünschen danke ich Anja Herdlitschke und Angela Rübeling. Ohne ihre Hilfe wäre diese Arbeit nicht möglich gewesen.

Ein großer Dank gilt Dr. Ingo Mey, der mir perfekte Unterstützung bei Computer-problemen aller Art geleistet hat und ohne dessen Hilfe und Matlab-Skripte ich ziemlich aufgeflogen wäre.

Basti, mit dem ich seit der Masterarbeit zusammen die Aufgaben im Arbeitskreis gemeistert habe, danke ich ebenfalls. Ich konnte mich stets auf seine Hilfsbereitschaft und seinen Rat verlassen.

Helen gilt mein Dank für das angenehme Arbeitsklima in unserem Büro und natürlich auch für die tolle Hilfsbereitschaft und Zusammenarbeit in allen Bereichen.

David danke ich für seine Unterstützung vor allem neben der Arbeit durch unzählige Fußballabende, BombSquad Sessions und Partysessions.

Jan gilt mein Dank für die schönen Jahre in der WG und ebenfalls für die legendären BombSquad Abende.

Moe danke ich für die tolle Zusammenarbeit vor allem bei der Organisation der Geschenke für den Arbeitskreis, für die Einkauftouren der Süßigkeitskasse und unsere unzähligen WhatsApp Diskussionen.

Den Mitgliedern des Arbeitskreises danke ich für die unzähligen Tipps und Ratschläge, sowie ihre Unterstützung bei Fragen und Problemen, natürlich auch für unsere alltägliche Mittags- und Kaffeepause, ohne die ich den Arbeitstag nicht überstanden hätte. Unsere Unternehmungen und Filmabende haben meinen Alltag darüber hinaus immer bereichert.

Desweitern danke ich meinen ehemaligen Arbeitskollegen Anna, Gesa und Edith, die mir den Anfang in die Doktorarbeit erheblich erleichtert haben

Ein besonderer Dank geht an Susi, für die zügige und sorgfältige Korrektur dieser Arbeit. Darüber hinaus habe ich unsere Sportsessions jede Woche, sei es Tennis, Squash oder Badminton gewesen, sehr genossen.

Marco und Gesa danke ich für die schönen Abende in der Zeit meiner Doktorarbeit, ob Fußball, Kino, lecker Essen gehen oder einfach nur einen Trinken.

Turbo gilt mein Dank für das Teilen der gleichen Begeisterung für Fußball, Filme oder Autos.

Jenny danke ich für den Rückhalt und das Teilen von besonderen Momenten über die letzten zwei Jahre.

Mein größter Dank gilt meiner Mutter, ich konnte mich stets auf ihre uneingeschränkte Unterstützung verlassen. Ihr Zuspruch und Rückhalt ermöglichte mir erst diese Herausforderung anzunehmen.